AWARD NUMBER: W81XWH-12-1-0132

TITLE: CpG-STAT3siRNA for Castration-Resistant Prostate Cancer Therapy

PRINCIPAL INVESTIGATOR: Marcin Kortylewski

CONTRACTING ORGANIZATION: City of Hope Beckman Research Institute
Duarte, CA 91010-3012

REPORT DATE: December 2015

TYPE OF REPORT:Final

PREPARED FOR: U.S. Army Medical Research and Materiel Command
Fort Detrick, Maryland 21702-5012

REPORT DOCUMENTATION PAGE

Form Approved
OMB No. 0704-0188

1. REPORT DATE	2. REPORT TYPE	3. DATES COVERED
December 2015	Final	28Sep2012 - 27Sep2015

4. TITLE AND SUBTITLE

CpG-STAT3siRNA for Castration-Resistant Prostate Cancer Therapy

5a. CONTRACT NUMBER

5b. GRANT NUMBER
W81XWH-12-1-0132

5c. PROGRAM ELEMENT NUMBER

6. AUTHOR(S)

Marcin Kortylewski, Ph.D.

E-Mail: mkortylewski@coh.org

5d. PROJECT NUMBER

5e. TASK NUMBER

5f. WORK UNIT NUMBER

7. PERFORMING ORGANIZATION NAME(S) AND ADDRESS(ES)

City of Hope Beckman Research Institute
Duarte, CA 91010-3012

8. PERFORMING ORGANIZATION REPORT NUMBER

9. SPONSORING / MONITORING AGENCY NAME(S) AND ADDRESS(ES)
U.S. Army Medical Research and Materiel Command
Fort Detrick, Maryland 21702-5012

10. SPONSOR/MONITOR'S ACRONYM(S)

11. SPONSOR/MONITOR'S REPORT NUMBER(S)

12. DISTRIBUTION / AVAILABILITY STATEMENT
Approved for Public Release; Distribution Unlimited

13. SUPPLEMENTARY NOTES

14. ABSTRACT

Majority of human prostate cancers activate STAT3 signaling which is associated with progression to castration-resistant phenotype. STAT3 is also activated in diverse immune cell associated with prostate cancers. Therefore, STAT3 is a highly desirable target for prostate cancer therapy. Within the three years of funding, we have completed feasibility studies using CpG-siRNA strategy to target tumorigenic STAT3 and NF-κB/RELA transcription factors in xenotransplanted models of TLR9+ CRPCs. We demonstrated that blocking TLR9/NF-κB/STAT3 signaling axis reduces self-renewal and tumor-initiating potential of prostate cancer cells *in vivo*. Next, we characterized TLR9+/phosphoSTAT3+ immune cell populations in CRPC patients. The comparison of blood samples from healthy, localized- and metastatic-stage patients' found accumulation of granulocytic myeloid-derived suppressor cells (G-MDSCs; $Lin^{-}HLA\text{-}DR^{-}CD14^{-}CD15^{+}CD33^{low}$) with progression of the disease. The G-MDSCs in prostate cancer patients expressed TLR9 and showed high levels of STAT3 activation which correlated with their ability to suppress T cell proliferation *in vitro*. We found that STAT3 induced expression of arginase which was mainly responsible for tolerogenic functions of MDSCs and we demonstrated that targeting STAT3 signaling in TLR9+ MDSCs using CpG-siRNA restores T cell proliferation. Finally, we completed feasibility studies demonstrating that local intratumoral injections of CpG-STAT3siRNA result in systemic antitumor immune responses and inhibit growth of distant tumor lesions.

15. SUBJECT TERMS
Castration-resistant Prostate Cancer, TLR9, STAT3, RELA, MDSC, Arginase

16. SECURITY CLASSIFICATION OF:			17. LIMITATION OF ABSTRACT	18. NUMBER OF PAGES	19a. NAME OF RESPONSIBLE PERSON
a. REPORT	b. ABSTRACT	c. THIS PAGE			19b. TELEPHONE NUMBER *(include area code)*
U	U	U	UU	57	USAMRMC

Table of Contents

CpG-STAT3 siRNA for Castration-Resistant Prostate Cancer Therapy
Revised Final Report: 28/09/2012 – 26/09/2015

Introduction

Majority of human prostate cancers show STAT3 activation, which strongly correlates with tumor progression towards hormone-refractory/castration-resistant phenotype (CRPC) and poor patients' survival[1-3]. In addition, STAT3 is activated in diverse immune cell associated with prostate tumors promoting immune tolerance, angiogenesis and metastasis[4, 5]. Because STAT3 operates in both cancer cells and non-malignant tumor-associated cells, it represents a highly desirable target for cancer therapy[5]. Inhibiting STAT3 has potential to eliminate the aggressive castration-resistant prostate cancer (CRPC) cells, which are not amenable to existing hormonal treatments or standard chemotherapies[1] but undergo apoptosis when STAT3 signaling is inhibited[6-8]. In addition, very recently STAT3 signaling was shown to promote stem-like cell phenotype in prostate cancers[9]. Pharmacological inhibition of proteins lacking enzymatic activity, including STAT3, is difficult and requires alternative approaches, such as silencing genes using siRNA. We previously generated a strategy for cell-specific delivery of siRNA using CpG oligonucleotides (ODNs) for targeting cells positive for Toll-like receptor 9 (TLR9)[10]. CpG-siRNAs are internalized specifically by TLR9-positive human/mouse immune cells and malignant cells, such as blood cancer cells or CRPCs[10, 11]. We also demonstrated that *in vivo* administration of CpG-*STAT3* siRNA breaks tumor immune tolerance, thereby inducing antitumor immune responses in syngeneic tumor models in mice[10]. In addition, intratumoral injections of CpG-*STAT3* siRNA were shown to induce direct tumor cell death in TLR9-positive human leukemia xenotransplants[11]. These results suggested the feasibility of using human-specific CpG-*STAT3* siRNA to simultaneously target both castration-resistant prostate cancer cells and tumor-associated immune cells, such as myeloid-derived suppressor cells (MDSCs). We hypothesized that targeting oncogenic and tolerogenic signaling using cell-specific CpG(A)-siRNA strategy will suppress tumor progression and generate potent antitumor immunity, with minimal adverse effects.

Keywords

Castration-Resistant Prostate Cancer, TLR9, STAT3, NF-κB, MDSC, CpG, siRNA, oligonucleotides

Accomplishments

The main objectives for this study remained unchanged: first was to optimize of the CpG(A)-siRNA strategy for targeting tumorigenic signaling in metastatic prostate cancer cells; second was to utilize this strategy for breaking immunosuppressive effects of the prostate cancer microenvironment.

Task 1. To optimize CpG(A)-siRNA strategy for direct inhibition of human CRPC cell survival and proliferation.

We previously validated STAT3 and NF-κB/RELA transcription factors as optimal targets for CpG-siRNA strategy in CRPC xenotransplants. During the whole funding period, we completed *in vitro* and *in vivo* studies within this aim which allow us to elucidate the molecular mechanisms underlying therapeutic effects of targeting TLR9 signaling. These studies allowed us to develop detailed methodology for the design and application of CpG-siRNA conjugates to deliver siRNA molecules into specific target cells in mice, including TLR9-positive prostate cancer cells. **Our recent publication in the *Methods Mol. Biol*. (Appendix 1),**[12] provides specifics of the CpG-siRNA oligonucleotide synthesis/purification, testing *in vitro* and local/systemic delivery into TLR9-positive cells *in vivo* (Figure 1). It also discusses critical troubleshooting points for target cell selection and optimizing gene silencing efficiency of CpG-siRNA conjugates.

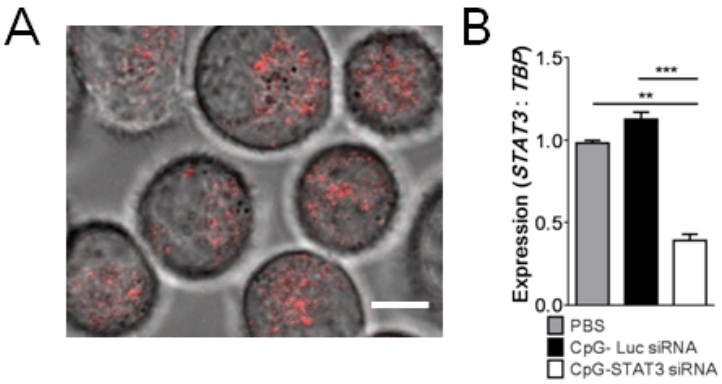

Figure 1. CpG-*STAT3*siRNA uptake *in vitro* and target gene silencing in DU145 prostate tumors *in vivo*. (A) The intracellular localization of the CpG-siRNACy3 (500 nM/1 h) was assessed using confocal time-lapse microscopy in living PC3 cells; scale bar = 100 μm. (B) The silencing effect of CpG-STAT3siRNA in experiment described in the main Figure 4B was verified using qPCR to measure and STAT3 (B) expression levels and normalizing to TBP expression; shown are means ± SEM (n = 5).[13]

Based on these findings, we optimized our CpG(A)-siRNA approach for targeting essential regulators of human CRPC cell survival and self-renewal identified within this aim. In this part of the study, we investigated a potential link between TLR9 expression and tumorigenic signaling in androgen-independent prostate cancer cells. Using limited dilution/serial transplantation experiments, we showed that TLR9 is essential for prostate cancer cells' potential to propagate and self-renew *in vivo*. Furthermore, we demonstrated that low expression or silencing of TLR9 limits the clonogenic potential and mesenchymal stem cell-like properties of LNCaP- and PC3-derived prostate cancer cell variants. Genome-wide transcriptional analysis of prostate cancer cells isolated from xenotransplanted TLR9-positive and -negative tumors revealed a unique gene expression signature, with prominent upregulation of inflammation and stem cell-related markers. We showed that TLR9 signaling orchestrated expression of critical stem cell-related genes such as *NKX3.1*, *KLF-4*, *BMI-1* and *COL1A1*, at both mRNA and protein levels. Our further analysis identified that TLR9-induced NF-κB/RELA and STAT3 transcription factors co-regulated *NKX3.1* and *KLF4* gene expression by directly binding to both promoters. Finally, we demonstrated the potential of using TLR9-targeted siRNA delivery to block RELA- and STAT3-dependent prostate cancer cell self-renewal *in vivo*. The intratumoral administration of CpG-*RELA*siRNA or CpG-*STAT3*siRNA but not control conjugates inhibited growth of established human prostate cancer xenografts in mice and reduced clonogenic potential of cancer cells. These results provided evidence that targeted inhibition of TLR9 signaling can be a therapeutic strategy for late-stage prostate cancer patients. **These studies were summarized in our recent publication in *Oncotarget* journal (Appendix 2).**[13]

Task 2. To assess the feasibility of using CpG(A)-*STAT3* siRNA to break tumor immune tolerance in metastatic CRPC.

Studies completed within this aim demonstrated that CpG(A)-*STAT3* siRNA allows for targeting and abrogating immunosuppressive activity of myeloid-derived suppressor cells (MDSC) accumulating in blood of prostate cancer patients during disease progression. Following on our immunohistochemical analyses, we confirmed the accumulation of $TLR9^+/STAT3P^+$ myeloid cells in lymph nodes of late-stage metastatic prostate cancer patients but not in tumor free control subjects. Further studies identified elevated levels of of granulocytic-myeloid-derived suppressor cell (G-MDSCs; $Lin^-HLA\text{-}DR^-CD15^{hi}CD33^{lo}$) accumulating in cancer patients' blood with disease progression. These $TLR9^+$ G-MDSCs showed high levels of STAT3 activation together with secretion of immunosuppressive mediators, such as arginase-1 and inhibited effector T-cell proliferation and activity (Figure 2, below).

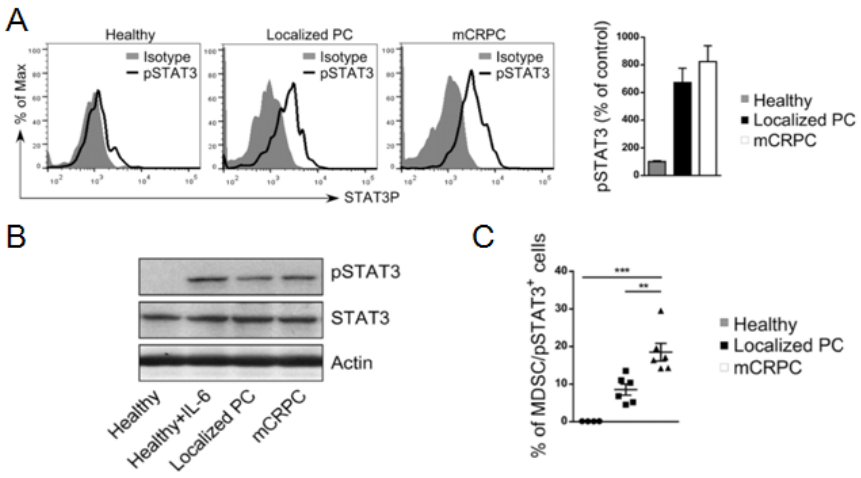

Figure 3. STAT3 activity is elevated in CD15HI MDSCs in prostate cancer patients. (A) Flow cytometric analysis of activated STAT3 (pSTAT3) in granulocytic MDSCs ($CD15^{HI}CD33^{LO}$) from patients with localized (n = 6) and metastatic (n=6) prostate cancers compared to granulocytes from healthy individuals (n=5). Shown are representative histogram overlays and bar graph summary of data from all patients; average of mean fluorescence intensities ± SD. (B) Prostate cancer patients' granulocytic cells show increased pSTAT3 without changes in the total STAT3 protein levels. Western blotting analysis comparing $CD15^+CD14^-$ cells isolated from PBMCs pooled from prostate cancer patients or healthy donors. (C) The percentage of G-MDSCs with activated STAT3 increases with prostate cancer progression; summary of results from all tested patients.

Functional studies showed that STAT3 blocking using CpG-*STAT3* siRNA abrogates immunosuppressive effects of patients-derived G-MDSCs on effector CD8 T cells. These effects depended on reduced expression and enzymatic activity of Arginase-1, a downstream STAT3 target gene and a potent T-cell inhibitor. Overall, we demonstrated the feasibility of using TLR9-targeted STAT3siRNA delivery strategy to alleviate MDSC-mediated immunosuppression in prostate cancer patients without the need for myeloid cell depletion. These findings together with the effect of STAT3 targeting on prostate cancer cell self-renewal and tumor propagating potential provide support for application of CpG-STAT3siRNA strategy to immunotherapy of advanced prostate cancers alone or in combination with immunotherapies, such as emerging T cell-based therapies. Disruption of STAT3 signaling in the tumor microenvironment with concurrent TLR9 stimulation has potential to disrupt the central immunosuppressive circuit paving way to effective antitumor immune responses without toxicities associated with pharmacological agents. **These studies were published in the *Clinical Cancer Research* journal (Appendix 3)[14] and discussed in the invited mini-review article in *OncoImmunology* (Appendix 4)[15].**

Task 3. To evaluate the CpG(A)-*STAT3* siRNA as a novel two-pronged approach to prostate cancer immunotherapy.

We completed studies *in vivo* focusing on the two pronged effects of CpG-*STAT3* siRNA on prostate cancer cells and on the tumor microenvironment using syngeneic (RM9) and xenotransplanted (DU145, PC3) tumor models in mice. To isolate the effect of CpG-*STAT3* siRNA on tumor-associated cells from direct targeting of $TLR9^+$ cancer cells we generated a panel of control $TLR9^-$ prostate cancer cells using

stable expression of *TLR9* shRNA. The TLR9 protein levels were undetectable in LNCaP cells, low in LNCaP-S17 and high in PC3 cells. Thus, to study the role of TLR9, we stably transduced the LNCaP and LNCaP-S17 cells using lentiviruses encoding either human TLR9 cDNA or mock vector; meanwhile the PC3 cells were transduced with either TLR9 shRNA or non-silencing control vector. Although, *in vitro* proliferation of various TLR9-expressing prostate cancer cell variants did not change, high TLR9 expression correlated with improved tumor engraftment and growth. As mentioned above (Task 1), TLR9 expression allowed for targeted delivery of CpG-*STAT3* siRNA into cancer cells **(Appendix 2)**.[13] On the contrary, TLR-negative prostate cancer cells were not directly targeted by CpG-siRNA strategy (Figure 3, below).

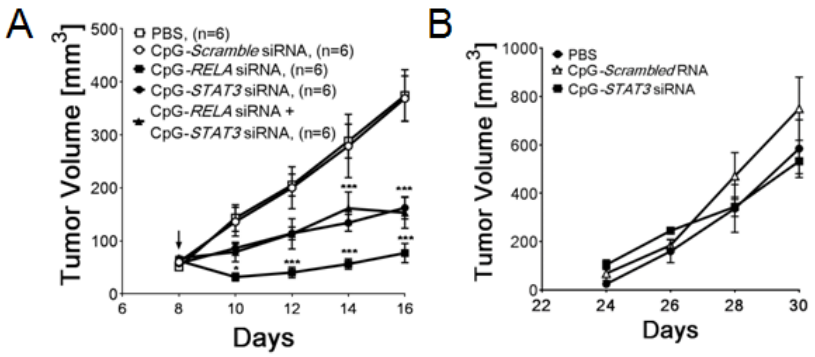

Figure 3. TLR9 expression in prostate cancer cells is critical for CpG-siRNA-mediated growth inhibitory effect. CpG-mediated silencing of *RELA* and/or *STAT3* inhibits growth of PC3/TLR9^{+} (A) but not PC3/TLR9^{-} (B) tumors in NSG mice. Mice were treated using IT injections of the indicated CpG-siRNA conjugates (5 mg/kg) or PBS every other day.

We demonstrated the role of tumor-microenvironment in promoting prostate cancer progression by comparison of human- and mouse-specific CpG-*STAT3* siRNA reagents against xenotransplanted TLR9^{+} human prostate cancers (Moreira and Kortylewski, manuscript in preparation). Both version of CpG-*STAT3* siRNA showed potent anti-tumor effect in the treated site but only mouse-specific reagent affected growth of tumors in distant/untreated site (Figure 4AB). This is the first evidence of abscopal effect after local intratumoral injections of CpG-*STAT3* siRNA which suggests that blocking STAT3 can induce systemic effects even in immunodeficient host, likely through activation of host innate immunity. We also verified CpG-*STAT3* siRNA efficacy in Ras/Myc oncogene-driven and STAT3-dependent mouse prostate tumors (RM1-9) which are strongly infiltrated by G-MDSCs (CD11b^{+}Ly6G^{+}) (Figure 4C).[16] These studies confirmed that local delivery of mouse-specific CpG-*STAT3* siRNA effectively inhibits growth of prostate tumors *in vivo* which results from two-pronged effect of blocking STAT3 in cancer cells and in tumor-associated immune cells (Figure 5).

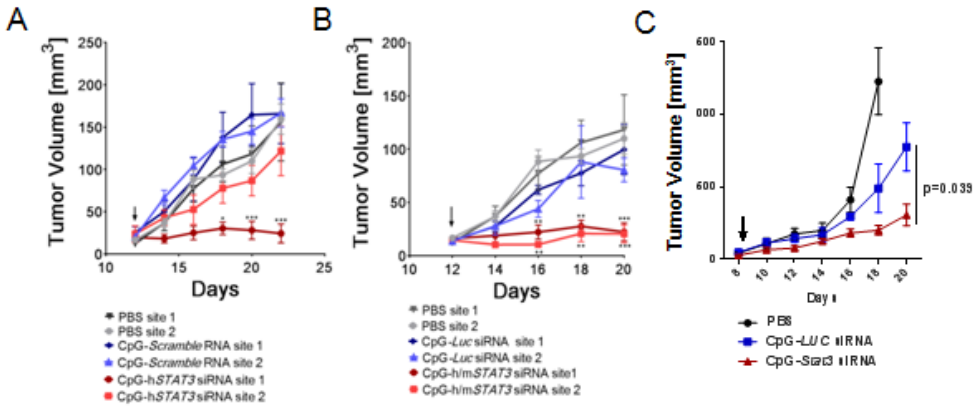

Figure 4. Local treatment using CpG-*STAT3*siRNA abrogates growth of xenotransplanted and syngeneic prostate cancers. (A, B) Two variants of CpG-*STAT3*siRNA, human-specific or human/mouse-specific inhibit growth of xenotransplanted DU145 tumors. NSG mice were injected using 1x10^{6} prostate cancer cells into two opposite flanks. When tumors were established, mice were injected intratumorally every other day using 5 mg/kg CpG-hSTAT3siRNA (in A) or CpG-h/mSTAT3siRNA (in B) or control non-targeting CpG-Luc siRNA and vehicle (PBS). Only tumors on one side were injected (site 1) while others were untreated (site 2). Shown are means ± SD (n = 6). Statistically significant differences were indicated by asterisks. (C) CpG-h/mSTAT3siRNA inhibits growth of RM9 prostate tumors in immunocompetent mice. C57BL/6 mice were challenged using 1x10^{5} RM9 mouse prostate cancer cells. After tumors were established, mice were injected intratumorally every other day using 5 mg/kg CpG-h/mSTAT3siRNA, control non-targeting CpG-Luc siRNA or PBS. Shown are means ± SD (n = 6).

Key Research Accomplishments

- CpG(A)-siRNA targeting STAT3 and NF-κB/RELA reduce tumor-initiating potential and viability of TLR9^{+} cancer cells in xenotransplanted prostate tumor models
- STAT3 and NF-κB/RELA co-regulate expression of prostate cancer stem cell-related genes, such as *NKX3.1*, *KLF4* and *COL1A1*
- The percentage of TLR9^{+}/STAT3P^{+} granulocytic MDSCs increases in patients' blood with prostate cancer progression
- CpG(A)-*STAT3* siRNA silences STAT3 and reduces arginase expression in patients' MDSCs, thereby restoring T cell activity
- Local injection of CpG-*STAT3* siRNA results in systemic antitumor effect beyond the treated tumor site.

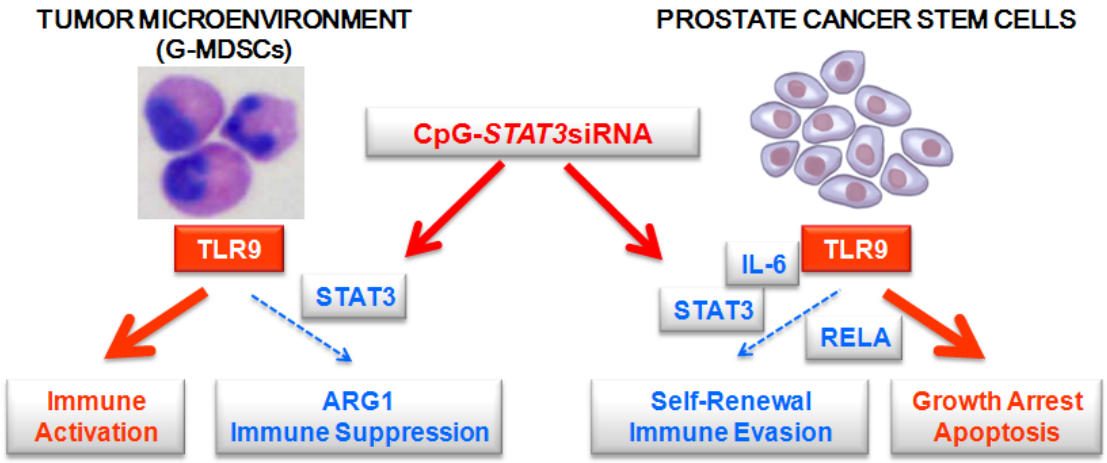

Figure 5. TLR9-targeted STAT3 inhibition allows for two-pronged therapeutic effect against prostate cancers. CpG-STAT3siRNA conjugates target STAT3 signaling in TLR9+ G-MDSCs, an immunosuppressive population of myeloid cells which accumulate during prostate cancer progression from localized to metastatic disease. STAT3 silencing reduces production of a potently immunosuppressive mediator, arginase-1 (ARG1), thereby restoring effector T cell proliferation and activity. As shown in a parallel study, CpG-siRNA strategy allows for delivery of therapeutic siRNAs to prostate cancer stem cells which express TLR9 and rely on NF-κB/STAT3 signaling for self-renewal and tumor-propagating potential. The combination of breaking immune suppression in the tumor microenvironment and decreasing cancer cell survival is likely to augment the overall therapeutic effect against prostate cancer. **Adapted from our mini-review article in *OncoImmunology* journal (Appendix 4).**[15]

Impact

Prostate cancer remains the most common malignancy in men in the United States[17]. Current chemotherapeutic approaches for CRPCs are plagued by toxic effects to normal tissues and modest antitumor activity as these modalities are by no means curative[18-20]. The emerging immunotherapies using autologous cellular vaccinations or immune checkpoint blockade proved limited by the immunosuppressive tumor microenvironment[21, 22]. CpG-*STAT3* siRNA strategy can overcome the challenges in therapy of high-risk or metastatic prostate cancers by disrupting the cross talk between cancer cells and tumor-associated immune cells and restoring antitumor immunity. There are no direct pharmacological inhibitors of oncogenic and immunosuppressive transcription factors such as STAT3 transcription factor. CpG(A)-siRNA oligonucleotides provide a unique and cell-specific method for targeting STAT3 in both prostate cancer cells and in the tolerogenic myeloid-derived suppressor cells in the tumor-microenvironment. This two-pronged

strategy is paradigm-shifting and highly likely to inspire other combinatorial cancer immunotherapies. Our results, summarized in several published manuscripts, provide a strong rationale for further development of CpG(A)-siRNA strategy for two-pronged CRPC immunotherapy which can lead to the development of a technology platform for broad application in cancer immunotherapy not limited to TLR9-positive malignancies.

References

1. Tam, L. et al. Expression levels of the JAK/STAT pathway in the transition from hormone-sensitive to hormone-refractory prostate cancer. *Br J Cancer* 97, 378-83 (2007).
2. Abdulghani, J. et al. Stat3 promotes metastatic progression of prostate cancer. *Am J Pathol* 172, 1717-28 (2008).
3. Seruga, B., Ocana, A. & Tannock, I.F. Drug resistance in metastatic castration-resistant prostate cancer. *Nat Rev Clin Oncol* 8, 12-23 (2011).
4. Yu, H., Kortylewski, M. & Pardoll, D. Crosstalk between cancer and immune cells: role of STAT3 in the tumour microenvironment. *Nat Rev Immunol* 7, 41-51 (2007).
5. Kortylewski, M. & Yu, H. Role of Stat3 in suppressing anti-tumor immunity. *Curr Opin Immunol* 20, 228-33 (2008).
6. Mora, L.B. et al. Constitutive activation of Stat3 in human prostate tumors and cell lines: direct inhibition of Stat3 signaling induces apoptosis of prostate cancer cells. *Cancer Res* 62, 6659-66 (2002).
7. Lee, S.O. et al. RNA interference targeting Stat3 inhibits growth and induces apoptosis of human prostate cancer cells. *Prostate* 60, 303-9 (2004).
8. Hedvat, M. et al. The JAK2 inhibitor AZD1480 potently blocks Stat3 signaling and oncogenesis in solid tumors. *Cancer Cell* 16, 487-97 (2009).
9. Schroeder, A. et al. Loss of androgen receptor expression promotes a stem-like cell phenotype in prostate cancer through STAT3 signaling. *Cancer Res* 74, 1227-37 (2013).
10. Kortylewski, M. et al. In vivo delivery of siRNA to immune cells by conjugation to a TLR9 agonist enhances antitumor immune responses. *Nat Biotechnol* 27, 925-32 (2009).
11. Zhang, Q. et al. TLR9-mediated siRNA delivery for targeting of normal and malignant human hematopoietic cells in vivo. *Blood* 121, 1304-15 (2013).
12. Hossain, D.M. et al. TLR9-targeted siRNA delivery in vivo. *Methods Mol Biol* 1364, 183-196 (2016).
13. Moreira, D. et al. TLR9 signaling through NF-kappaB/RELA and STAT3 promotes tumor-propagating potential of prostate cancer cells. *Oncotarget* 6, 302-313 (2015).
14. Hossain, D.M. et al. TLR9-Targeted STAT3 Silencing Abrogates Immunosuppressive Activity of Myeloid-Derived Suppressor Cells from Prostate Cancer Patients. *Clin Cancer Res* 21, 283-293 (2015).
15. Pal, S. & Kortylewski, M. Breaking Bad Habits: Targeting MDSCs to Alleviate Immunosuppression in Prostate Cancer. *OncoImmunology* e-pub (2015).
16. Xu, J. et al. CSF1R signaling blockade stanches tumor-infiltrating myeloid cells and improves the efficacy of radiotherapy in prostate cancer. *Cancer Res* 73, 2782-94 (2013).
17. Cancer Facts & Figures 2015. *Atlanta: American Cancer Society* (2015).
18. Tannock, I.F. et al. Docetaxel plus prednisone or mitoxantrone plus prednisone for advanced prostate cancer. *N Engl J Med* 351, 1502-12 (2004).
19. Petrylak, D.P. et al. Docetaxel and estramustine compared with mitoxantrone and prednisone for advanced refractory prostate cancer. *N Engl J Med* 351, 1513-20 (2004).
20. de Bono, J.S. et al. Prednisone plus cabazitaxel or mitoxantrone for metastatic castration-resistant prostate cancer progressing after docetaxel treatment: a randomised open-label trial. *Lancet* 376, 1147-54 (2010).
21. Kantoff, P.W. et al. Sipuleucel-T immunotherapy for castration-resistant prostate cancer. *N Engl J Med* 363, 411-22 (2010).
22. Topalian, S.L. et al. Safety, activity, and immune correlates of anti-PD-1 antibody in cancer. *N Engl J Med* 366, 2443-54 (2012).

Changes/Problems

There were no significant changes to the original experimental plan as outlined in the Statement of Work.

Products

1. Hossain D.M.S., Moreira D., Zhang Q., Nechaev S., Swiderski P., Kortylewski M. TLR9-targeted siRNA delivery in vivo. ***Methods Mol. Biol***., 1364, 183-196, 2016. PMID: 26472451
2. Moreira D.F., Zhang Q., Hossain D.M.S., Nechaev S., Li H., Kowolik C.M., D'Apuzzo M., Forman S., Jones J.O., Pal S.K., Kortylewski M. TLR9 signaling through NF-κB/RELA and STAT3 promotes tumor-propagating potential of prostate cancer cells. ***Oncotarget***, 6, 17302-17313, 2015. PMID: 26046794
3. Hossain D.M.S., Pal S.K., Moreira D.F., Duttagupta P., Zhang Q., Won H., Jones J.O., D'Apuzzo M., Forman S.J., Kortylewski M. TLR9-Targeted STAT3 Silencing Abrogates Immunosuppressive Activity of Myeloid-Derived Suppressor Cells from Prostate Cancer Patients. ***Clin Cancer Res***., 3145, 2015. PMID: 25967142
4. Pal S.K. and Kortylewski M. Breaking Bad Habits: Targeting MDSCs to Alleviate Immunosuppression in Prostate Cancer. ***OncoImmunology***, 2015 (in press; e-pub ahead of print; DOI: *10.1080/2162402X.2015.1078060*)).
5. Moreira D.F., Zhang Q., Hossain D.M.S., Nechaev S., Li H., Kowolik C.M., D'Apuzzo M., Forman S., Jones J.O., Pal S.K., Kortylewski M. Eliminating TLR9+ prostate cancer stem cells in vivo using NF-κB/RELA- or STAT3-targeting CpG-siRNA conjugates (poster presentation). Annual Meeting of the American Society of Gene and Cell Therapy (ASGCT), New Orleans, 2015.
6. Hossain D.M.S., Pal S.K., Moreira D.F., Duttagupta P., Zhang Q., Won H., Jones J.O., D'Apuzzo M., Forman S.J., Kortylewski M. TLR9-Targeted STAT3 Silencing Abrogates Immunosuppressive Activity of Myeloid-Derived Suppressor Cells from Prostate Cancer Patients (poster presentation). Annual Meeting of the American Society of Gene and Cell Therapy (ASGCT), New Orleans, 2015.
7. Hossain D.M.S., Pal. S. K., Moreira D., Forman S., Kortylewski M.: TLR9-Targeted STAT3 Silencing Abrogates Immunosuppressive Activity of Myeloid-Derived Suppressor Cells from Prostate Cancer Patients (abstract and poster presentation). Annual Meeting of the Society for Immunotherapy Cancer (SITC), National Harbor, MD, November 2014.
8. Kortylewski M.: CpG-STAT3 siRNA for Castration-Resistant Prostate Cancer Therapy (oral presentation), Advances in Prostate Cancer Research, AACR-Prostate Cancer Foundation Conference, San Diego, CA, 2014.
9. Moreira D., Zhang Q., Hossain D.M.S., Nechaev S., Li H., Kowolik C.M., D'Apuzzo M., Forman S., Jones J., Pal S. K., M. Kortylewski M: TLR9 signaling through NF-κB and STAT3 promotes tumor-propagating potential of prostate cancer cells; abstract and poster presentation at the Prostate Cancer Foundation Meeting, San Diego, CA, October 2014
10. Kortylewski M.: Immunostimulatory CpG-siRNAs: An Opportunity for Combinatorial Cancer Therapy (oral presentation) the 3rd Symposium on Translational Genomics, NCI/NIH, Bethesda, MD, 2014.
11. Generation of control prostate cancer models (PC3, DU145, RM9) with or without TLR9 expression or with inducible TLR9 to compare effects of CpG-siRNAs on prostate cancer cells and on the tumor microenvironment.

Participants and Other Collaborating Organizations

1. Marcin Kortylewski, Ph.D. (PI), Beckman Research Institute at City of Hope
2. Qifang Zhang, Ph.D. (postdoctoral fellow), Beckman Research Institute at City of Hope
3. Dayson Moreira, Ph.D. (postdoctoral fellow), Beckman Research Institute at City of Hope

Special Reporting Requirements

N/A

Appendices

1. Hossain D.M.S., Moreira D., Zhang Q., Nechaev S., Swiderski P., Kortylewski M. TLR9-targeted siRNA delivery in vivo. ***Methods Mol. Biol***., 1364, 183-196, 2016. PMID: 26472451
2. Moreira D.F., Zhang Q., Hossain D.M.S., Nechaev S., Li H., Kowolik C.M., D'Apuzzo M., Forman S., Jones J.O., Pal S.K., Kortylewski M. TLR9 signaling through NF-κB/RELA and STAT3 promotes tumor-propagating potential of prostate cancer cells. ***Oncotarget***, 6, 17302-17313, 2015. PMID: 26046794
3. Hossain D.M.S., Pal S.K., Moreira D.F., Duttagupta P., Zhang Q., Won H., Jones J.O., D'Apuzzo M., Forman S.J., Kortylewski M. TLR9-Targeted STAT3 Silencing Abrogates Immunosuppressive Activity of Myeloid-Derived Suppressor Cells from Prostate Cancer Patients. ***Clin Cancer Res***., 3145, 2015. PMID: 25967142
4. Pal S.K. and Kortylewski M. Breaking Bad Habits: Targeting MDSCs to Alleviate mmunosuppression in Prostate Cancer. ***OncoImmunology***, 2015
(in press; e-pub ahead of print; DOI: *10.1080/2162402X.2015.1078060*)

Chapter 15

TLR9-Targeted SiRNA Delivery In Vivo

Dewan Md Sakib Hossain, Dayson Moreira, Qifang Zhang, Sergey Nechaev, Piotr Swiderski, and Marcin Kortylewski

Abstract

The SiRNA strategy is a potent and versatile method for modulating expression of any gene in various species for investigational or therapeutic purposes. Clinical translation of SiRNA-based approaches proved challenging, mainly due to the difficulty of targeted SiRNA delivery into cells of interest and the immunogenic side effects of oligonucleotide reagents. However, the intrinsic sensitivity of immune cells to nucleic acids can be utilized for the delivery of SiRNAs designed for the purpose of cancer immunotherapy. We have demonstrated that synthetic ligands for the intracellular receptor TLR9 can serve as targeting moiety for cell-specific delivery of SiRNAs. Chemically synthesized CpG-SiRNA conjugates are quickly internalized by TLR9-positive cells in the absence of transfection reagents, inducing target gene silencing. The CpG-SiRNA strategy allows for effective targeting of TLR9-positive cells in vivo after local or systemic administration of these oligonucleotides into mice.

Key words TLR9, SiRNA, CpG, Cancer, Myeloid cells, Leukemia, Oligonucleotides

1 Introduction

The discovery of RNA interference (RNAi) mediated by small-interfering RNA (SiRNA) created a unique opportunity for targeting almost any disease-related gene for therapeutic purposes [1–3]. The SiRNA-based therapies can overcome the challenges of non-enzymatic proteins, such as transcription factors. Preclinical studies in various disease models, including cancer, demonstrated in vivo efficacy of RNAi in rodents [2] and in nonhuman primates [4]. Recent, first-in-human clinical trial confirmed gene silencing after systemic delivery of SiRNA to cancer patients [5]. Broad application of SiRNAs is still limited by the lack of cell-specific delivery, insufficient intracellular uptake, and cytoplasmic release. The effective target gene silencing usually requires encapsulating SiRNA into chemical formulations that may contribute to toxicities and side effects [1, 2]. Previously, several strategies have been

Kato Shum and John Rossi (eds.), *SiRNA Delivery Methods: Methods and Protocols*, Methods in Molecular Biology, vol. 1364, DOI 10.1007/978-1-4939-3112-5_15,

implemented to enhance targeted cell delivery by conjugating SiRNAs with cholesterol, cationic peptides, cell-specific antibodies, RNA aptamers, or ligands for cell surface receptors [3, 6]. However, many of these strategies result in endosomal entrapment of SiRNAs with limited cytoplasmic release and thereby limited effect on target mRNAs [2].

We have recently developed an original method to deliver therapeutic SiRNAs into specific target cells by targeting endosomal receptor Toll-like receptor 9 (TLR9) [7]. TLR9-positive cells recognize and internalize single-stranded oligodeoxyribonucleotides containing an unmethylated CpG motif (CpG ODN) [8, 9]. The conjugates of CpG ODNs to Dicer substrate SiRNAs (CpG-SiRNAs) [10] are actively internalized by human and mouse TLR9-positive cells, without any transfection reagents [7, 11]. The CpG-SiRNA conjugates interact with Dicer after uptake into early endosomes (EE). Importantly, TLR9 plays essential role in facilitating the release of uncoupled SiRNA from EE and trafficking to RNA-induced silencing complexes (RISC) on the surface of endoplasmic reticulum (ER) [12, 13]. The CpG-SiRNA processing results in efficient target gene silencing in various human and mouse TLR9-positive cells in vivo. These include hematopoietic cells, such as dendritic cells (DCs), macrophages, and B cells, as well as in certain blood cancers, e.g., in acute myeloid leukemia (AML), multiple myeloma, or B cell lymphoma (BCL) [7, 11, 14]. The efficacy studies in mice demonstrated direct and/or immune-mediated antitumor activity of CpG-SiRNAs targeting various tumorigenic factors, including *STAT3, STAT5, RELA/p65, BCL2L1*, or *S1PR1* [11, 15, 16]. Overall, CpG-SiRNA strategy allows for a two-pronged targeting of both cancer cells and immune cells to augment therapeutic effects. In this chapter, we describe methods for the design and application of CpG-SiRNA conjugates to deliver SiRNA into specific target cells in mice, starting from the oligonucleotide synthesis to local/systemic delivery into TLR9-positive cells in vivo. Additionally, we discuss critical troubleshooting points for target cell selection and optimizing gene silencing efficiency of CpG-SiRNA conjugates.

2 Materials

2.1 CpG-siRNA Design and Synthesis

1. The CpG-SiRNA conjugates consist of Dicer substrate SiRNA (25/27mer) [10] linked to the class A CpG/D19 (type A) or CpG1668 (type B) for human- or mouse-optimized versions of the reagent, respectively.
2. The two strands of the CpG-SiRNA are synthesized separately using Akta OligoPilot100 (GE) as follows:
   - SiRNA(SS)—25mer sense strand with or without fluorochrome added to the 3′ end (*see* **Note 1**).

- 5′-NNNNNNNNNNNNNNNNNNNNNdNdN-3′
- N = ribonucleotide; dN = deoxyribonucleotide.
- CpG-SiRNA(AS)—27mer antisense strand.
- *Human version* 5′-GGGGGGGG-linker-3′.
- *Mouse version* 5′-TCCATGACGTTCCTGATGCT-linker-NNNNNNNNNNNNNNNNNNNNNNNNN-3′.
- The linker consists of 5 units of the C3 Spacer (Glen Research, Sterling, VA); underlined are phosphorothioated residues. The second nucleotide from the 3′ end of CpG-SiRNA(AS) strand can be 2′O-methyl-modified to improve stability.

3. Both oligonucleotides are aliquoted and stored as lyophilized pellets of 50 nmol each below –20 °C until use.

2.2 Tissue Digestion

1. 10× Collagenase D stock solution: Determine enzyme activity in Wunsch units and prepare 4000 U Collagenase D per 1 mL of HBSS with calcium and magnesium; before use dilute in HBSS to 1× solution for tissue digestion.
2. 10× DNase I stock solution: Dissolve 10 mg DNase I in 1 mL of HBSS, and before use dilute in HBSS to 1× solution for tissue digestion.
3. 10× ACS buffer: For 1 L, dissolve 89.9 g NH_4Cl, 10.0 g $KHCO_3$, and 370 mg EDTA in milli-Q water, then adjust to pH 7.3, and dilute to 1× buffer solution in water for erythrocyte lysis.
4. Histopaque®-1083 for isolating viable cells from mouse tissues.

2.3 7 M Urea/ Polyacrylamide (PAGE) Gel

1. 10× TBE: For 500 mL, dissolve 54 g Tris base, 27.6 g boric acid, and 10 mL 0.5 M EDTA, pH 8.0 in water, adjust to pH 8.3, and dilute to 1× solution for gel running and staining.
2. 8 M Urea: For 200 mL, dissolve 96.1 g urea in water, and filter the solution.
3. 7 M Urea/20 % acrylamide solution: For 200 mL, dissolve 88.2 g urea in 100 mL of 40 % acrylamide/bis-acrylamide solution (19:1), adjust volume to 200 mL using milli-Q water and filter the solution, *see* Table 1.
4. Ethidium bromide: Use 2 μL of ethidium bromide solution (10 mg/mL) in 25 mL of 1× TBE buffer for gel staining.
5. Double-stranded RNA marker.
6. Nuclease-free water: DNase/RNase-free water.

Table 1
Composition of 7 M urea/15 % PAGE

Reagent	For 10 mL
7 M Urea/20 % acrylamide solution	7.5 mL
8 M Urea	1.5 mL
10× TBE	1 mL
APS (10 %)	80 μL
TEMED	7 μL

2.4 Flow Cytometry Reagents

1. Staining buffer: 1× PBS, 2 % FBS and 0.1 % NaN_3.
2. Antibodies: Fluorescently labeled antibodies specific to surface markers on immune and cancer cells.
3. Fc Block: Anti-CD16/CD32 antibody to block unspecific binding by Fcγ receptors.
4. Viability dye: 7AAD.
5. Flow cytometer: BD Accuri C6.

2.5 Time-Lapse Confocal Microscopy Reagents, Instruments and Software

1. Culture dishes: 35/14 mm #1.5 glass bottom tissue culture dishes.
2. Microscope: cLSM510-Meta inverted confocal microscope (Zeiss, Thornwood, NY).
3. Acquisition software: LSM software v.4.2 SP1 (Zeiss).
4. Post-acquisition analysis software: LSM Image Browser v.4.2.0.121 (Zeiss).

2.6 In Vivo CpG-siRNA Delivery

1. Syringes: 1 mL U-100 insulin syringe with 30G needle to inject CpG-SiRNA conjugates diluted in 1× PBS in vivo.
2. Anesthetic agents: Anesthesia induction chamber including isoflurane and oxygen supply.
3. Mice: For in vivo experiments C57BL/6 and NOD/SCID/IL-2RγKO (NSG) mice were purchased from National Cancer Institute (Frederick, MD) and the Jackson Laboratory (Bar Harbor, ME), respectively.

3 Methods

3.1 Hybridization of CpG-siRNA Conjugates

1. Add 250 μL of DNase/RNase-free water to each of the two 50 nmol aliquots of CpG-SiRNA(AS) and SiRNA(SS), mix well at 37 °C for 5 min, and make sure that both oligonucleotides are completely dissolved.

2. Combine both strands in a new 1.5 mL sterile tube to make 100 μM stock solution of CpG-SiRNA conjugate (use amber tubes for fluorescently labeled reagents).
3. Place the tube at 80 °C for 1 min; promptly transfer to the 37 ° C water bath and incubate for 1 h.
4. Spin down and aliquot hybridized CpG-SiRNA conjugates into desired volumes for long-term storage at −80 °C.

3.2 Oligonucleotide Quality Control on the 7 M Urea/PAGE Gels

1. Assemble the gel plates in the gel casting chamber, prepare 7 M urea/15 % PAGE gel according to Table 1 and pour quickly between gel plates, insert comb, and allow polymerizing for 30 min.
2. Dismount the polymerized gel from casting chamber and assemble into gel apparatus according to manufacturer's instruction.
3. Fill the gel chamber with 1× TBE, carefully remove the comb, wash all wells and pre-run for 30 min.
4. Dilute oligonucleotides to 10 μM, use 2 μL of diluted samples to mix with 0.5 μL of 0.5 M EDTA, pH 8.0 and 3 μL of 2× RNA loading dye, load into the wells together with the RNA marker, and run the gel at 250 V for 1 h.
5. Remove the gel and carefully transfer into a dish containing 1× TBE plus ethidium bromide, stain for 15–20 min, and then examine the gel on the UV transilluminator (Fig. 1) (*see* **Note 2**).

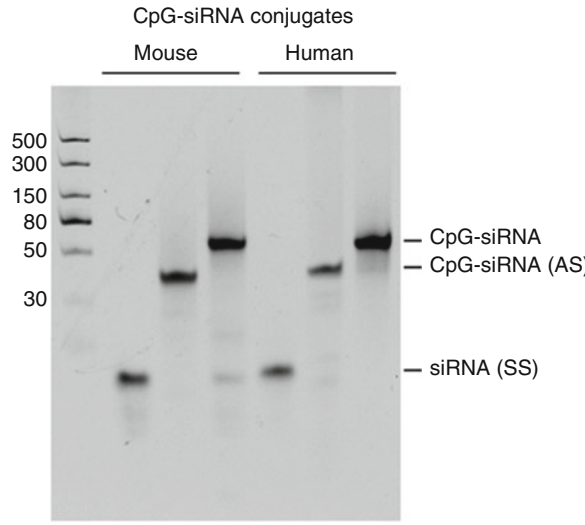

Fig. 1 Quality control for the hybridized CpG-siRNA constructs. Mouse and human versions of siRNA(SS), CpG-siRNA(AS), and CpG-siRNA conjugate were loaded on the 7 M urea/15 % PAGE gel. After electrophoresis gel was stained using ethidium bromide to visualize oligonucleotides compared to a dsRNA marker

3.3 The Cytofluorimetric Assessment of CpG-siRNA Internalization by Target Cells In Vitro

1. Culture the desired number of cells (usually 10^6 cells/mL) in the appropriate medium or, if using freshly isolated primary cells (*see* Subheadings 3.7–3.9), allow cells to adjust to the in vitro culture condition for 2–4 h (*see* **Note 3**).
2. Treat cells with various doses (10–500 nM) of fluorescently labeled CpG-SiRNA constructs, then collect cells at desired times to verify cellular uptake.
3. Collect cells, resuspend each sample in 100 μL of the staining buffer, add 1 μL of the Fc Block for 10 min, then stain cells with a combination of fluorescently labeled antibodies specific to immune cell markers for 20–30 min on ice, wash once with 2 ml of the staining buffer, and resuspend in the staining buffer plus 7AAD for exclusion of dead cells for the analysis using flow cytometry (Fig. 2a, b) (*see* **Note 4**).

3.4 Time-Lapse Confocal Microscopy to Verify Internalization of CpG-siRNA In Vitro

1. Plate and culture cells overnight at a desired density (usually 10^5 cells/well) in the appropriate medium using the 35/14 mm #1.5 glass-bottom tissue culture dishes.
2. Next day, wash cells twice in phenol red-free cell culture medium, then replace it with complete culture medium, and add fluorescently labeled CpG-SiRNA at 100–500 nM concentration.
3. Transfer culture dishes to the microscope chamber with environmental control (37 °C at 5 % CO_2), and incubate for desired times (0.25–48 h).
4. Acquire images at various time increments using cLSM510-Meta inverted confocal microscope, C-Apochromat 40×/1.2 water-immersed objective and LSM software v.4.2 SP1 (Zeiss).
5. Use LSM Image Browser v.4.2.0.121 for post-acquisition analysis (Zeiss) (Fig. 3) (*see* **Note 5**).

3.5 Local Peritumoral Delivery of CpG-siRNA to Target Cell Populations In Vivo

1. Prepare 7–10-week-old mice (C57BL/6 or NSG for syngeneic or xenotransplanted tumor models, respectively).
2. Inject tumor cells suspended in sterile PBS (usually $0.1–1 \times 10^6$ cells/100 μL) to generate subcutaneous (SC) tumor model.
3. After tumor size exceeds ~5 mm in diameter, prepare for injections of CpG-SiRNA.
4. Prepare solution of fluorescently-labeled CpG-SiRNA (e.g., CpG-SiRNA^{Cy3}) at 1–5 mg/kg (20–100 μg) in 100 μL of sterile PBS.
5. Use insulin syringe with 30G injection needle laid parallel to the skin and inserted flatly onto the tumor.

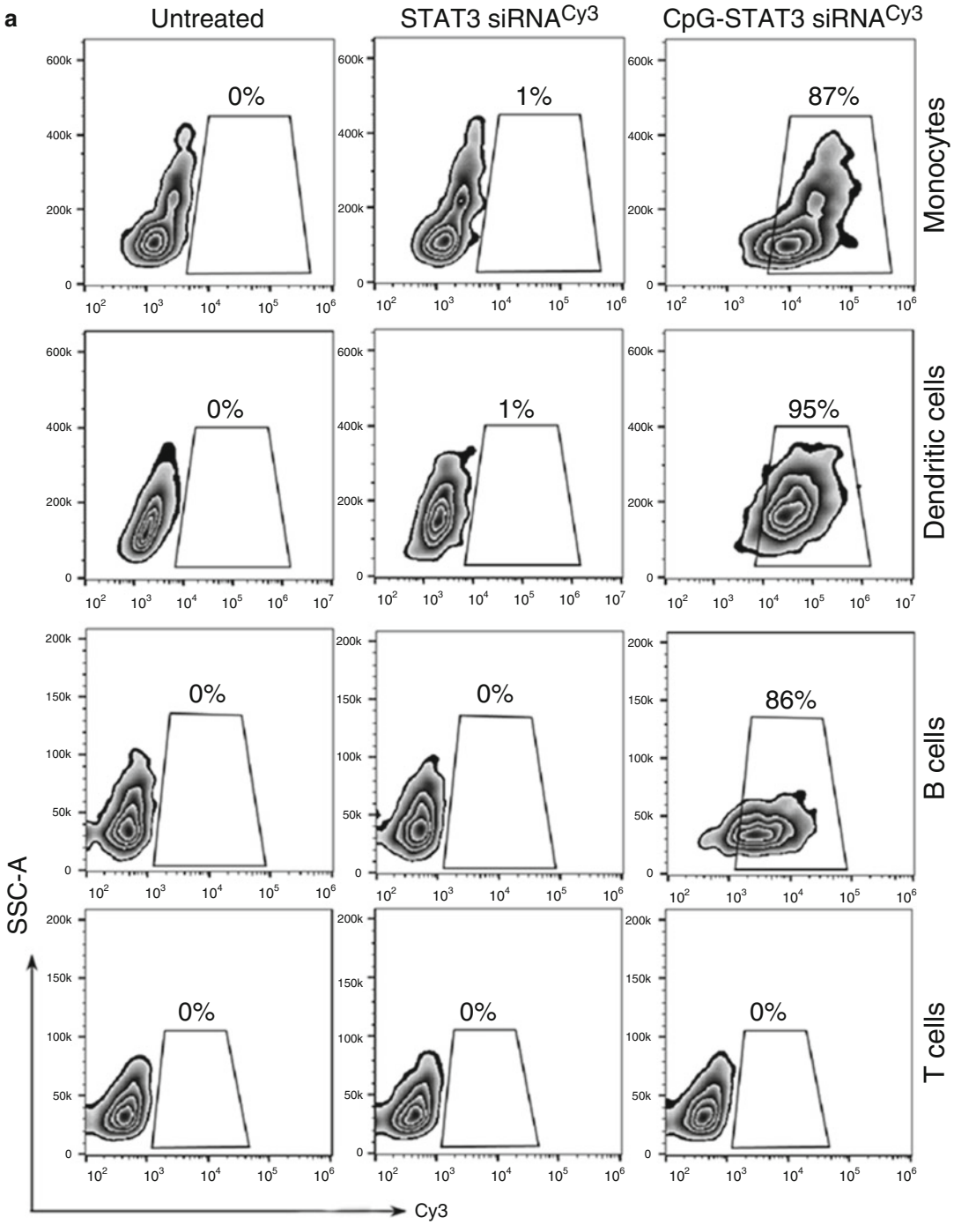

Fig. 2 Human immune and leukemic cells efficiently internalize CpG-siRNA conjugates in vitro. (**a**) Targeted delivery of CpG-*STAT3* siRNA into different primary human immune cells in vitro. Human PBMCs were incubated with fluorescently labeled CpG(A)-*STAT3* siRNA^{Cy3} or unconjugated *STAT3* siRNA^{Cy3} at 500 nM concentration for 1 h without any transfection reagents. Percentages of Cy3$^+$ monocytes (CD14$^+$), plasmacytoid dendritic cells (BDCA2$^+$), B cells (CD19$^+$), and T cells (CD3$^+$) were assessed by flow cytometry. (**b**) CpG-siRNA internalization by human MM (KMS.11) and AML (MV4-11, KG1a) cells. Cells were incubated with 500 nM Cy3-labeled CpG-*STAT3* siRNA for 1 h. The percentage of Cy3$^+$ leukemic cells was analyzed by flow cytometry

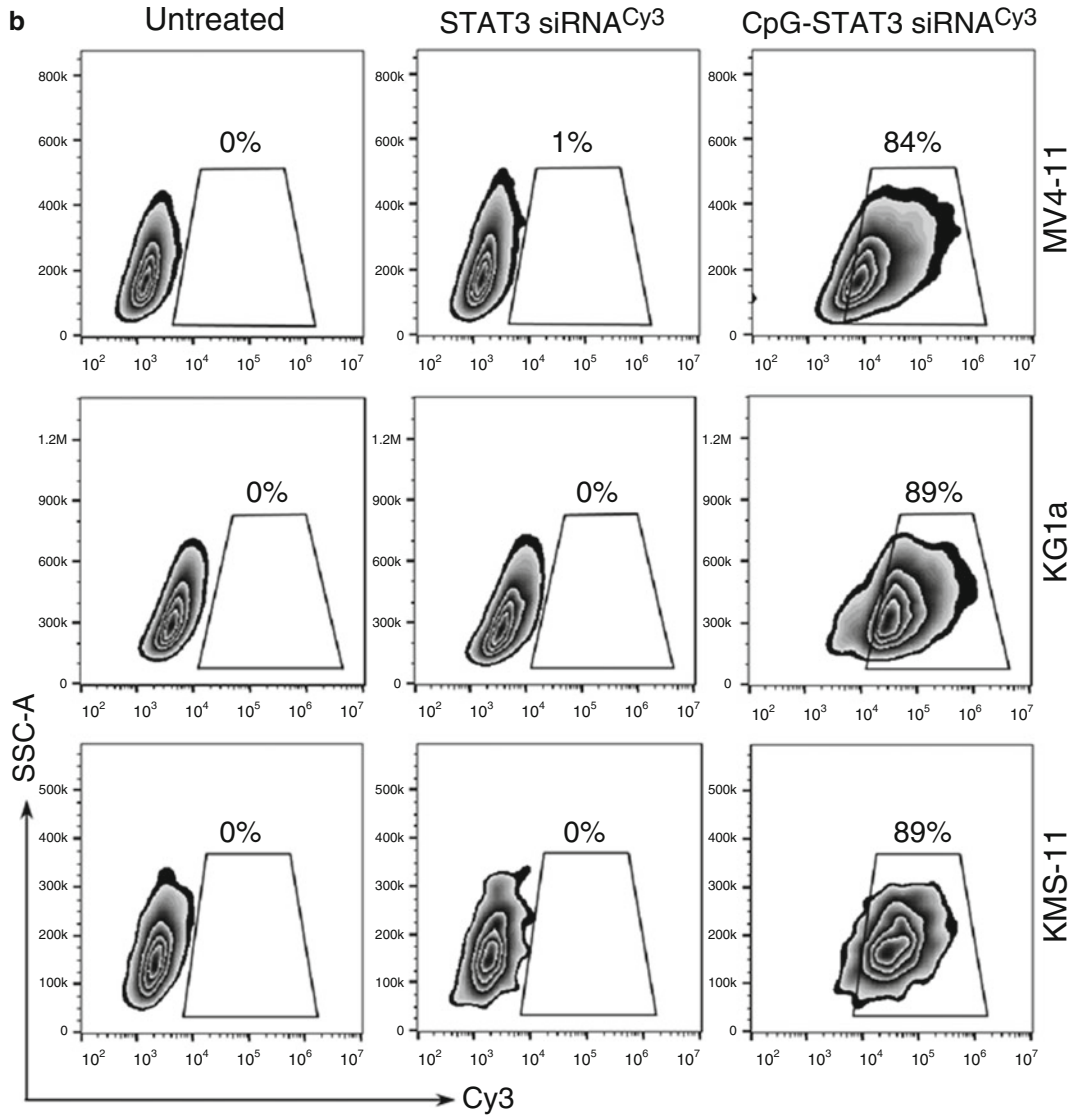

Fig. 2 (continued)

6. Slowly inject CpG-SiRNA solution in four different locations (~25 μL/location) without completely withdrawing the needle to reach maximum area without puncturing skin on the opposite side (*see* **Note 6**).
7. After the appropriate time (usually 1–24 h), euthanize mice, harvest tumors, tumor-draining, and peripheral lymph nodes, and prepare single-cell suspensions as described in Subheading 3.7 followed by the flow cytometric analysis of the oligonucleotide internalization as in Subheading 3.3.

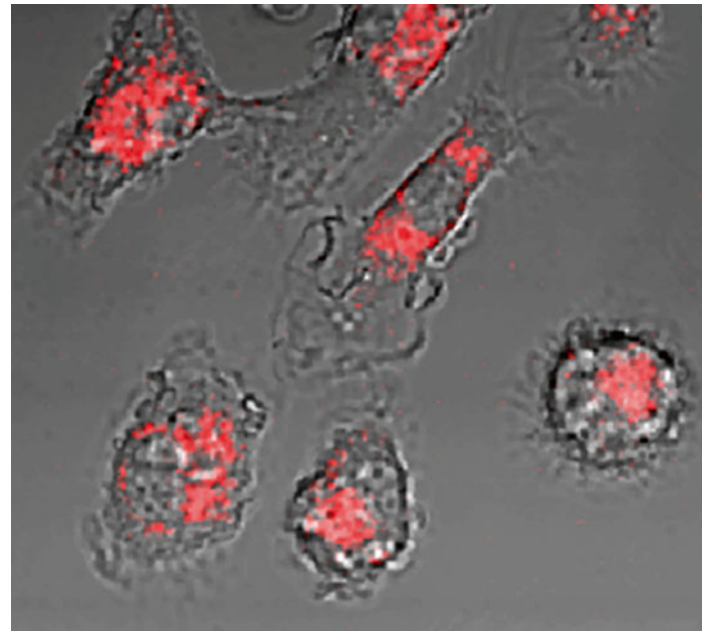

Fig. 3 Intracellular localization of CpG-siRNA after in vitro uptake. Representative images from time-lapse confocal microscopy of cultured primary bone-marrow derived macrophages incubated in the presence of 500 nM CpG-siRNA^{Cy3} for 0.5 h

3.6 Systemic Delivery of CpG-siRNA to Target Cell Populations In Vivo

1. Prepare 7–10-week-old mice (C57BL/6 or NSG for syngeneic or xenotransplanted tumor models, respectively) and anesthetize using isoflurane inhalation.
2. Prepare solution of fluorescently labeled CpG-SiRNA (e.g., CpG-SiRNA^{Cy3}) at 1–5 mg/kg in 200 μL of sterile PBS.
3. Position the anesthetized mouse on its side, use index finger and thumb to draw back skin of above and below the eye then carefully insert the 30G needle at ~45° angle at the corner of the eye, lateral to the medial canthus.
4. Slowly inject the CpG-SiRNA solution into the retrobulbar sinus then remove needle gently and apply ointment to reduce strain (*see* **Note 7**).
5. After the desired time (usually 1–24 h) euthanize mice, collect blood and harvest various organs (e.g., liver, spleen, kidney, bone marrow) to evaluate biodistribution of the fluorescently labeled oligonucleotides using as described in Subheadings 3.3, 3.7 and 3.8 (Fig. 4) (*see* **Notes 8** and **9**).

3.7 Isolation of Cells from Soft Tissues and Tumors

1. Transfer harvested tissues into Petri dishes and wash twice with HBSS.
2. Add 5–10 mL of 1× Collagenase D (400 U/mL) and 1× DNase I (1 mg/mL) and mince tissues into small cubes (~1–2 mm in diameter) using surgical scissors, and incubate for 30 min/37 °C.

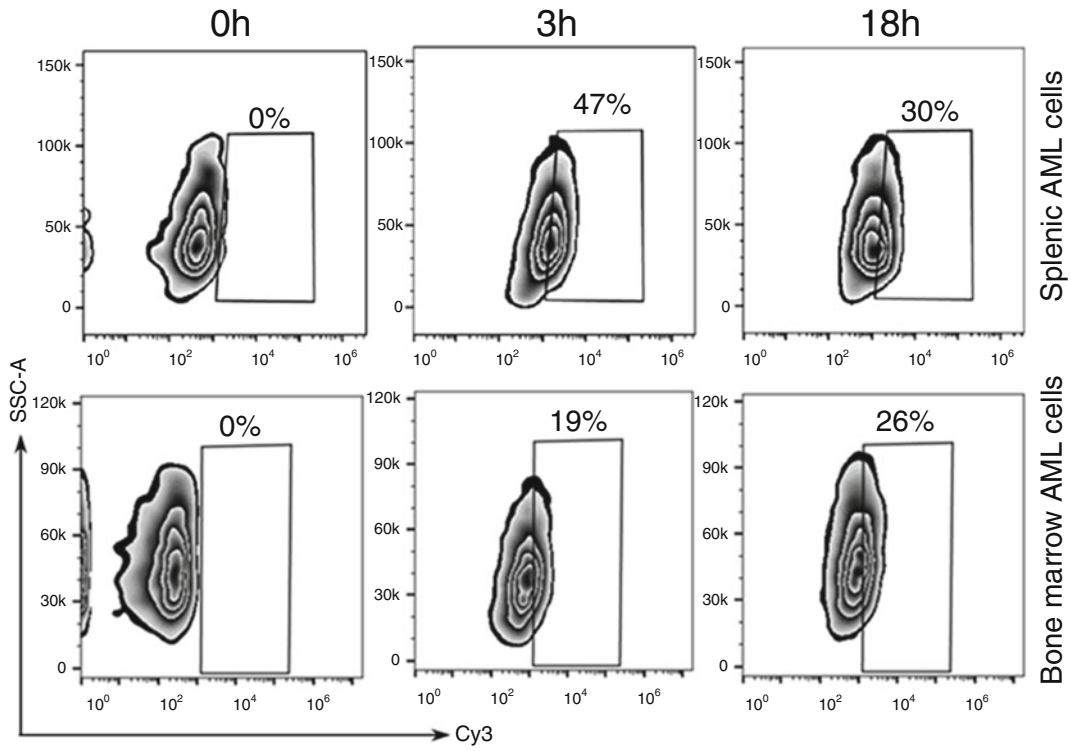

Fig. 4 CpG-*Stat3* siRNA is efficiently internalized by AML cells in vivo. C57BL/6 mice bearing *Cbfb-MYH11/Mpl+* AML were injected with a single dose of CpG-*Stat3* siRNA^{Cy3} (5 mg/kg). Uptake of fluorescently labeled siRNA was assessed using flow cytometry in AML cells isolated from spleen and bone marrow 3 or 18 h after injection

3. Add 10 mM EDTA (tissue culture grade) to stop enzymatic reaction and then pipette up and down to disperse tissues into single-cell suspension.
4. Filter cell suspensions through 70 μm cell strainers into 50 mL tubes, adjust volume to 20–30 mL with HBSS without calcium and magnesium and spin down at 500 × *g*/5 min/18 °C.
5. To lyse erythrocytes, add 5 mL of 1× ACS buffer to the cell pellet, resuspend, and incubate for 3 min/RT.
6. Add 25 mL HBSS without calcium and magnesium to stop the lysis, spin down, and resuspend cells into 10 mL HBSS without calcium and magnesium. To isolate viable cells, pipet 10 mL of cell suspension into 50 mL tube then carefully underlay with 5 mL of Histopaque®-1083 equilibrated to RT and centrifuge tubes at 400 × *g*/30 min/18 °C.
7. Collect viable cells from the interphase without touching the pellet, resuspend in HBSS without calcium and magnesium, spin down again, and then resuspend again for cell counting (Fig. 5) (*see* **Note 10**).

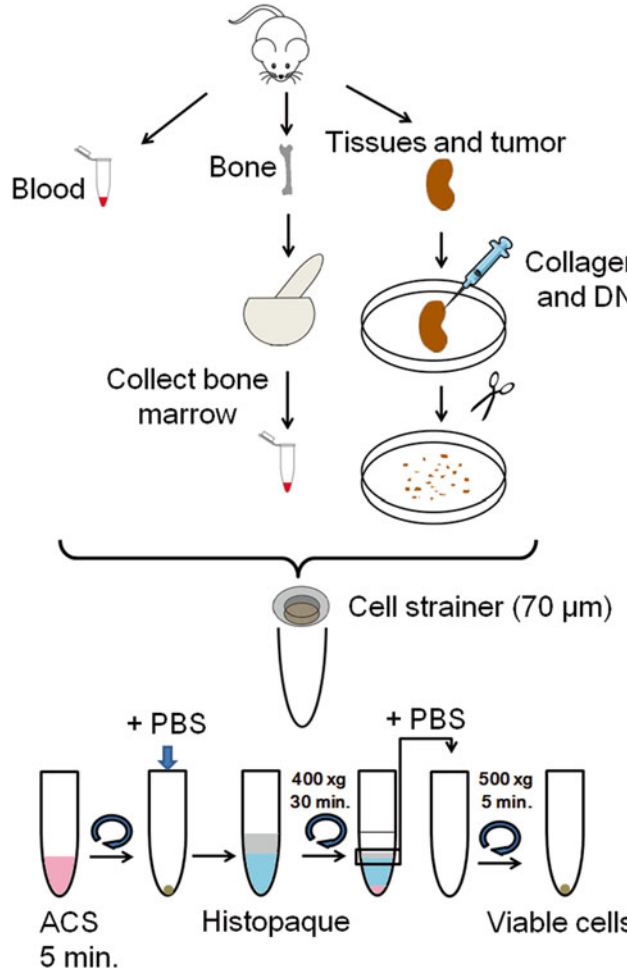

Fig. 5 Schematic of blood, bone, and soft tissue processing to assess organ and cellular biodistribution of CpG-siRNA conjugates

3.8 Isolation of Cells from the Bone Marrow

1. Euthanize mice, remove tibia and femur and place them in tubes with PBS.
2. Cleanly remove rests of muscles from bones, place them in a mortar and add 5 mL of PBS/3 % FBS, crush all bones using pestle for 1–2 min, and rinse with 1 mL of PBS/3 % FBS.
3. Aspirate the cell suspension up and down using 5 mL pipette, and then filter the content of the mortar through a 70 µm strainer into 50 mL tube and spin down at 500 × *g* for 5 min.
4. To lyse erythrocytes, add 5 mL of 1× ACS buffer to the cell pellet, resuspend, and incubate for 3 min/RT.
5. Add 25 mL PBS then spin down and re-suspend cells into 10 mL PBS.

6. To isolate viable cells, pipet 10 mL of cell suspension into 50 mL tube, then carefully underlay with 5 mL of Histopaque®-1083 equilibrated to RT, and centrifuge tubes at 400 × *g*/30 min/18 °C.
7. Collect viable cells from the interphase without touching the pellet, resuspend in HBSS without calcium and magnesium, spin down, and resuspend the cell pellet again for cell counting (Fig. 5).

3.9 Processing of Blood Cells

1. Transfer collected blood into 15 mL tube containing 3–4 mL ACS buffer to lyse blood cells.
2. Incubate for 5–10 min at RT and spin down 500 × *g* for 5 min.
3. Wash cell pellet twice with PBS.
4. Count cell number and proceed to next experiment (Fig. 5).

4 Notes

1. The choice of fluorochrome and its position in the conjugate depends on the application. For uptake and biodistribution studies, it is best to label 3′ end of the SiRNA(SS) to prevent interference with the intracellular processing of the conjugate. For in vivo applications, more intensive fluorochromes are preferred, e.g., Cy3 or Alexa 488 rather than fluorescein.
2. Differences in concentrations or formation of secondary structures between CpG part of the molecule and the SiRNA(AS) could potentially interfere with proper hybridization of both oligonucleotides. Therefore, it is important to confirm the quality and the proper formation of hybridized duplex using gel electrophoresis.
3. For selection of optimal target cells, it is critical to confirm TLR9 expression. Cells lacking TLR9 internalize CpG-SiRNA but endosomal retention of the SiRNA is likely to prevent gene silencing effect [12].
4. Majority of TLR9-positive immune cells and malignant cells, such as leukemia and lymphoma, internalize the conjugate within 1–4 h at concentrations from 100 to 500 nM. Higher concentrations of the CpG-SiRNA usually do not improve uptake any further.
5. The purpose of testing conjugate uptake using confocal microscopy is to confirm that SiRNA is present intracellularly rather than associated with target cell surface. The exact localization of the construct cannot be distinguished by standard flow cytometry.

6. For peritumoral injections, it is important not to withdraw needle completely and to avoid additional puncturing of the skin which can result in leakage of the reagent. It is also advisable to hold the needle in position for few seconds after injecting the total 100 μL to allow for penetration of the solution deeper into tissues to minimize potential reflux.
7. In case of retroorbital injections, mice should not receive more than single injection per day. Additional injections are possible only when using alternate eyes with 1–2 days in between.
8. Efficient in vivo delivery of the SiRNA to target cells depends on their ability to quickly internalize CpG-SiRNA (within 0.5–1 h). The best results are usually achieved targeting normal and malignant myeloid cells in vitro and in vivo.
9. Conjugate degradation by serum nucleases as well as rapid kidney clearance limits CpG-SiRNA half-life in mouse circulation. Chemical modification of the oligonucleotide backbone and the conjugation of CpG-SiRNA to polyethylene glycol (PEG) can improve the pharmacokinetic profile of these conjugates.
10. To induce target gene silencing in vivo, mice should be treated using CpG-SiRNA conjugates for at least 2 days using daily injections of the reagent.

Acknowledgments

This work was supported by the Department of Defense grant number W81XWH-12-1-0132, Prostate Cancer Foundation, STOP CANCER Allison Tovo-Dwyer Memorial Career Development Award and by the National Cancer Institute of the National Institutes of Health under grant numbers R01CA155367 (to M.K.). The content is solely the responsibility of the authors and does not necessarily represent the official views of the NIH.

References

1. Snead NM, Rossi JJ (2012) RNA interference trigger variants: getting the most out of RNA for RNA interference-based therapeutics. Nucleic Acid Ther 22:139–146
2. Rettig GR, Behlke MA (2012) Progress toward in vivo use of siRNAs-II. Mol Ther 20:483–512
3. Davidson BL, McCray PB Jr (2011) Current prospects for RNA interference-based therapies. Nat Rev Genet 12:329–340
4. Zimmermann TS, Lee AC, Akinc A, Bramlage B, Bumcrot D, Fedoruk MN, Harborth J, Heyes JA, Jeffs LB, John M, Judge AD, Lam K, McClintock K, Nechev LV, Palmer LR, Racie T, Rohl I, Seiffert S, Shanmugam S, Sood V, Soutschek J, Toudjarska I, Wheat AJ, Yaworski E, Zedalis W, Koteliansky V, Manoharan M, Vornlocher HP, MacLachlan I (2006) RNAi-mediated gene silencing in non-human primates. Nature 441:111–114
5. Davis ME, Zuckerman JE, Choi CH, Seligson D, Tolcher A, Alabi CA, Yen Y, Heidel JD, Ribas A (2010) Evidence of RNAi in humans from systemically administered siRNA via targeted nanoparticles. Nature 464:1067–1070

6. Whitehead KA, Langer R, Anderson DG (2009) Knocking down barriers: advances in siRNA delivery. Nat Rev Drug Discov 8:129–138
7. Kortylewski M, Swiderski P, Herrmann A, Wang L, Kowolik C, Kujawski M, Lee H, Scuto A, Liu Y, Yang C, Deng J, Soifer HS, Raubitschek A, Forman S, Rossi JJ, Pardoll DM, Jove R, Yu H (2009) In vivo delivery of siRNA to immune cells by conjugation to a TLR9 agonist enhances antitumor immune responses. Nat Biotechnol 27:925–932
8. Krieg AM (2012) CpG still rocks! Update on an accidental drug. Nucleic Acid Ther 22:77–89
9. Kawai T, Akira S (2010) The role of pattern-recognition receptors in innate immunity: update on Toll-like receptors. Nat Immunol 11:373–384
10. Amarzguioui M, Lundberg P, Cantin E, Hagstrom J, Behlke MA, Rossi JJ (2006) Rational design and in vitro and in vivo delivery of Dicer substrate siRNA. Nat Protoc 1:508–517
11. Zhang Q, Hossain DM, Nechaev S, Kozlowska A, Zhang W, Liu Y, Kowolik CM, Swiderski P, Rossi JJ, Forman S, Pal S, Bhatia R, Raubitschek A, Yu H, Kortylewski M (2013) TLR9-mediated siRNA delivery for targeting of normal and malignant human hematopoietic cells in vivo. Blood 121:1304–1315
12. Nechaev S, Gao C, Moreira D, Swiderski P, Jozwiak A, Kowolik CM, Zhou J, Armstrong B, Raubitschek A, Rossi JJ, Kortylewski M (2013) Intracellular processing of immunostimulatory CpG-siRNA: toll-like receptor 9 facilitates siRNA dicing and endosomal escape. J Control Release 170:307–315
13. Stalder L, Heusermann W, Sokol L, Trojer D, Wirz J, Hean J, Fritzsche A, Aeschimann F, Pfanzagl V, Basselet P, Weiler J, Hintersteiner M, Morrissey DV, Meisner-Kober NC (2013) The rough endoplasmatic reticulum is a central nucleation site of siRNA-mediated RNA silencing. EMBO J 32:1115–1127
14. Hossain DM, Dos Santos C, Zhang Q, Kozlowska A, Liu H, Gao C, Moreira D, Swiderski P, Jozwiak A, Kline J, Forman S, Bhatia R, Kuo YH, Kortylewski M (2014) Leukemia cell-targeted STAT3 silencing and TLR9 triggering generate systemic antitumor immunity. Blood 123:15–25
15. Deng J, Liu Y, Lee H, Herrmann A, Zhang W, Zhang C, Shen S, Priceman SJ, Kujawski M, Pal SK, Raubitschek A, Hoon DS, Forman S, Figlin RA, Liu J, Jove R, Yu H (2012) S1PR1-STAT3 signaling is crucial for myeloid cell colonization at future metastatic sites. Cancer Cell 21:642–654
16. Moreira D, Zhang Q, Hossain DM, Nechaev S, Li H, Kowolik CM, D'Apuzzo M, Forman S, Jones J, Pal SK, Kortylewski M (2015) TLR9 signaling through NF-κB/RELA and STAT3 promotes tumor-propagating potential of prostate cancer cells. Oncotarget 6:17302–17313

TLR9 signaling through NF-κB/RELA and STAT3 promotes tumor-propagating potential of prostate cancer cells

Dayson Moreira[1], Qifang Zhang[1], Dewan Md S. Hossain[1], Sergey Nechaev[1,8], Haiqing Li[2], Claudia M. Kowolik[3], Massimo D'Apuzzo[4], Stephen Forman[5], Jeremy Jones[6], Sumanta K. Pal[7], Marcin Kortylewski[1]

[1]Department of Cancer Immunotherapeutics & Tumor Immunology, Beckman Research Institute at City of Hope, Duarte, CA 91010, USA

[2]Bioinformatics Core Facility, Beckman Research Institute at City of Hope, Duarte, CA 91010, USA

[3]Department of Molecular Medicine, Beckman Research Institute at City of Hope, Duarte, CA 91010, USA

[4]Department of Pathology, Beckman Research Institute at City of Hope, Duarte, CA 91010, USA

[5]Department of Hematologic Malignancies, Beckman Research Institute at City of Hope, Duarte, CA 91010, USA

[6]Department of Cell Biology, Beckman Research Institute at City of Hope, Duarte, CA 91010, USA

[7]Department of Medical Oncology, Beckman Research Institute at City of Hope, Duarte, CA 91010, USA

[8]Irell & Manella Graduate School of Biological Sciences, Beckman Research Institute at City of Hope, Duarte, CA 91010, USA

Correspondence to:
Marcin Kortylewski, **e-mail:** mkortylewski@coh.org

Keywords: *TLR9, prostate cancer, RELA, STAT3, tumor-propagating cells*

Received: *April 29, 2015* ***Accepted:*** *May 09, 2015* ***Published:*** *May 22, 2015*

ABSTRACT

Prostate cancer progression was associated with tumorigenic signaling activated by proinflammatory mediators. However, the etiology of these events remains elusive. Here, we demonstrate that triggering of the innate immune receptor, Toll-like Receptor 9 (TLR9), in androgen-independent prostate cancer cells initiates signaling cascade leading to increased tumor growth and progression. Using limited dilution/serial transplantation experiments, we show that TLR9 is essential for prostate cancer cells' potential to propagate and self-renew *in vivo*. Furthermore, low expression or silencing of TLR9 limits the clonogenic potential and mesenchymal stem cell-like properties of LNCaP- and PC3-derived prostate cancer cell variants. Genome-wide transcriptional analysis of prostate cancer cells isolated from xenotransplanted TLR9-positive and -negative tumors revealed a unique gene expression signature, with prominent upregulation of inflammation- and stem cell-related markers. TLR9 signaling orchestrated expression of critical stem cell-related genes such as *NKX3.1, KLF-4, BMI-1* and *COL1A1*, at both mRNA and protein levels. Our further analysis identified that TLR9-induced NF-κB/RELA and STAT3 transcription factors co-regulated *NKX3.1* and *KLF4* gene expression by directly binding to both promoters. Finally, we demonstrated the feasibility of using TLR9-targeted siRNA delivery to block RELA- and STAT3-dependent prostate cancer cell self-renewal *in vivo*. The intratumoral administration of CpG-*RELA*siRNA or CpG-*STAT3*siRNA but not control conjugates inhibited growth of established prostate tumors and reduced clonogenic potential of cancer cells. Overcoming cancer cell self-renewal and tumor-propagating potential by targeted inhibition of TLR9 signaling can provide therapeutic strategy for late-stage prostate cancer patients.

INTRODUCTION

In developed countries, prostate cancer is the second leading cause of male cancer-related deaths with lack of effective therapies for late-stage cancer patients [1]. The initiation, progression and metastasis of prostate cancers is thought to be associated with chronic or recurrent inflammation as underscored by numerous studies and epidemiological evidence [2, 3].

Cellular reactions to infection, tissue stress and injury involve activation of Toll-like receptors (TLRs) in various hematopoietic cells [4]. More recent studies found that TLRs, such as TLR9, are expressed by solid tumors including prostate cancers [5]. Cancer cells can also upregulate TLR9 in response to genotoxic stress caused by irradiation or chemotherapy [6]. Rather than becoming immunogenic, TLR9^{+} prostate cancers are reportedly less differentiated, more aggressive and prone to reoccur [7, 8]. TLR9 recognizes DNA molecules harboring unmethylated CpG motifs, typical for bacterial DNA [4]. Recent studies documented that mitochondrial DNA (mtDNA) released as a result of sterile tissue injury activates TLR9 causing pathologic inflammatory responses [9, 10]. Downstream TLR9 signaling involves NF-κB transcription factor, which regulate expression of proinflammatory and survival mediators [4]. In immune cells, TLR9 signaling is tightly controlled at multiple levels by the signal transducer and activator of transcription 3 (STAT3) [11, 12]. STAT3 is an essential negative feedback inhibitor for TLR9 signaling which is activated by NF-κB-induced cytokines such as IL-6 or IL-10 [9, 13, 14]. Little is known about downstream effects of TLR9 signaling in human cancer cells. However, there is compelling evidence on the role of NF-κB and STAT3 in prostate cancer cell proliferation, survival and androgen-independence. [15–18]

In the current study, we investigated whether inflammatory TLR9 signaling in prostate cancer cells provides a set of molecular targets driving tumor aggressiveness and tumor-propagating potential. These studies provide insights into tumorigenic role of inflammation in advanced prostate tumors.

RESULTS

TLR9 promotes prostate cancer cell engraftment and progression *in vivo*

Previous studies reported expression of the innate immune receptor TLR9 in human prostate cancer cells [5, 7, 8]. We verified these findings by histopathology on 48 primary prostate cancer specimens. Although TLR9 expression showed inter- and intratumoral variation, all samples showed at least low level of cytoplasmic TLR9 (Figure 1A). The staining intensity correlated with increased Gleason grade for the majority of samples (Supplementary Table S1). To assess whether TLR9 contributes to prostate cancer progression, we selected three prostate cancer models: parental LNCaP cells, LNCaP-S17 cells stably expressing IL-6 and PC3-luc cells as representing less or more advanced stages in the progression to androgen-independence, respectively [19]. The TLR9 protein levels were undetectable in LNCaP, low in LNCaP-S17 and high in PC3 cells (Figure 1B, inlays). To study the role of TLR9, we stably transduced the LNCaP and LNCaP-S17 cells using lentiviruses encoding either human *TLR9* cDNA (LNCaP-TLR9^{+} and LN-TLR9^{HI}) or mock vector (LNCaP-TLR9^{-} and LN-TLR9^{LO}); meanwhile the PC3 cells were transduced with either *TLR9* shRNA (PC-TLR9^{LO}) or non-silencing control vector (PC-TLR9^{HI}) (Figure 1B, inlays). In both LNCaP and PC3 cell variants higher levels of TLR9 expression and activation (by CpG ODN stimulation) correlated with increased mRNA and protein levels of IL-6, an important STAT3 activator and a contributor to prostate cancer progression [19]. As expected, these effects were blunted in LNCaP-S17 cells overexpressing IL-6 (Supplementary Figure S1). The *in vitro* proliferation of these cancer cells variants did not significantly change (Supplementary Figure S2AB). To evaluate TLR9 effect on prostate tumor progression, we injected LNCaP, LNCaP-S17 and PC3 cell variants subcutaneously into immunodeficient NSG mice. Both LNCaP-TLR9^{+} and LN-TLR9^{HI} cells formed progressively growing tumors in contrast to poorly tumorigenic LNCaP-TLR9^{-} and LN-TLR9^{LO} cells (Figure 1B, left/middle). Although the PC-TLR9^{LO} tumors became palpable within two weeks, their growth was strongly delayed compared to PC-TLR9^{HI} tumors (Figure 1B, right). Overall, in all tested prostate cancer models, high TLR9 expression correlated with tumor engraftment and growth.

TLR9 increases frequency of prostate cancer stem-like cells with self-renewal properties

Prior studies linked increased tumorigenicity to a population of prostate cancer stem cells which enable serial tumor transplantation [20, 21]. To assess frequency of tumor-propagating cell (TPC) and their self renewal potential in variants of LNCaP-S17 and PC3 cells, we used limited-dilution/clonal tumor-initiation assays [21]. The LN-TLR9^{LO} tumors showed limited and delayed engraftment in NSG mice, thus preventing us from the TPC assessment within the timeframe of our analysis (Figure 1C). In contrast, the TPC frequency in LN-TLR9^{HI} tumors was high and comparable to TPC numbers in the PC-TLR9^{HI} model (Figure 1C, first panel). The silencing of TLR9 in PC-TLR9^{LO} cells resulted in ~200-fold reduction in the TPC frequency (Figure 1C, second panel) which corresponded to the previously

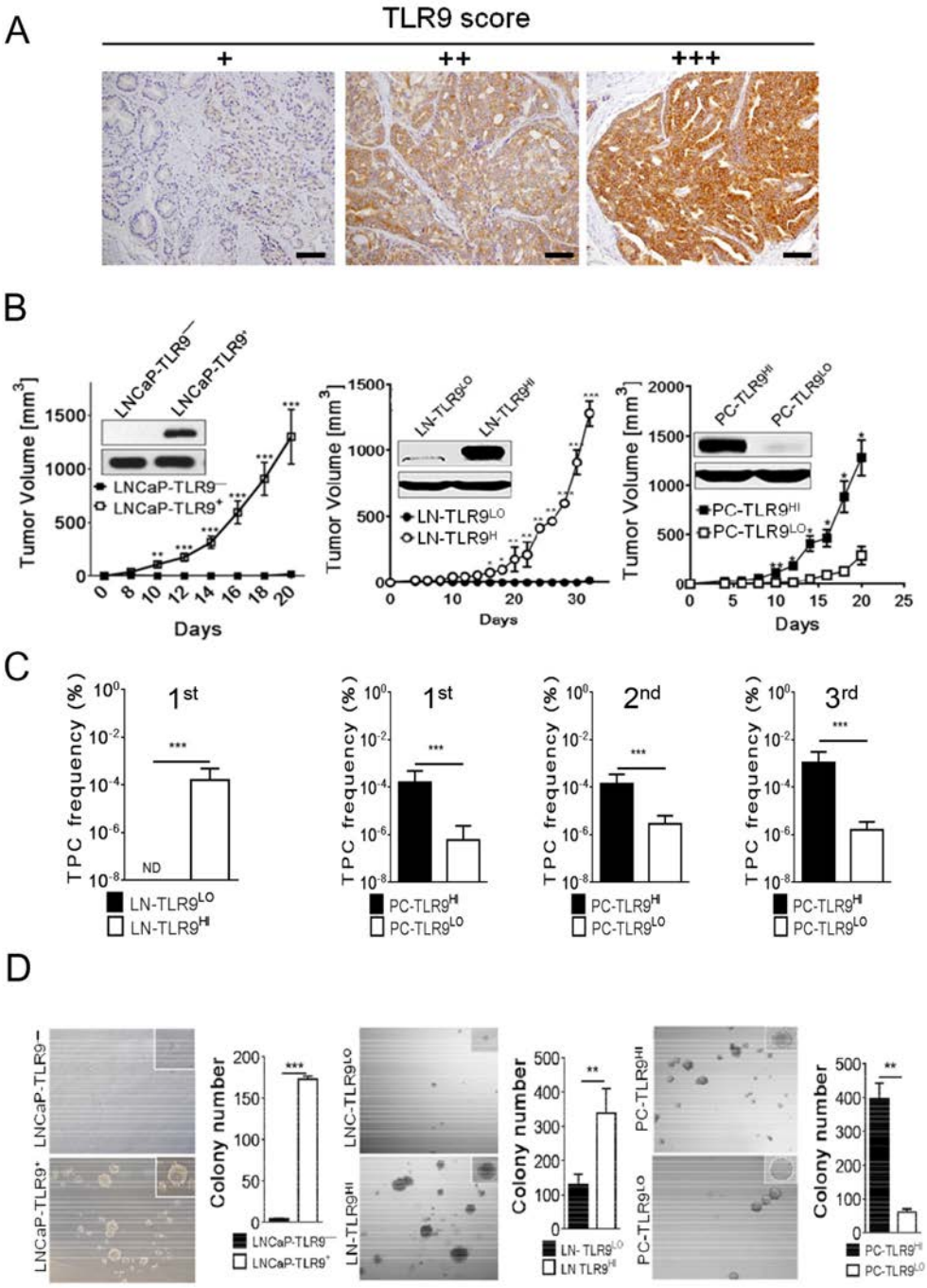

Figure 1: Higher frequency of self-renewing tumor-propagating cells (TPC) in TLR9 + prostate tumors. A. The advanced human prostate cancers express TLR9 as assessed by immunohistochemical staining and pathological evaluation on sections from primary prostate cancers; scale bars = 10 μm. TLR9 levels were assessed within foci of carcinoma representative of the final Gleason score and the cytoplasmic staining was scored as: negative, no staining; +, staining in < 20% of carcinoma cells; ++, weak to moderate staining in > 20% of carcinoma cells; +++, strong/diffuse staining in > 20% of carcinoma cells. **B.** TLR9 expression promotes engraftment and growth of prostate cancer xenotransplants. Human TLR9 was either expressed in LNCaP and LNCaP-S17 cancer cells (with low basal levels of TLR9) or silenced in PC3 cells (with high basal levels of TLR9) using lentiviral systems. The protein levels of TLR9 were assessed using Western blotting; β-actin was used as a loading control (inlays). The immunodeficient NSG mice were injected subcutaneously using 5×10^6 LNCaP- (left panel), LNCaP-S17- (middle panel), or PC3-derived cell variants (right panel). Tumor growth was measured at the indicated times; means ± SEM (n = 5). The results represent three independent experiments. **C.** The primary, secondary and tertiary TPC frequencies were measured in LN-TLR9^{LO} and LN-TLR9^{HI} or in PC-TLR9^{LO} and PC-TLR9^{HI} tumors using limiting dilution analysis *in vivo*; shown are means and 95% CI. **D.** Prostate cancer cells expressing TLR9 have augmented clonogenic potential. Cancer cells freshly isolated from xenotransplanted LNCaP (left), LNCaP-S17 (middle panel) or PC3 (right panel) variants were grown in 3D cultures to form colonies. Shown are the representative images and numbers of spheroid colonies; means ± SEM (n = 5).

observed delayed PC-TLR9^{LO} tumor engraftment (Figure 1B, right). To confirm the enhanced self-renewal properties of PC-TLR9^{HI} cells, we transplanted tumor cells using limited dilution, from primary into secondary and then tertiary recipients (Figure 1C, three right panels). The significant reduction in the TPC frequency was consistent throughout serial transplantations of PC3 variants. Differences in TPC frequencies between prostate cancer variants could reflect changes in putative stem-like/progenitor cell populations [20, 21]. We used standard colony/sphere formation assays to verify whether TLR9 expression affects clonogenic potential of prostate cancer cells. Within 7–14 days, both LNCaP-TLR9^{+} and LN-TLR9^{HI} cells formed prostatospheroids while LNCaP-TLR9^{-} and LN-TLR9^{LO} cells were only loosely clustered (Figure 1D, left/middle). Both variants of PC3 cell created large and regular prostatospheres, however the number of colonies was reduced 8-fold after TLR9 silencing (Figure 1D, right).

Prostate cancer cells often demonstrate bone marrow mesenchymal stem cells' features [22]. Under *in vitro* stimulation both LNCaP and PC3 cancer cells differentiate into either osteoblast- or adipocyte-like cells [22]. Thus, we tested whether upregulation of TLR9 levels will stimulate such properties of prostate cancer cells. Depending on culture conditions, both LN-TLR9^{HI} and PC-TLR9^{HI} cells differentiated into adipocyte- or osteoblast-like cells while prostate cancer cells with low levels of TLR9 failed to differentiate (Supplementary Figure S3). Together with our prior results, these observations support the notion that TLR9 expression in prostate cancer cells promotes tumor-propagating and stem cell-like phenotype, which is likely responsible for enhanced aggressiveness.

TLR9 orchestrates expression of tumorigenic and stem cell-related genes in prostate cancer cells

TLR9 regulates expression of genes critical for function of non-malignant immune cells [4] but the TLR9 downstream gene targets in cancer cells are mostly unknown. We employed whole transcriptome profiling to dissect the TLR9's role in prostate cancer cells (Supplementary Figure S4). Altogether, our results revealed the potential link between TLR9 signaling and gene networks involved in stem cell maintenance and renewal. For validating this prediction, we selected a set of prostate cancer stem cell-specific genes: *BMI-1*, *NKX3.1* and *SOX-4*; mesenchymal stem cell-related *COL1A1*; and critical regulators of pluripotent embryonic stem cells (ESC): *KLF-4*, *SOX-2*, *OCT-4* and *NANOG*. [23–26] The qPCR analysis of total RNA samples isolated from cultured LNCaP-TLR9 variants or *in vivo* grown LN-TLR9^{HI} and LN-TLR9^{LO} tumors showed the significant upregulation of majority of the tested stem cell-related genes after TLR9 expression (Figure 2A, top/middle). Correspondingly, the silencing of TLR9 in PC3 cells (PC-TLR9^{LO}) significantly downregulated of the majority (6/8) of tested genes, except for canonical ESC factors *NANOG* and *OCT4* (Figure 2A, bottom; Supplementary Figure S5A-B). In addition, TLR9 expression correlated with the protein levels of NKX3.1, KLF-4, BMI-1 and COL1A1 in both LNCaP-S17 and PC3 cells (Figure 2B). When seeded in 2D culture at clonal density, PC3 cells form two types of keratinocyte-like colonies: the dispersed paraclones and the regularly-shaped holoclones. The latter type reportedly harbors stem-like cells with self-renewal potential [27]. Our initial studies indicated that TLR9 expression correlated with the number of holoclones formed by LNCaP, LNCaP-S17 and PC3 cell variants (Supplementary Figure S6). Thus, we combined immunofluorescent staining with clonal cell-dilution assays to evaluate TLR9, NKX3.1 and BMI-1 expression in PC3 cell variants. In fact, PC-TLR9^{HI} cell holoclones showed higher than paraclones levels of TLR9 (Figure 2C, top). Furthermore, we observed that BMI-1 and NKX3.1 were expressed exclusively in PC-TLR9^{HI} holoclones (Figure 2C, middle and bottom). These results suggested that TLR9 drives the transcriptional program, which promotes the stem cell-like phenotype in prostate cancer cells.

NF-κB and *STAT3* cooperate to mediate TLR9-induced effects in prostate cancer cells

The IPA analysis of our RNAseq data suggested NF-κB/RELA and STAT3 as top mediators of TLR9-dependent gene expression in prostate cancer cells (Supplementary Figure S5C). To elucidate TLR9-mediated transcriptional regulation, we focused on two key prostate cancer stem cell-related genes: *NKX3.1* and *KLF-4*. The CpG-induced upregulation of *NKX3.1* and *KLF4* was inhibited by the silencing of either *NF-κB/RELA* or *STAT3* in both LNCaP-TLR9^{+} (Figure 3A) and LN-TRL9^{HI} cells (Figure 3B). Next, we used the chromatin immunopreciptation (ChIP) and qPCR assays to test whether TLR9 stimulates binding of NF-κB/RELA and/or STAT3 to *NKx3.1* or *KFL-4* promoter regions in LN-TLR9^{HI} cells. In fact, within an hour after TLR9 activation both NF-κB/RELA and STAT3 were recruited to *NKX3.1* and *KFL-4* promoters (Figure 3C). NF-κB/RELA and STAT3 potentially partner in transcriptional regulation of tumorigenic genes in cancer cells [16]. We used Re-ChIP assays to assess whether these TFs bind to the same DNA regulatory elements in *NKX3.1* and *KFL-4* promoters. The sequential immunoprecipitation using STAT3- and then NF-κB/RELA-specific antibodies yielded promoter regions from both *NKX3.1* and *KLF-4* (Figure 3C). We further evaluated these results using ChIP/Re-ChIP assays in PC3-TLR9^{LO} and PC3-TLR9^{HI} cells. As expected, CpG stimulation induced binding of NF-κB/RELA together with STAT3 to the *NKX3.1* promoter in PC3-TLR9^{HI} but

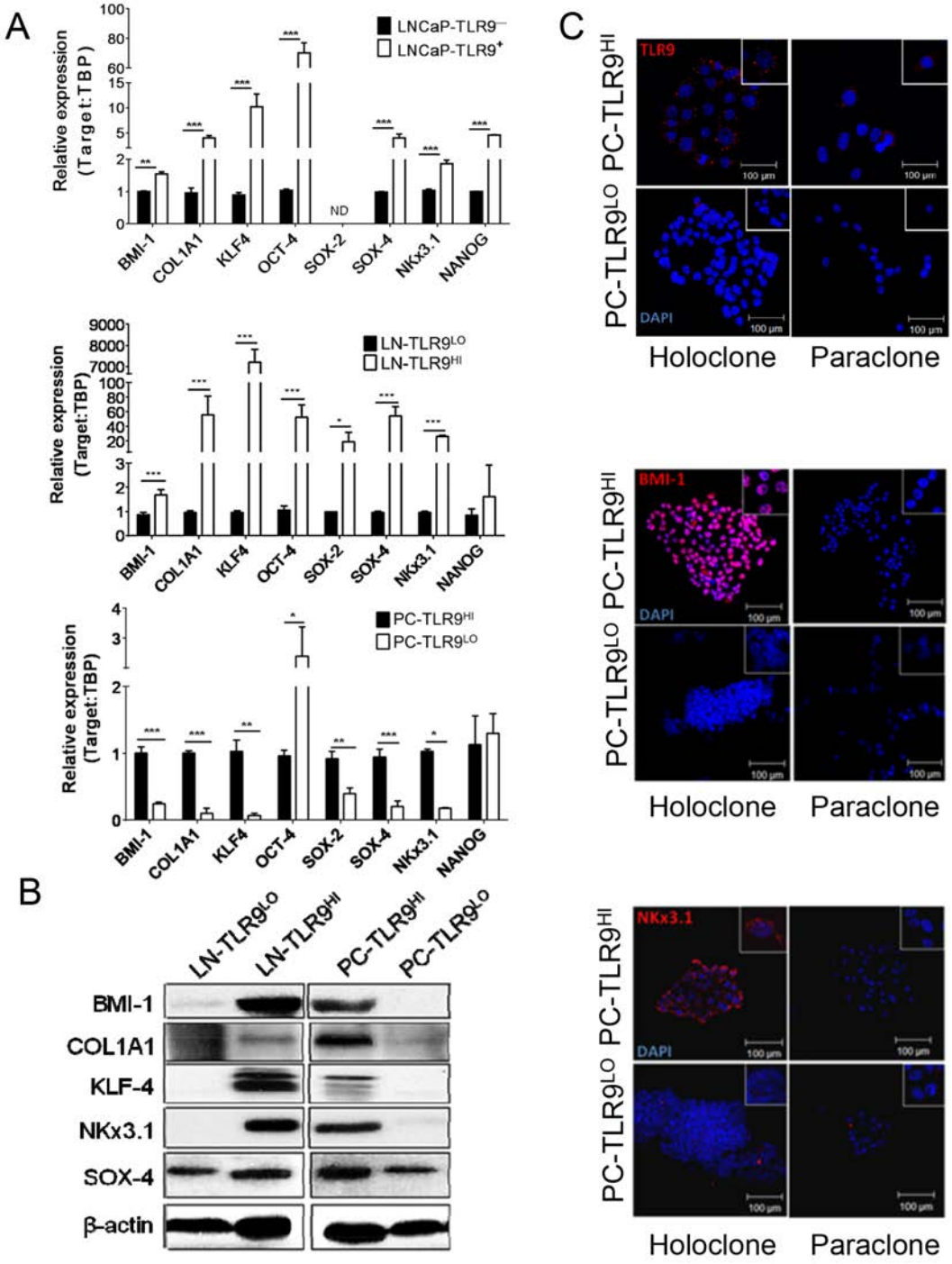

Figure 2: TLR9 orchestrates expression of prostate cancer stem cell-related genes. A. The mRNA expression of *BMI-1, COL1A1, KLF4, OCT-4, SOX-2, SOX-4*, *NKX3.1* and *NANOG* was assessed by qPCR in RNA samples isolated from LNCaP cells (top) or xenotransplanted LNCaP-S17 (middle) and PC3 (bottom) tumor variants; means ± SEM (n = 3). **B.** Protein levels of the selected stem cell-related factors as indicated were assessed using Western blotting; β-actin was used as a loading control. **C.** Intracellular localization of TLR9 (top), BMI-1 (middle) and NKX3.1 (bottom) shown in red with DAPI for staining nuclei (blue) in holo-/paraclones formed by PC-TLR9^{LO} or PC-TLR9^{HI} cells *in vitro* and analyzed using immunofluorescent microscopy; scale bar = 100 µm.

not in PC3-TLR9^{LO} cells (Figure 3D, left). NF-κB/RELA and STAT3 similarly collaborate for the transcriptional regulation of *KLF-4* in PC3-TLR9^{HI} cells (Figure 3D, right). TLR9 silencing reduced STAT3 binding to *KLF-4* promoter, although it did not affect NF-κB/RELA. It is likely that the interaction with STAT3 supports but is not required for NF-κB binding to *KLF-4* promoter. Taken together, our results suggest that NF-κB/RELA and STAT3

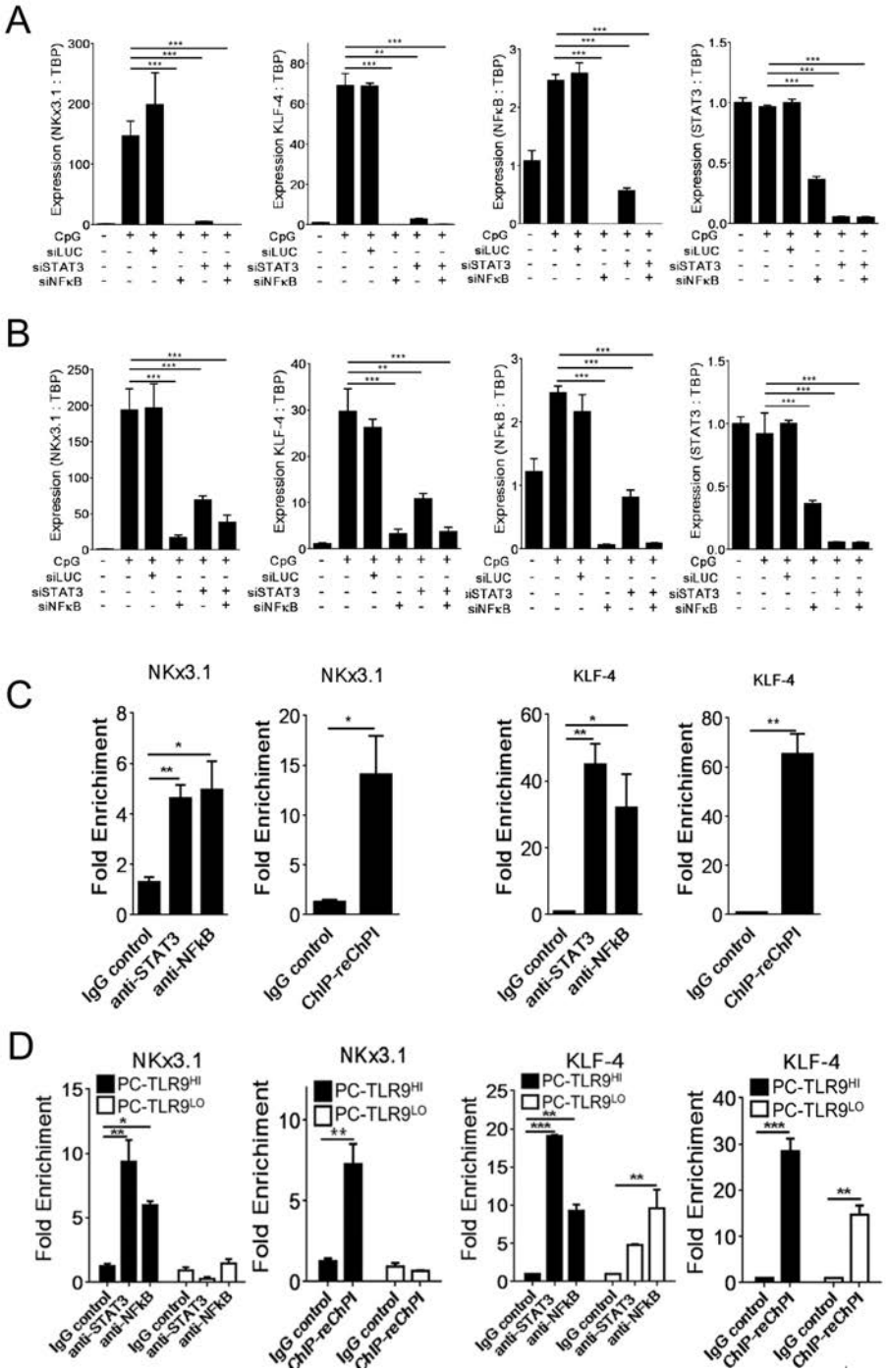

Figure 3: NF-κB and STAT3 co-regulate expression of NKX3.1 and KLF-4 prostate cancer stem cell-related genes downstream from TLR9. A, B. Both NF-κB and STAT3 are required for TLR9-dependent expression of *NKX3.1* and *KLF-4* genes. 10^6 LNCaP-TLR9$^+$ (A) or LN-TLR9^{HI} cells (B) were transfected using Lipofectamine 2000 (Invitrogen) and siRNAs specific to *NF-κB/RELA*, *STAT3* or *Luciferase* as a negative control (40 nm/L). After 24 h, cells were treated using CpG ODN (1 μg/mL) for another 24 h or left untreated. The mRNA levels of *NKX3.1* and *KLF4* as well as *NF-κB/RELA* and *STAT3* for verification of target gene silencing were assessed by qPCR and normalized to *TBP* expression. Shown are results from two independent experiments; means ± SEM. **C.** TLR9 activation in prostate cancer cells induces binding of both NF-κB/RELA and STAT3 to promoters of stem cell-related genes. The LN-TLR9^{HI} cells were stimulated using CpG as above. NF-κB/RELA and STAT3 binding to *NKX3.1* (left two graphs) and *KLF4* (right two graphs) promoters was evaluated using ChIP assays with qPCR analyses. In addition, a portion of the anti-STAT3 immunoprecipitate was subjected to a second round of immunoprecipitation using NF-κB/RELA antibody (re-Chip) as indicated. **D.** TLR9 silencing reduces NF-κB/RELA and STAT3 recruitment to *NKX3.1* and *KLF4* promoters in PC3 cells. ChIP (left) and Re-ChIP assays (right) were performed using PC-TLR9^{LO} and PC-TLR9^{HI} cells treated using CpG ODN for 1 h. *NKX3.1* and *KLF4* promoter-binding activities of NF-κB/RELA and STAT3 were assessed as fold enrichment in two independent experiments; mean ± SEM (n = 4).

cooperate to various extents in orchestrating expression of TLR9-induced prostate cancer stem cell-related genes.

Targeted inhibition of NF-κB and STAT3 signaling in TLR9-positive tumor-propagating cells inhibits growth of human prostate cancers *in vivo*

While targeting stem cell-like cells could overcome therapeutic resistance of late-stage cancers, the task remains challenging [21]. TLR9 expression in prostate cancer propagating cells creates an opportunity to use this receptor as a target for the delivery of therapeutic molecules, such as CpG-siRNA [28]. As we previously demonstrated, siRNAs linked to TLR9 ligands (e.g. CpG ODNs) are internalized by hematopoietic cells, followed by the TLR9-mediated cytoplasmic siRNA release and target gene silencing [28]. We verified that in the absence of any transfection reagents *in vitro*, TLR9-positive PC3-luc and DU145 prostate cancer cells, efficiently internalize CpG-siRNA (Figure 4A and Supplementary Figure S7A). Next, we evaluated the impact of silencing *NF-κB/RELA* or *STAT3* on the growth of PC3-luc and DU145 tumors. The intratumoral injections of CpG-*RELA*siRNA alone, CpG-*STAT3*siRNA alone or combination thereof, but not CpG-scrambled RNA, induced target gene silencing and inhibited growth of PC3 tumors. The observed therapeutic effects were more pronounced for targeting *RELA* rather than *STAT3* or both transcription factors together. In contrast, similar experiments using DU145 tumors showed comparable growth inhibitory effects of both CpG-*RELA*siRNA and CpG-*STAT3*siRNA (Figure 4B, right; Supplementary Figure S7B). These results may reflect various degree of STAT3-dependency in both tumor models as well as less effective silencing of STAT3 compared to RELA in target cells (Figure 3C). Importantly, the colony-forming assays confirmed that intratumoral injections of CpG-*RELA*siRNA and CpG-*STAT3*siRNA reduced clonogenic potential of tumor cells (Figure 4D). Consistently with our earlier studies, we did not observe target gene silencing or any antitumor effects of CpG-*STAT3*siRNA in TLR9-negative tumor xenotransplants in immunodeficient mice (Supplementary Figure S8) [28]. Our ongoing studies using syngeneic prostate cancer models should reveal the complete therapeutic potential of immunostimulatory CpG-siRNAs.

Previous *in vitro* studies suggested that TLR9 promotes prostate cancer cell proliferation and/or invasiveness [7]. However, to our knowledge this is the first report of TLR9′s role in promoting prostate cancer cells' self-renewal and tumor-propagating potential. This is a result of the concerted expression of genes related to cancer stem cell maintenance through NF-κB/RELA and STAT3 as downstream mediators of TLR9 signaling. Finally, we demonstrate the feasibility to use TLR9-mediated siRNA delivery for targeting prostate cancer-propagating cells *in vivo*, thereby halting tumor progression. Targeting of TLR9$^+$ tumor-propagating cells alone or in combination with antiproliferative agents has potential to address an unmet need for treatment of patients with advanced and poorly differentiated prostate cancers.

DISCUSSION

Previous studies reported that prostate cancer cells express innate immune receptors, such as TLR9, normally restricted to the hematopoietic cell lineage [2, 5, 7]. Rather than becoming immunogenic, TLR9$^+$ prostate cancers were less differentiated, more aggressive and prone to reoccur [8, 29]. Our study reconciles these observations as it identifies a novel function of TLR9 signaling in cancer cells and underscores the role of inflammation in prostate cancer progression. We demonstrate for the first time that TLR9 expression promotes tumor-propagating potential of prostate cancer cells *in vivo*. The TLR9$^+$ prostate cancer cells have increased both clonogenic potential and the ability to differentiate into osteoblast- or adipocyte-like cells similarly as bone marrow mesenchymal stem cells. These phenotypic changes are associated with concerted expression of tumorigenic mediators, including a set of genes related to cancer stem cell maintenance and tumor-propagating potential. We identify NF-κB/RELA and STAT3 as two critical downstream mediators of TLR9 signaling. Both NF-κB/RELA and STAT3 coordinate transcription *NKX3.1* and *KLF4* stem cell-related genes. Finally, silencing of *RELA* or *STAT3* specifically in TLR9$^+$ tumor-propagating cells inhibits growth of established prostate cancers *in vivo*.

Our results align with earlier reports demonstrating elevated TLR9 expression in prostate cancers with higher Gleason scores and in the cell lines established from more advanced tumor stages such as PC3 or DU145 [5, 7, 29]. Previous *in vitro* studies suggested that TLR9 activity promotes cancer cell proliferation [30] and/or invasiveness [7]. However, to our knowledge this is the first report of TLR9's role in promoting prostate cancer cells' self-renewal and tumor-propagating potential. Several studies suggested the existence of undifferentiated population of prostate cancer stem cells with self-renewing potential, which enable serial tumor transplantation in immunodeficient mice [20, 21, 31]. Growing evidence also links prostate cancer stem cells to castration resistance and tumor recurrence [20, 32]. We found that TLR9 expression is essential for prostate cancer cells ability to differentiate into adipocytes or osteoblasts [22]. Given the similarity between prostate cancer cells and bone marrow mesenchymal stem cells, TLR9$^+$ tumor-propagating cells may play a role in the metastatic tumor spread to bone. This possibility will be explored in our

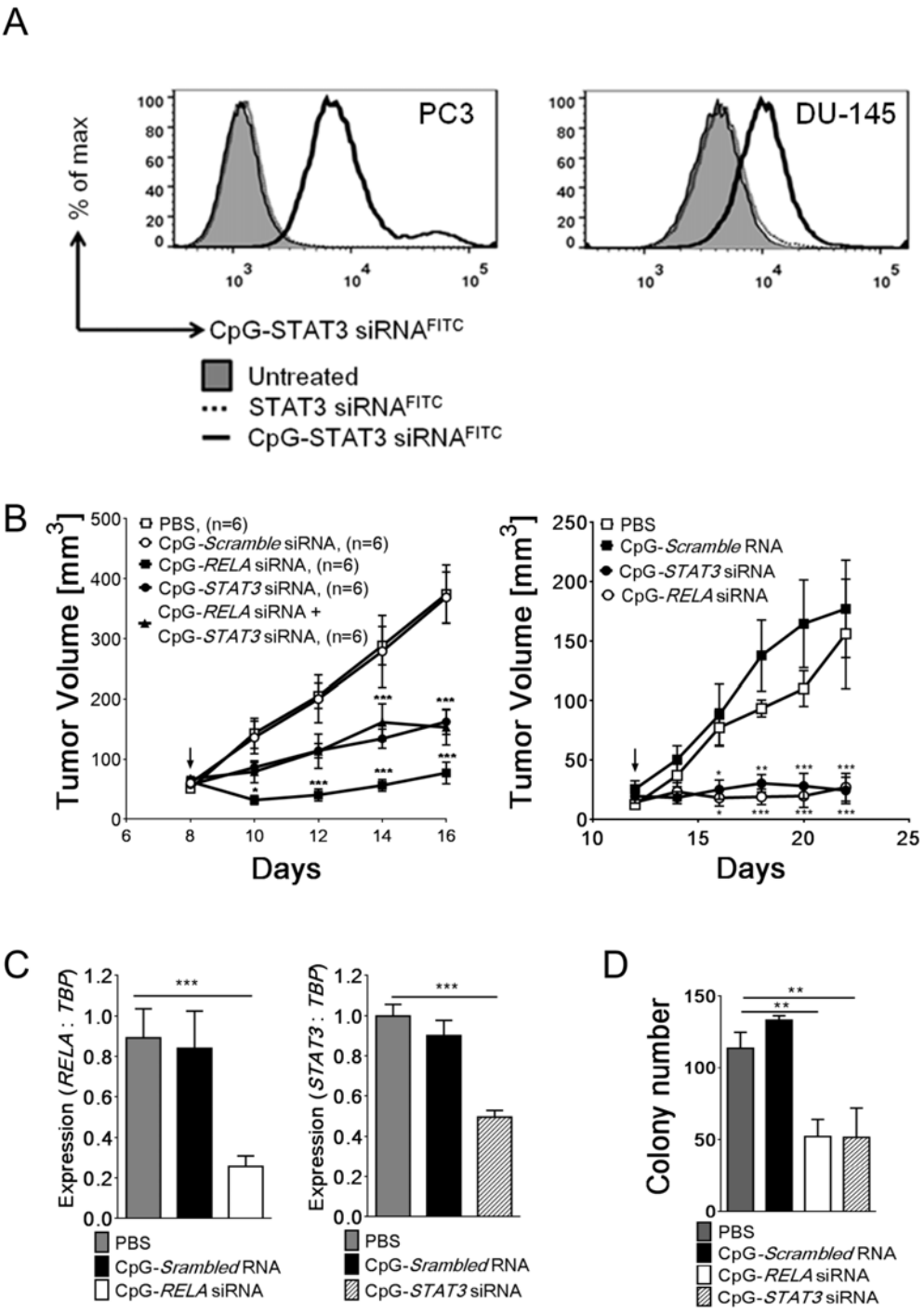

Figure 4: TLR9-targeted silencing of RELA or STAT3 inhibits growth and clonogenic potential of prostate tumors. A. Internalization of naked CpG-siRNA conjugates by PC3-luc and DU145 prostate cancer cells in the absence of transfection reagents. Cells were incubated with fluorescently-labeled CpG-*STAT3*siRNA^{FITC} or unconjugated *STAT3*siRNA^{FITC} (500 nM) for 1 h and the level of uptake was analyzed using flow cytometry. **B.** CpG-mediated silencing of *RELA* and/or *STAT3* inhibits growth of PC3-luc (left) and DU145 (right) prostate tumors in NSG mice. After tumors well established (as shown by arrows), the established PC3-luc tumors were treated using IT injections of the indicated CpG-siRNA conjugates, CpG-scrambled RNA control (5 mg/kg) or PBS every other day while measuring tumor volumes. **C.** The silencing effect of CpG-siRNA conjugates in PC3 cells were verified using qPCR to measure *RELA* (left) and *STAT3* (right) expression levels and normalizing to *TBP* expression; shown are means ± SEM ($n = 6$). **D.** *In vivo* treatments using CpG-*RELA*siRNA or CpG-*STAT3*siRNA reduce clonogenic potential of PC3 prostate cancer cells. Tumor cells isolated from NSG mice treated as indicated were used for colony-forming assays; shown are mean numbers of colonies ± SEM ($n = 5$).

further studies. Noteworthy, recent studies suggested that non-stem cancer cells can dedifferentiate into tumorigenic cells [33]. The notion of stem cell phenotype reversibility find some support in our findings that forced expression or silencing of TLR9 can affect tumor-propagating potential of prostate cancer cells. As recently demonstrated, TLR9 expression in cancer cells is upregulated in response to genotoxic stress caused by irradiation or chemotherapy [6]. Therefore, expansion of cancer stem cell population could result from TLR9-mediated response to environmental conditions, thereby limiting the outcome of cytotoxic tumor therapies. In fact, sterile tissue injury or tumor irradiation can stimulate TLR9 signaling *in vivo* through release of natural TLR9 agonists such as mitochondrial DNA [9, 10, 34].

Downstream TLR9 signaling involves NF-κB activation and indirectly induces STAT3 signaling. [4, 9, 11] In our studies, TLR9 expression upregulated several well known activators of tumorigenic STAT3 signaling in prostate cancer cells, such as EGFR, IL-6 and VEGF [12]. We demonstrate that TLR9/NF-κB/STAT3 signaling axis operates in prostate cancer cells to promote expression of tumorigenic and stem cell-related genes. While both NF-κB and STAT3 are well known mediators of prostate carcinogenesis and progression, their collaboration in promoting prostate cancer-propagating cells has not yet been shown [15, 35]. As suggested by both our transcriptome and protein analyses, the link between TLR9/NF-κB and STAT3 signaling likely relies on IL-6 secretion by cancer cells. IL-6 is known for inducing rapid STAT3 phosphorylation through the IL-6R-associated Janus family kinases (JAKs) [36]. IL-6-mediated activation of STAT3 in human prostate cancers is well documented and related to androgen-independence [17, 37]. As recently suggested, IL-6/STAT3 signaling also promotes stem cell-like phenotype of cancer cells [38]. We cannot exclude the contribution of other signaling pathways to transcriptional activity induced by TLR9. In fact, based on our *in vitro* experiments TLR9-triggered gene expression is sensitive not only to inhibitors of NF-κB and STAT3, but also to Src and PI3K/Akt inhibitors (Moreira unpublished data). Recent reports demonstrated synergism between IL-6/STAT3 and PI3K/Akt or Src pathways in promoting prostate cancer aggressiveness and progression [37, 39]. Our findings underscore the possibility that these signaling pathways converge to orchestrate functionally overlapping set of genes. As shown by this study, TLR9/NF-κB/STAT3 signaling coordinates expression of genes related to differentiation and renewal of normal or cancer stem cells. Several of the identified targets genes are known mediators of prostate cancer cell "stemness" and self-renewal, such as *NKx3.1* [24], *BMI-1* [23], and *SOX-4* [25]; some are also embryonic stem cell (ESC) regulators, such as *KLF4* and *SOX2* [40]. However, TLR9 signaling is not required for expression of the two canonical ESC transcription factors *NANOG* and *OCT4*. This is in contrast to recently shown direct TLR4/NANOG signaling in liver cancer-initiating cells [41], which may indicate diversity of molecular mechanisms regulating stem cell phenotype in various solid tumors.

While targeting stem cell-like cells gained interest as a potential method to overcome therapeutic resistance of late-stage cancers, such task remains challenging [21, 31]. TLR9 expression in prostate cancer cells creates an opportunity to use this receptor as a target for the delivery of therapeutic molecules, such as CpG-siRNA conjugates [42]. Doses and uptake of CpG-siRNA by $TLR9^+$ human prostate cancer cells were comparable to our previous observations in blood cancer models [28]. The proof-of-principle experiments using CpG-siRNAs to target tumorigenic NF-κB/RELA and STAT3 signaling in xenotransplanted $TLR9^+$ prostate tumors confirmed therapeutic efficacy of such strategy. Targeting either of the two tumorigenic transcription factors inhibited tumor growth and reduced clonogenic potential of tumor cells. Overall, our findings suggest that TLR9-mediated siRNA delivery targets prostate cancer-propagating cells, thereby halting tumor progression. Further *in vivo* studies will elucidate effects of inhibiting TLR9-mediated signaling, which should trigger differentiation of cancer-propagating cells into tumor cells with potentially greater sensitivity to standard therapies [43]. Therefore, targeting $TLR9^+$ tumor-propagating cells alone or in combination with expanding panel of antiproliferative agents, can address an unmet need for treatment of patients with advanced and poorly differentiated prostate cancers.

MATERIALS AND METHODS

Pathological analysis

Investigation has been conducted in accordance with the ethical standards and according to the Declaration of Helsinki and according to national and international guidelines and has been approved by the authors' institutional review board. Prostate cancer specimens from patients' samples were acquired from the Biospecimen Repository (COH) with the prior Institutional Review Board approvals (IRB09213), with written, informed consent of all patients. 4 μm sections prepared from the selected 48 prostate cancer specimens were deparafiinized, stained using human TLR9-specific antibodies (IMG305a; Imgenex) and evaluated by a pathologist (COH).

Cell lines

Human prostate cancer cells: DU145, PC3 expressing luciferase and STAT3 (PC3-luc; Supplementary Figure S7C), LNCaP-S17 (LN-S17) stably expressing IL-6 [19] were kindly provided by Dr. Richard Jove (Vaccine&Gene Therapy Institute, FL), while LNCaP were purchased from ATCC. All cells were authenticated and clear from

contamination by other cell types (Biosynthesis, Lewisville, TX). The PC-TLR9^{LO} and PC-TLR9^{HI} cells were generated using lentiviral transduction of pKLO-puro.1-shTLR9 or control pKLO-puro.1 vectors (Sigma-Aldrich) into PC3-luc cells, respectively, followed by selection of stable cell lines in puromycin (1.5 μg/ml). The sequence of shTLR9 was: 5′-CCGGCCACTTCTATAACCGGAACTTCTCGAGAAG TTCCGGTTATAGAACTGGTTTTTG-3′. To generate the LNCaP-TLR9^{+} and LN-TLR9^{HI} cells, the full length human TLR9 cDNA (Addgene) was cloned into pLVX-EF1α vector and lentivirally transduced into LNCaP and LN-S17 cells to select stable clones.

In vitro spheroid and clonogenic assays

For the spheroid formation assays, 24-well culture dishes coated with 0.6%(w/v) agarose were overlayed using 1×10^4 of freshly isolated tumor cells suspended in the agarose-medium mixture (RMPI/10%(v/v) FCS/0.3%(w/v) agarose). The colonies were counterstained and counted after 1–2 weeks of culture. The clonogenic assay design was reported by others [27].

In vivo experiments

NOD/SCID/IL-2RγKO mice (NSG), aged 6–8 weeks, were purchased from the Jackson Laboratory. Mouse care and experimental procedures were performed under pathogen-free conditions following protocols approved by the Institutional Animal Care and Use Committee (COH). The limited-dilution assays to calculate tumor-propagating cell frequency were performed as described elsewhere using the ELDA software to calculate frequencies and probability estimates [21]. The CpG-siRNA design was described previously [28]. The sequence of the CpG-*RELA*siRNA (deoxyribonucleotides are underlined; asterisks indicate phosphothioation sites): CpG-siRNA(antisense strand): 5′ G*G*TGCATCGATGCAGG*G*G*G*G-Linker-UCC UUUUACGUUUCUCCUCAAUCCGGU 3′ siRNA(sense strand): 5′ CGGAUUGGAGAAACGUAAAAGGA 3′.

Western blotting

Total cellular lysates were prepared as previously reported [28] and analyzed using antibodies specific to TLR9 (Imgenex), tyrosine-phosphorylated STAT3, total STAT3, BMI-1, COL1A1, KLF4, NKX3.1, SOX-4 (Santa Cruz) and β-actin (Sigma).

Quantitative real-time PCR

The RNA extraction, reverse transcriptase and real time PCR reactions were performed using CFX96 Real-Time PCR Detection System (Bio-Rad) and the specific pairs of primers designed for *BMI-1, COL1A1, KLF4, NANOG, NKX3.1, OCT-4, SOX2* and *SOX4* (sequences provided in the Supplementary Materials) as previous described [28]. The data were normalized to the *TBP* levels and the relative gene expression levels were calculated using the $2^{-\Delta\Delta Ct}$ method.

Flow cytometry

For uptake studies, following the incubation with fluorescently-labeled oligonucleotides cells were analyzed using C6 flow cytometer (BD Biosciences) and analyzed using FlowJo software (Tree Star).

Chromatin Immunoprecipitation (ChIP) assays

ChIP assays were carried out with a EipTect ChIP OneDay (Qiagen) following the manufacturer's instructions. For ChIP-re-ChIP assay, the immunoprecipitates were subjected to a second round of immunoprecipitation. The presence of specific DNA fragments was quantified using qPCR and specific primers listed in the Supplementary Methods.

Statistics

Unpaired *t* test was used to calculate two-tailed *P* value to estimate statistical significance of differences between two treatment groups. One- or two-way ANOVA plus Bonfeerroni post-test were applied to assess differences between multiple groups or in tumor growth kinetics experiments, respectively. Statistically significant *P* values were indicated in figures as follows: ***, $P < 0.001$; **, $P < 0.01$ and *, $P < 0.05$. Data were analyzed using Prism software v. 6.01 (GraphPad).

ACKNOWLEDGMENTS

We are grateful to Drs. Ya-Huei Kuo and Ian Talisman (COH) for critical reading of the manuscript and to the staff of Light Microscopy, Analytical Cytometry, Pathology Cores and Animal Resource Center for assistance (COH).

CONFLICTS OF INTEREST

The authors declare no conflict of interest.

GRANTS SUPPORT

This work was supported by the Department of Defense grant W81XWH-12–1-0132, Movember-Prostate Cancer Foundation, Margaret E.Early Medical Research Trust, STOP CANCER Allison Tovo-Dwyer Memorial Award (to M.K.) and by the National Cancer Institute of the NIH under grants R01CA155367 (to M.K.), P30CA033572 (to COH) and by the Brazil National Counsel of Technological and Scientific Development (CNPq) 20196/2011–2 (to D.M.). The content is solely the responsibility of the authors and

does not necessarily represent the official views of the NIH.

Editorial note

This paper has been accepted based in part on peer-review conducted by another journal and the authors' response and revisions as well as expedited peer-review in Oncotarget.

REFERENCES

1. DeSantis CE, Lin CC, Mariotto AB, Siegel RL, Stein KD, Kramer JL, Alteri R, Robbins AS, Jemal A. Cancer treatment and survivorship statistics, 2014. CA: a cancer journal for clinicians. 2014.
2. De Marzo AM, Platz EA, Sutcliffe S, Xu J, Gronberg H, Drake CG, Nakai Y, Isaacs WB, Nelson WG. Inflammation in prostate carcinogenesis. Nat Rev Cancer. 2007; 7:256–269.
3. Sfanos KS, De Marzo AM. Prostate cancer and inflammation: the evidence. Histopathology. 2012; 60:199–215.
4. Kawai T, Akira S. The role of pattern-recognition receptors in innate immunity: update on Toll-like receptors. Nat Immunol. 2010; 11:373–384.
5. Rayburn ER, Wang W, Zhang Z, Li M, Zhang R, Wang H. Experimental therapy of prostate cancer with an immunomodulatory oligonucleotide: effects on tumor growth, apoptosis, proliferation, and potentiation of chemotherapy. Prostate. 2006; 66:1653–1663.
6. Shatz M, Menendez D, Resnick MA. The human TLR innate immune gene family is differentially influenced by DNA stress and p53 status in cancer cells. Cancer Res. 2012; 72:3948–3957.
7. Ilvesaro JM, Merrell MA, Swain TM, Davidson J, Zayzafoon M, Harris KW, Selander KS. Toll like receptor-9 agonists stimulate prostate cancer invasion *in vitro*. Prostate. 2007; 67:774–781.
8. Gonzalez-Reyes S, Fernandez JM, Gonzalez LO, Aguirre A, Suarez A, Gonzalez JM, Escaff S, Vizoso FJ. Study of TLR3, TLR4, and TLR9 in prostate carcinomas and their association with biochemical recurrence. Cancer Immunol Immunother. 2011; 60:217–226.
9. Gao C, Kozlowska A, Nechaev S, Li H, Zhang Q, Hossain DM, Kowolik CM, Chu P, Swiderski P, Diamond DJ, Pal SK, Raubitschek A, Kortylewski M. TLR9 Signaling in the Tumor Microenvironment Initiates Cancer Recurrence after Radiotherapy. Cancer Res. 2013; 73:7211–7221.
10. Zhang Q, Raoof M, Chen Y, Sumi Y, Sursal T, Junger W, Brohi K, Itagaki K, Hauser CJ. Circulating mitochondrial DAMPs cause inflammatory responses to injury. Nature. 2010; 464:104–107.
11. Murray PJ, Smale ST. Restraint of inflammatory signaling by interdependent strata of negative regulatory pathways. Nat Immunol. 2012; 13:916–924.
12. Yu H, Pardoll D, Jove R. STATs in cancer inflammation and immunity: a leading role for STAT3. Nat Rev Cancer. 2009; 9:798–809.
13. Vicari AP, Chiodoni C, Vaure C, Ait-Yahia S, Dercamp C, Matsos F, Reynard O, Taverne C, Merle P, Colombo MP, O'Garra A, Trinchieri G, Caux C. Reversal of tumor-induced dendritic cell paralysis by CpG immunostimulatory oligonucleotide and anti-interleukin 10 receptor antibody. J Exp Med. 2002; 196:541–549.
14. Kortylewski M, Kujawski M, Herrmann A, Yang C, Wang L, Liu Y, Salcedo R, Yu H. Toll-like receptor 9 activation of signal transducer and activator of transcription 3 constrains its agonist-based immunotherapy. Cancer Res. 2009; 69:2497–2505.
15. Ben-Neriah Y, Karin M. Inflammation meets cancer, with NF-kappaB as the matchmaker. Nat Immunol. 2011; 12:715–723.
16. Lee H, Deng J, Xin H, Liu Y, Pardoll D, Yu H. A Requirement of STAT3 DNA Binding Precludes Th-1 Immunostimulatory Gene Expression by NF-{kappa}B in Tumors. Cancer Res. 2011; 71:3772–3780.
17. Mora LB, Buettner R, Seigne J, Diaz J, Ahmad N, Garcia R, Bowman T, Falcone R, Fairclough R, Cantor A, Muro-Cacho C, Livingston S, Karras J, Pow-Sang J, Jove R. Constitutive activation of Stat3 in human prostate tumors and cell lines: direct inhibition of Stat3 signaling induces apoptosis of prostate cancer cells. Cancer Res. 2002; 62:6659–6666.
18. Zerbini LF, Wang Y, Cho JY, Libermann TA. Constitutive activation of nuclear factor kappaB p50/p65 and Fra-1 and JunD is essential for deregulated interleukin 6 expression in prostate cancer. Cancer Res. 2003; 63:2206–2215.
19. Lou W, Ni Z, Dyer K, Tweardy DJ, Gao AC. Interleukin-6 induces prostate cancer cell growth accompanied by activation of stat3 signaling pathway. Prostate. 2000; 42:239–242.
20. Qin J, Liu X, Laffin B, Chen X, Choy G, Jeter CR, Calhoun-Davis T, Li H, Palapattu GS, Pang S, Lin K, Huang J, Ivanov I, Li W, Suraneni MV, Tang DG. The PSA(-/lo) prostate cancer cell population harbors self-renewing long-term tumor-propagating cells that resist castration. Cell Stem Cell. 2012; 10:556–569.
21. Kreso A, van Galen P, Pedley NM, Lima-Fernandes E, Frelin C, Davis T, Cao L, Baiazitov R, Du W, Sydorenko N, Moon YC, Gibson L, Wang Y, Leung C, Iscove NN, Arrowsmith CH, et al. Self-renewal as a therapeutic target in human colorectal cancer. Nat Med. 2014; 20:29–36.
22. Zhau HE, He H, Wang CY, Zayzafoon M, Morrissey C, Vessella RL, Marshall FF, Chung LW, Wang R. Human prostate cancer harbors the stem cell properties of bone marrow mesenchymal stem cells. Clin Cancer Res. 2011; 17:2159–2169.
23. Lukacs RU, Memarzadeh S, Wu H, Witte ON. Bmi-1 is a crucial regulator of prostate stem cell self-renewal and malignant transformation. Cell stem cell. 2010; 7:682–693.

24. Wang X, Kruithof-de Julio M, Economides KD, Walker D, Yu H, Halili MV, Hu YP, Price SM, Abate-Shen C, Shen MM. A luminal epithelial stem cell that is a cell of origin for prostate cancer. Nature. 2009; 461:495–500.

25. Scharer CD, McCabe CD, Ali-Seyed M, Berger MF, Bulyk ML, Moreno CS. Genome-wide promoter analysis of the SOX4 transcriptional network in prostate cancer cells. Cancer Res. 2009; 69:709–717.

26. Wernig M, Meissner A, Foreman R, Brambrink T, Ku M, Hochedlinger K, Bernstein BE, Jaenisch R. *In vitro* reprogramming of fibroblasts into a pluripotent ES-cell-like state. Nature. 2007; 448:318–324.

27. Li H, Chen X, Calhoun-Davis T, Claypool K, Tang DG. PC3 human prostate carcinoma cell holoclones contain self-renewing tumor-initiating cells. Cancer Res. 2008; 68:1820–1825.

28. Zhang Q, Hossain DM, Nechaev S, Kozlowska A, Zhang W, Liu Y, Kowolik CM, Swiderski P, Rossi JJ, Forman S, Pal S, Bhatia R, Raubitschek A, Yu H, Kortylewski M. TLR9-mediated siRNA delivery for targeting of normal and malignant human hematopoietic cells *in vivo*. Blood. 2013; 121:1304–1315.

29. Vaisanen MR, Vaisanen T, Jukkola-Vuorinen A, Vuopala KS, Desmond R, Selander KS, Vaarala MH. Expression of toll-like receptor-9 is increased in poorly differentiated prostate tumors. Prostate. 2010; 70:817–824.

30. Kundu SD, Lee C, Billips BK, Habermacher GM, Zhang Q, Liu V, Wong LY, Klumpp DJ, Thumbikat P. The toll-like receptor pathway: a novel mechanism of infection-induced carcinogenesis of prostate epithelial cells. Prostate. 2008; 68:223–229.

31. Yang T, Rycaj K, Liu ZM, Tang DG. Cancer stem cells: constantly evolving and functionally heterogeneous therapeutic targets. Cancer Res. 2013; 74:2922–2927.

32. Germann M, Wetterwald A, Guzman-Ramirez N, van der Pluijm G, Culig Z, Cecchini MG, Williams ED, Thalmann GN. Stem-like cells with luminal progenitor phenotype survive castration in human prostate cancer. Stem cells (Dayton, Ohio). 2012; 30:1076–1086.

33. Magee JA, Piskounova E, Morrison SJ. Cancer stem cells: impact, heterogeneity, and uncertainty. Cancer Cell. 2012; 21:283–296.

34. Oka T, Hikoso S, Yamaguchi O, Taneike M, Takeda T, Tamai T, Oyabu J, Murakawa T, Nakayama H, Nishida K, Akira S, Yamamoto A, Komuro I, Otsu K. Mitochondrial DNA that escapes from autophagy causes inflammation and heart failure. Nature. 2012; 485: 251–255.

35. Jin R, Yi Y, Yull FE, Blackwell TS, Clark PE, Koyama T, Smith JA Jr., Matusik RJ. NF-kappaB gene signature predicts prostate cancer progression. Cancer Res. 2014; 74:2763–2772.

36. Heinrich PC, Behrmann I, Haan S, Hermanns HM, Muller-Newen G, Schaper F. Principles of interleukin (IL)-6-type cytokine signalling and its regulation. Biochem J. 2003; 374:1–20.

37. Drake JM, Graham NA, Lee JK, Stoyanova T, Faltermeier CM, Sud S, Titz B, Huang J, Pienta KJ, Graeber TG, Witte ON. Metastatic castration-resistant prostate cancer reveals intrapatient similarity and interpatient heterogeneity of therapeutic kinase targets. Proc Natl Acad Sci U S A. 2013; 110:E4762–4769.

38. Schroeder A, Herrmann A, Cherryholmes G, Kowolik C, Buettner R, Pal S, Yu H, Muller-Newen G, Jove R. Loss of androgen receptor expression promotes a stem-like cell phenotype in prostate cancer through STAT3 signaling. Cancer Res. 2013; 74:1227–1237.

39. Smith DA, Kiba A, Zong Y, Witte ON. Interleukin-6 and oncostatin-M synergize with the PI3K/AKT pathway to promote aggressive prostate malignancy in mouse and human tissues. Mol Cancer Res. 2013; 11:1159–1165.

40. Bae KM, Su Z, Frye C, McClellan S, Allan RW, Andrejewski JT, Kelley V, Jorgensen M, Steindler DA, Vieweg J, Siemann DW. Expression of pluripotent stem cell reprogramming factors by prostate tumor initiating cells. The Journal of urology. 2010; 183:2045–2053.

41. Chen CL, Tsukamoto H, Liu JC, Kashiwabara C, Feldman D, Sher L, Dooley S, French SW, Mishra L, Petrovic L, Jeong JH, Machida K. Reciprocal regulation by TLR4 and TGF-beta in tumor-initiating stem-like cells. J Clin Invest. 2013; 123:2832–2849.

42. Kortylewski M, Swiderski P, Herrmann A, Wang L, Kowolik C, Kujawski M, Lee H, Scuto A, Liu Y, Yang C, Deng J, Soifer HS, Raubitschek A, Forman S, Rossi JJ, Pardoll DM, et al. In vivo delivery of siRNA to immune cells by conjugation to a TLR9 agonist enhances antitumor immune responses. Nat Biotechnol. 2009; 27:925–932.

43. Rane JK, Pellacani D, Maitland NJ. Advanced prostate cancer—a case for adjuvant differentiation therapy. Nat Rev Urol. 2012; 9:595–602.

Published OnlineFirst May 12, 2015; DOI: 10.1158/1078-0432.CCR-14-3145

Clinical Cancer Research

TLR9-Targeted STAT3 Silencing Abrogates Immunosuppressive Activity of Myeloid-Derived Suppressor Cells from Prostate Cancer Patients

Dewan M. S. Hossain[1], Sumanta K. Pal[2], Dayson Moreira[1], Priyanka Duttagupta[1], Qifang Zhang[1], Haejung Won[1], Jeremy Jones[3], Massimo D'Apuzzo[4], Stephen Forman[5], and Marcin Kortylewski[1]

Abstract

Purpose: Recent advances in immunotherapy of advanced human cancers underscored the need to address and eliminate tumor immune evasion. The myeloid-derived suppressor cells (MDSC) are important inhibitors of T-cell responses in solid tumors, such as prostate cancers. However, targeting MDSCs proved challenging due to their phenotypic heterogeneity.

Experimental Design: Myeloid cell populations were evaluated using flow cytometry on blood samples, functional assays, and immunohistochemical/immunofluorescent stainings on specimens from healthy subjects, localized and metastatic castration-resistant prostate cancer patients.

Results: Here, we identify a population of $Lin^{-}CD15^{HI}CD33^{LO}$ granulocytic MDSCs that accumulate in patients' circulation during prostate cancer progression from localized to metastatic disease. The prostate cancer–associated MDSCs potently inhibit autologous $CD8^{+}$ T cells' proliferation and production of IFNγ and granzyme-B. The circulating MDSCs have high levels of activated STAT3, which is a central immune checkpoint regulator. The granulocytic $pSTAT3^{+}$ cells are also detectable in patients' prostate tissues. We previously generated an original strategy to silence genes specifically in Toll-like Receptor-9 (TLR9) positive myeloid cells using CpG-siRNA conjugates. We demonstrate that human granulocytic MDSCs express TLR9 and rapidly internalize naked CpG-*STAT3*siRNA, thereby silencing *STAT3* expression. STAT3 blocking abrogates immunosuppressive effects of patients-derived MDSCs on effector $CD8^{+}$ T cells. These effects depended on reduced expression and enzymatic activity of Arginase-1, a downstream STAT3 target gene and a potent T-cell inhibitor.

Conclusions: Overall, we demonstrate the accumulation of granulocytic MDSCs with prostate cancer progression and the feasibility of using TLR9-targeted *STAT3*siRNA delivery strategy to alleviate MDSC-mediated immunosuppression. *Clin Cancer Res; 1–12. ©2015 AACR.*

Introduction

Prostate cancer remains the most common malignancy in men in the United States (1). Although localized prostate cancers are curable with surgery or standard therapeutic regimens, the 5-year survival rate of patients with the advanced metastatic tumors is reduced to 20% to 30%. Androgen deprivation therapies control the recurrent disease only for limited time until the development of metastatic castration-resistant prostate cancers (mCRPC). Current chemotherapeutic regimens for mCRPC have limited efficacy and are plagued by the highly toxic effects to normal tissues (2). The first FDA-approved immunotherapeutic approach to mCRPC, using autologous cellular vaccinations, showed promising although modest improvement in patients' survival (3). Growing evidence suggests that prostate tumor microenvironment can block immune responses using a wide array of immune checkpoint mechanisms likely extending beyond PD-1 blockade (4–7). Human tumors recruit and expand population of potently immunosuppressive myeloid-derived suppressor cells (MDSC) that were associated with progression and poor patients' survival (8–10). Depending on the expression of lineage-specific immune markers, MDSCs can be divided into $CD14^{+}CD15^{LO}CD33^{HI}$ monocytic MDSCs (M-MDSC) and $CD14^{-}CD15^{HI}CD33^{LO}$ granulocytic MDSCs (G-MDSC), also known as polymorphonuclear neutrophil-MDSCs (PMN-MDSC; ref. 8). The generation of MDSCs is a result of tumor-induced skewing of monocyte differentiation from macrophages/DCs into M-MDSCs and later into G-MDSCs, a dominant myeloid population in cancer patients' circulation (11). First study that reported circulating prostate cancer–associated MDSCs in patients with the localized disease identified these cells as $CD14^{+}$/HLA-DR^{-} M-MDSCs (12). Whether G-MDSCs are contributing to prostate cancer progression remains unknown. However, there is accumulating evidence linking G-MDSCs with immunosuppression in human

[1]Department of Cancer Immunotherapeutics & Tumor Immunology, Beckman Research Institute at City of Hope, Duarte, California. [2]Department of Medical Oncology and Experimental Therapeutics, Beckman Research Institute at City of Hope, Duarte, California. [3]Department of Cancer Biology, Beckman Research Institute at City of Hope, Duarte, California. [4]Department of Pathology, Beckman Research Institute at City of Hope, Duarte, California. [5]Department of Hematology and Hematopoietic Cell Transplantation, Beckman Research Institute at City of Hope, Duarte, California.

Note: Supplementary data for this article are available at Clinical Cancer Research Online (http://clincancerres.aacrjournals.org/).

Corresponding Authors: Marcin Kortylewski, Department of Cancer Immunotherapeutics & Tumor Immunology, Beckman Research Institute at City of Hope, 1500 East Duarte Rd., Duarte, CA 91010. Phone: 626-256-4673, ext. 64120; Fax: 626-471-3602; E-mail: mkortylewski@coh.org; and Sumanta K. Pal, spal@coh.org

doi: 10.1158/1078-0432.CCR-14-3145

Published OnlineFirst May 12, 2015; DOI: 10.1158/1078-0432.CCR-14-3145

Translational Relevance

Despite the initial efficacy of hormone therapies, prostate tumors eventually progress to metastatic castration-resistant prostate cancers (mCRPC), which resist current therapies and also the emerging immunotherapeutic regimens. The advanced prostate cancers develop a potently immunosuppressive microenvironment which partly relies on the heterogeneous population of myeloid-derived suppressor cells (MDSC). We identified a specific population of granulocytic MDSCs that accumulated in patients' circulation during prostate cancer progression from localized to metastatic disease. These $TLR9^+$ MDSCs showed high levels of immunosuppressive mediators, STAT3 and Arginase-1, and inhibited effector T-cell proliferation and activity. Targeting MDSCs using CpG-*STAT3*-siRNA strategy alleviated their immunosuppressive functions, restoring T-cell activity. With the ongoing clinical translation of CpG-*STAT3*siRNA conjugates to therapy of hematologic malignancies, our results underscore the potential of utilizing these oligonucleotide reagents to immunotherapy of advanced prostate cancers.

genitourinary tumors, such as renal and bladder cancers (13–16). Preclinical studies in mouse tumor models showed that MDSC depletion or targeting their expansion and recruitment increases the effectiveness of cancer therapies, including anti-PD-1 immunotherapies (8, 17). We also recently observed that resistance of renal carcinoma patients to pazopanib, a multi-receptor tyrosine kinase inhibitor and antitangiogenic agent, correlated with accumulation of $CD15^+$ G-MDSCs in circulation compared with patients responding to therapy (18).

The expansion of MDSCs in the tumor microenvironment is induced by cancer-derived mediators, such as VEGF, HGF, G-CSF, IL6, and IL10 (19). Downstream signaling induced by majority of these factors converges on signal transducer and activator of transcription 3 (STAT3), which plays central role in the expansion and function of MDSCs (19, 20). Tumor-induced STAT3 activation in myeloid cells inhibits differentiation while enhancing their survival through upregulation of Bcl-X_L, c-Myc, and cyclin D1 (19, 20). In addition, STAT3 promotes immunosuppressive functions of MDSCs by stimulating expression of Arginase-1, ROS, iNOS, and IDO (19, 21). Targeting STAT3 is therefore an attractive strategy to alleviate MDSC-mediated immunosuppression in the tumor microenvironment without the need for myeloid cell depletion. However, as a molecule without enzymatic activity, STAT3 has proven to be a challenging target for pharmacologic inhibition. Small-molecule tyrosine kinase inhibitors are an alternative strategy to target STAT3, but therapeutic effects in most clinical trials were short lived (22).

We previously generated an original method to silence genes specifically in human and mouse $TLR9^+$ myeloid cells using siRNA molecules conjugated to CpG oligonucleotides (23, 24). Targeted TLR9 activation and STAT3 blocking using CpG-*STAT3* siRNA alone, or in combination with radiotherapy, overcame immunosuppression and generated antitumor immune responses against various solid tumors in mice (23, 25). In the present study, we demonstrate that a population of G-MDSCs with high levels of STAT3 activity and Arginase-1 expression is associated with progression of prostate cancers from localized to metastatic disease. We also tested the feasibility of using CpG-*STAT3*siRNA to abrogate immunosuppressive functions of prostate cancer–associated G-MDSCs on effector T-cell activities. Overall, these studies provide a rational for application of CpG-*STAT3* siRNA strategy to immunotherapy of human prostate cancers.

Materials and Methods

Patients

Blood specimens were collected prospectively (after informed consent was obtained) from patients under two independent protocols, IRB-11020 and IRB-10058 (COH). In the IRB-11020, selected patients were diagnosed with high-risk localized prostate cancers. Blood specimens were collected at the baseline before patients underwent prostatectomy. Patients in the IRB-10058 were diagnosed with metastatic castration-resistant prostate cancers (mCRPC) and were later treated with docetaxel chemotherapy. Blood specimens were collected at baseline and after 4 months of docetaxel chemotherapy applied in 3 weekly cycles. Prostatectomy specimens were acquired from patients with high-risk, localized prostate cancers under IRB-10151 protocol (COH). Each protocol and the relevant informed consent were approved by the institutional scientific review committee, data safety monitoring board, and the institutional review board at City of Hope. All patients enrolled provided written informed consent, and the study was conducted in accordance with the amended Declaration of Helsinki and the International Conference on Harmonization Guidelines.

PBMC isolation and flow cytometry

PBMCs and plasma were separated using Vacutainer CPT tubes (BD Biosciences) within 2 hours after collection by centrifugation at 1,800 $\times g$ for 20 minutes at room temperature. Fresh PBMCs were used for phenotypic analysis of myeloid immune cell populations, 1×10^6 of PBMCs were preincubated with FcγIII/IIR-specific antibody to block unspecific binding and then stained with fluorescently-labeled antibodies to HLA-DR, CD11b, CD14, CD3, CD19, CD56, CD114, CD15, or CD33 (eBiosciences). For analysis of intracellular markers, we used PBMCs previously frozen in optimized Cryostor CS5 media (Biolife). Freeze–thaw procedure reduced CD15 staining causing decrease in the percentage of $CD15^{HI}CD33^{LO}$ cells (Supplementary Fig. S1), however, reductions of G-MDSC percentages were consistent between various patients. Thus, it was feasible and acceptable to compare identically handled cryopreserved samples to assess relative changes of G-MDSC population during disease progression. For intracellular staining, PBMCs were first stained for surface markers, then fixed and permeabilized using BD fixation and perm/wash buffer, respectively, following the manufacturer's recommendations. After blocking in human serum, cells were stained using fluorescently-labeled antibodies specific to TLR9 (eBiosciences), tyrosine 705-phosphorylated STAT3 (pSTAT3; BD Biosciences), or Arginase-1 (R&D Systems). Flow cytometric data were collected on BD-Accuri C6 Flow Cytometer (BD Biosciences) or MACSQuant (Miltenyi Biotec) and analyzed using FlowJo software (TreeStar).

MDSC isolation and treatment

For analysis of immunosupressive functions, myeloid cell populations were isolated from fresh blood samples using

Published OnlineFirst May 12, 2015; DOI: 10.1158/1078-0432.CCR-14-3145

FACSAriaIII cell sorter (BD Biosciences) or magnetic enrichment (STEMCELL Technologies). For the latter, $CD14^+$ cells were first removed from total PBMCs using specific antibodies (eBiosciences) and then $CD14^-CD15^+$ cells were selected using CD15-specific antibodies (eBiosciences). Purity of isolated cells was evaluated by flow cytometry, which detected single-cell population (data not shown). For the analysis of STAT3 activation and ARG1 expression, frozen PBMCs were thawed and cultured for at least 2 hours in 20% plasma from the same patient. These conditions were sufficient to restore the maximum levels of STAT3 signaling as determined in preliminary studies (Supplementary Fig. S2). Then selected myeloid cell populations were isolated using high-speed cell sorting using FACS-Aria (BD Biosciences) or magnetic separation using specific antibodies (STEMCELL Technologies). For the latter, after removal of $CD14^+$ myeloid cells from total PBMCs using CD14-specific antibodies (eBiosciences), the $CD14^-CD15^+$ cells were enriched from the remaining PBMCs using CD15-specific antibody (eBiosciences). For uptake studies, enriched MDSCs were treated using different concentrations of FITC-labeled CpG-*STAT3* siRNA followed by flow cytometry to assess the uptake. The sequences of human cell-specific CpG-siRNAs were reported before (23, 24). All CpG-siRNA conjugates were synthesized at DNA/RNA Synthesis Core (COH) by using 5 units of C3 carbon chain, $(CH_2)_3$ (Glen Research) to link the D19 oligodeoxyribonucleotides to antisense strands (AS) of siRNAs. The resulting constructs were hybridized to complementary siRNA sense strands (SS) to generate CpG-siRNA conjugates. To test the effect of STAT3 or Arginase-1 inhibition on MDSC function, the isolated MDSCs were treated with 500 nmol/L of CpG-*STAT3* siRNA or 20 μmol/L nor-NOHA (Cayman Chemical Company) and then cocultured with autologous T cells.

T-cell assays

$CD3^+$ T cells were isolated from patients' PBMCs using specific antibodies plus magnetic bead-enrichment (STEMCELL Technologies) and then labeled using carboxyfluorescein succinimidyl ester (CFSE; Life Technologies). CFSE-labeled cells were then incubated with Human T-cell Activator CD3/CD28 Dynabeads (Life Technologies) for 3 days with or without $CD15^{HI}CD33^{LO}$ MDSCs isolated from same patient. Proliferation of $CD3^+$ T cells were evaluated as CFSE dilution using flow cytometry. To determine IFNγ and granzyme-B response in $CD8^+$ T cells in same experimental condition, Golgi stop (BD Biosciences) was added for last 6 hours to the MDSC–T-cell cocultures and harvested cells were immunostained with specific antibodies to CD3, CD8, IFNγ, and granzyme-B (BD Biosciences) according to the manufacturer's protocol. Unstimulated $CD3^+$ T cells from each patient served as a negative control.

Quantitative real-time PCR and protein assays

For quantitative PCR (qPCR), total RNA was extracted from isolated MDSCs using the RNeasy Plus kit (Qiagen). After cDNA synthesis using iScript kit (Bio-Rad), samples were analyzed using sets of probes from the Universal Probe Library and specific primer pairs for human *STAT3*: 5′-CTGCCTAGATCGGCTAGAAAAC-3′, 5′-CCCTTTGTAGGAAACTTTTTGC-3′, UPL #25; *TLR9*: 5′-TGTGAAGCATCCTTCCCTGTA-3′, 5′-GAGAGACAGCGGGTGCAG-3′, UPL #56. SsoAdvanced SYBR Green Supermix (Bio-Rad) was used to analyze human *ARG-1, iNOS, and IDO* expression in patient MDSCs with following sets of primers: *ARG-1*: 5′-GTTTCTCAAGCAGACCAGCC-3′ and 5′-GCTCAAGTGCAGCAAAGAGA-3′; *iNOS*: 5′-ATTCTGCTGCTTGCTGAGGT-3′ and 5′-TTCAAGACCAAATTCCACCAG-3′; *IDO:* 5′-CATCTGCAAATCGTGACTAAG-3′ and 5′-CAGTCGACACATTAACCTTCCTTC-3′. Sequence-specific amplification was analyzed on the CFX96 Real-Time PCR Detection System (Bio-Rad). The data were normalized to the *TBP* expression and the relative expression levels were calculated using the $2^{-\Delta\Delta Ct}$ method. Concentrations of cytokines and growth factors were assessed in plasma specimens using Human Cytokine 30-plex protein assay (Invitrogen) on FLEXMAP 3D System (Luminex) at the Clinical Immunobiology and Correlative Studies Laboratory (City of Hope).

Arginase activity assay

Arginase-1 enzymatic activity in $CD15^{HI}CD33^{LO}$ cell lysates and blood serum from different stage prostate cancer patients were measured using the QuantiChrom Arginase Assay Kit (BioAssay Systems). To prepare lysates, isolated MDSCs were lysed with 10 mmol/L Tris-HCL (pH 7.4) containing protease inhibitors (Complete Mini; Roche) and 0.4% Triton X-100 for 15 minutes on ice. For blood serum samples, urea was removed using Amicon Ultra-0.5 centrifugal filter devices (Millipore).

Immunohistochemistry and confocal microscopy

For immunohistochemical analysis, 4-μm sections were deparaffinized and immunostained using antibodies specific for CD15 (Abcam) or pSTAT3 (Cell Signaling Technology). The slides were analyzed first using upright AX70 microscope (Olympus) followed by whole-slide imaging using NanoZoomer scanner and NDP v.2.5 software (Hamamatsu Photonics). To assess the morphology of $CD15^{HI}CD33^{LO}$ and $CD15^{LO}CD33^{HI}$ populations, sorted cells were cytospinned on glass slides and dried for 10 minutes at room temperature. Slides were then vertically submersed in methanol for 15 minutes, stained briefly using Differential Quick Stain kit (Polyscienecs, Inc), coverslipped with mounting medium (Vector Labs), and imaged using upright AX70 microscope (Olympus). For *in vitro* uptake studies, $CD15^+CD14^-$ cells enriched from prostate cancer patient were incubated with fluorescently labeled CpG-*STAT3*siRNA^{FITC} (500 nmol/L) for various times. Cell were then fixed using 1.6% paraformadehyde, permeabilized using 0.5% Triton/PBS, and washed. After a cytospin onto the poly-L-lysine (Sigma–Aldrich) coated slides, cells were mounted in VECTASHIELD Hard-set mounting medium with DAPI (Vector Labs) for confocal microscopy. The confocal imaging was carried out using a ×63 oil immersion objective on LSM-510 Meta inverted confocal microscope (Zeiss).

Statistical analysis

The Unpaired *t* test was used to calculate the two-tailed *P* value to estimate statistical significance of differences between two experimental groups. One- or two-way ANOVA plus Bonferroni posttest were applied to assess the statistical significance of differences between multiple treatment groups or patients from different stages and healthy donors. Statistically significant *P* values are indicated in the figures with asterisks: ***, $P < 0.001$; **, $P < 0.01$; *, $P < 0.05$. Data were analyzed using Prism v.6.0 software (GraphPad).

Published OnlineFirst May 12, 2015; DOI: 10.1158/1078-0432.CCR-14-3145

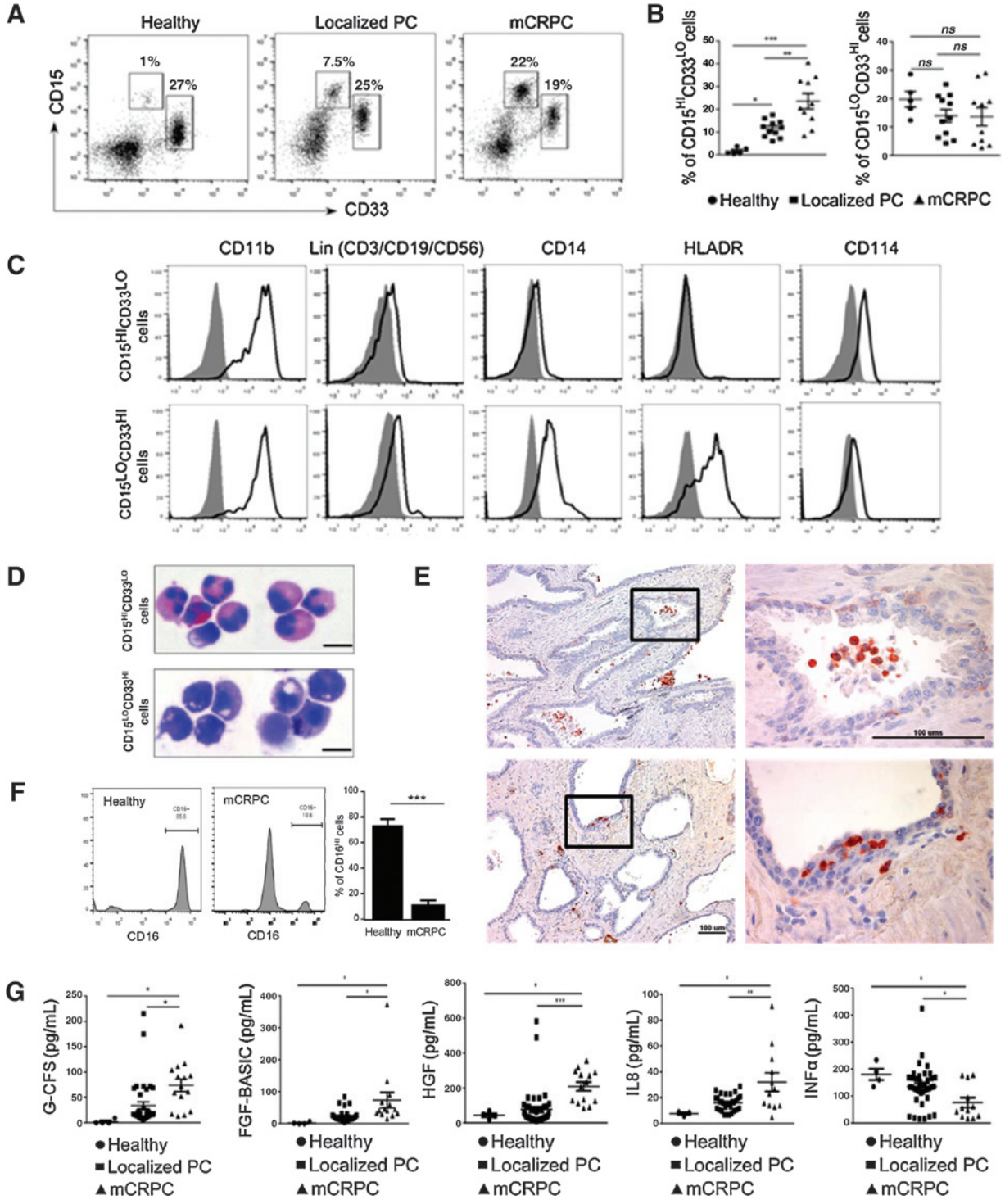

Figure 1.

CD15^{HI} myeloid cells accumulate in peripheral blood and tumor tissues in prostate cancer patients with disease progression. A and B, flow cytometric analysis of fresh PBMCs from healthy subjects and prostate cancer patients with localized or metastatic disease. Representative dot plots (A) and graphs combining data from all subjects (B) showing percentages of CD15^{HI}CD33^{LO} or CD15^{LO}CD33^{HI} cells in prostate cancer patients' circulation at localized prostate cancers (PC; $n = 11$) or metastatic tumors (mCRPC; $n = 10$) compared with healthy donors ($n = 5$). Shown are means ± SD. C, representative histograms showing expression of lineage markers (Lin = CD3/CD19/CD56), CD11b, CD14, HLA-DR, and CD114 (G-CSFR) among CD15^{LO}CD33^{HI} (top row) and CD15^{HI}CD33^{LO} (bottom row) cells. D, cellular morphology of sorted, cytospinned, and stained CD15^{HI}CD33^{LO} or CD15^{LO}CD33^{HI} myeloid cells. Representative microphotographs showing monocytic (top) and granulocytic polymorphonuclear (PMN) phenotype (bottom) of CD15^{HI}CD33^{LO} and CD15^{LO}CD33^{HI} cells, respectively. E, CD15^{+} cells in cancer patients' prostate tissues have granulocytic and PMN phenotype. (*Continued on the following page.*)

Published OnlineFirst May 12, 2015; DOI: 10.1158/1078-0432.CCR-14-3145

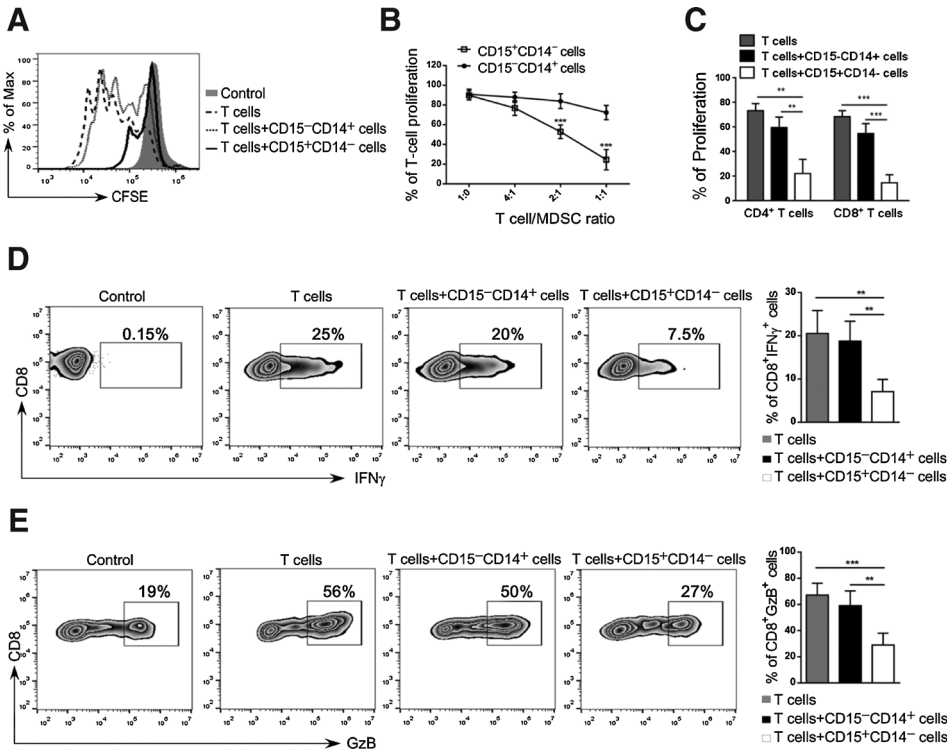

Figure 2.
$CD15^{HI}$ MDSCs isolated from prostate cancer patients inhibit proliferation and activity of autologous T cells. A to C, $CD15^{+}CD14^{-}$ granulocytic and $CD15^{-}CD14^{+}$ monocytic cell populations freshly enriched from metastatic prostate cancer patients' PBMCs were cultured separately with autologous T cells in presence of CD3-/CD28-specific antibodies for stimulation. A, representative flow cytometry data showing T-cell proliferation assessed by CFSE dilution after 3 days of coculture. B, combined results of T-cell proliferation assays from 5 patients showing percentage of total T-cell proliferation at different T:myeloid cell ratios. C, proliferation of $CD4^{+}$ and $CD8^{+}$ T cells when incubated at 1:1 ratio with or without the indicated myeloid cell populations; means ± SD ($n = 5$). D and E, $CD15^{+}CD14^{-}$ myeloid cells inhibit production of IFNγ and granzyme B by activated $CD8^{+}$ T cells. T cells were cocultured with either one of myeloid cell populations at 1:1 ratio as above. The intracellular levels of IFNγ and granzyme B were measured using flow cytometry. Representative dot plots and bar graphs showing percentages of $CD8^{+}IFN\gamma^{+}$ T cells (D) and $CD8^{+}$Granzyme-B^{+} T cells (E) after 3 days of culture; shown are means ± SD ($n = 5$). Asterisks, statistically significant differences.

Results

Prostate cancer progression is associated with the accumulation of circulating $CD15^{HI}CD33^{LO}$ granulocytic myeloid cells

We used flow cytometry to phenotype immune cell populations in blood derived from patients with localized or metastatic prostate cancers compared to healthy subjects. As shown in Fig. 1A and B, increased percentages of circulating myeloid cell subsets were more sensitive indicators of tumor presence and progression than changes in lymphoid cell populations, such as regulatory T cells, or in plasmacytoid DCs (Supplementary Fig. S3). Compared with controls, both groups of prostate cancer patients showed significant accumulation of blood $CD15^{HI}CD33^{LO}$ granulocytic myeloid cells, whereas the percentage of $CD15^{LO}CD33^{HI}$ myeloid cells did not change (Fig. 1B). In addition, the percentage of $CD15^{HI}CD33^{LO}$ granulocytic myeloid cells was increased more than twice in mCRPC patients compared with patients with localized tumors (Fig. 1B). The percentage of $CD15^{HI}CD33^{LO}$ myeloid cells in mCRPC patients remained elevated even after standard docetaxel treatment regimen (Supplementary Fig. S4). Further phenotypic characterization indicated that both myeloid cell populations share expression of the common myeloid marker CD11b while being negative for lineage-markers CD3, CD19, and CD56 (Fig. 1C). However, monocytic-lineage marker CD14 and HLA-DR molecules were expressed only by $CD15^{LO}CD33^{HI}$ and not by $CD15^{HI}CD33^{LO}$ (Fig. 1C). Therefore, $CD15^{HI}CD33^{LO}$ cells resemble the granulocytic subtype of MDSCs as also indicated by G-CSFR/CD114 expression, which is associated with this subpopulation (Fig. 1C; ref. 26). To verify this observation, we next analyzed cytomorphology of both populations after cell sorting. As expected, $CD15^{HI}CD33^{LO}$ cells show polymorphonuclear (PMN) morphology typical for granulocytic cells (top) compared with mononuclear $CD15^{LO}CD33^{HI}$ cells (bottom; Fig. 1D). The

(*Continued.*) Representative results of immunohistochemical staining on FFPE sections from two different patients (top and bottom); scale bar, 100 μm. F, mature $CD16^{HI}$ neutrophils are only minor fraction of circulating $CD15^{HI}CD33^{LO}$ cells in prostate cancer patients. The expression of CD16 was assessed on granulocytic cells from healthy subjects or prostate cancer patients. Shown are representative dot plot graphs (two left panels) and the summary of results from 6 different patients (right bar graph); means ± SD ($n = 6$). G, plasma levels of G-CSF and several other growth factors/chemokines increase with prostate cancer progression in contrast to reduced levels of proinflammatory IFNα. Luminex-based analysis of plasma samples from prostate cancer patients with localized ($n = 25$) or metastatic tumors ($n = 15$) compared with healthy individuals ($n = 4$). Asterisks, statistically significant differences; means ± SD.

Published OnlineFirst May 12, 2015; DOI: 10.1158/1078-0432.CCR-14-3145

PMN features of $CD15^+$ cells, such as partly segmented nuclei, were also detectable in immunohistochemical stainings of prostatectomy sections derived from mCRPC patients (Fig. 1E). However, flow cytometric results detected only a small fraction of mature $CD16^{HI}$ neutrophils within $CD15^{HI}CD33^{LO}$ cell compartment, which indicates that majority of these cells are immature granulocytes (Fig. 1F). Other studies demonstrated the involvement of various cytokines and growth factors in stimulating MDSC expansion (G-CSF, HGF, bFGF), recruitment (IL8), or differentiation (IFNα; ref. 19). Our further comparative analysis of plasma samples from patients with localized versus metastatic tumors indicated correlation between the elevated numbers of $CD15^{HI}CD33^{LO}$ cells and the increase in plasma concentrations of G-CSF, HGF, bFGF, and IL8 with the concomitant reduction of proinflammatory IFNα (Fig. 1G). Overall, prostate cancer progression from localized to metastatic disease correlates with changes of cytokine/growth factor environment that may promote accumulation of circulating $CD15^{HI}CD33^{LO}$ granulocytic cells.

G-MDSCs inhibit proliferation and activity of autologous T cells

We next verified whether prostate cancer–associated $CD15^+$ granulocytic cells show immunosuppressive activity. The effect on the proliferation and activities of autologous T cells was assessed using $CD14^-CD15^+$ cells enriched from mCRPC patients. The $CD14^+CD15^-$ monocytes were used as a negative control. As shown in Fig. 2A and B, the $CD14^-CD15^+$ myeloid cells reduced CD3/CD28-driven T-cell proliferation to approximately 50% at 2:1 or approximately 80% at 1:1 ratio of T cells to myeloid cells, respectively. In contrast, the presence of $CD14^+CD15^-$ monocytes did not significantly alter T-cell proliferation. The $CD14^-CD15^+$ myeloid cells had similar effect on both autologous $CD8^+$ and $CD4^+$ T cells (Fig. 2C) as well as on allogeneic T cells (Supplementary Fig. S5). The $CD14^-CD15^+$ myeloid cells but

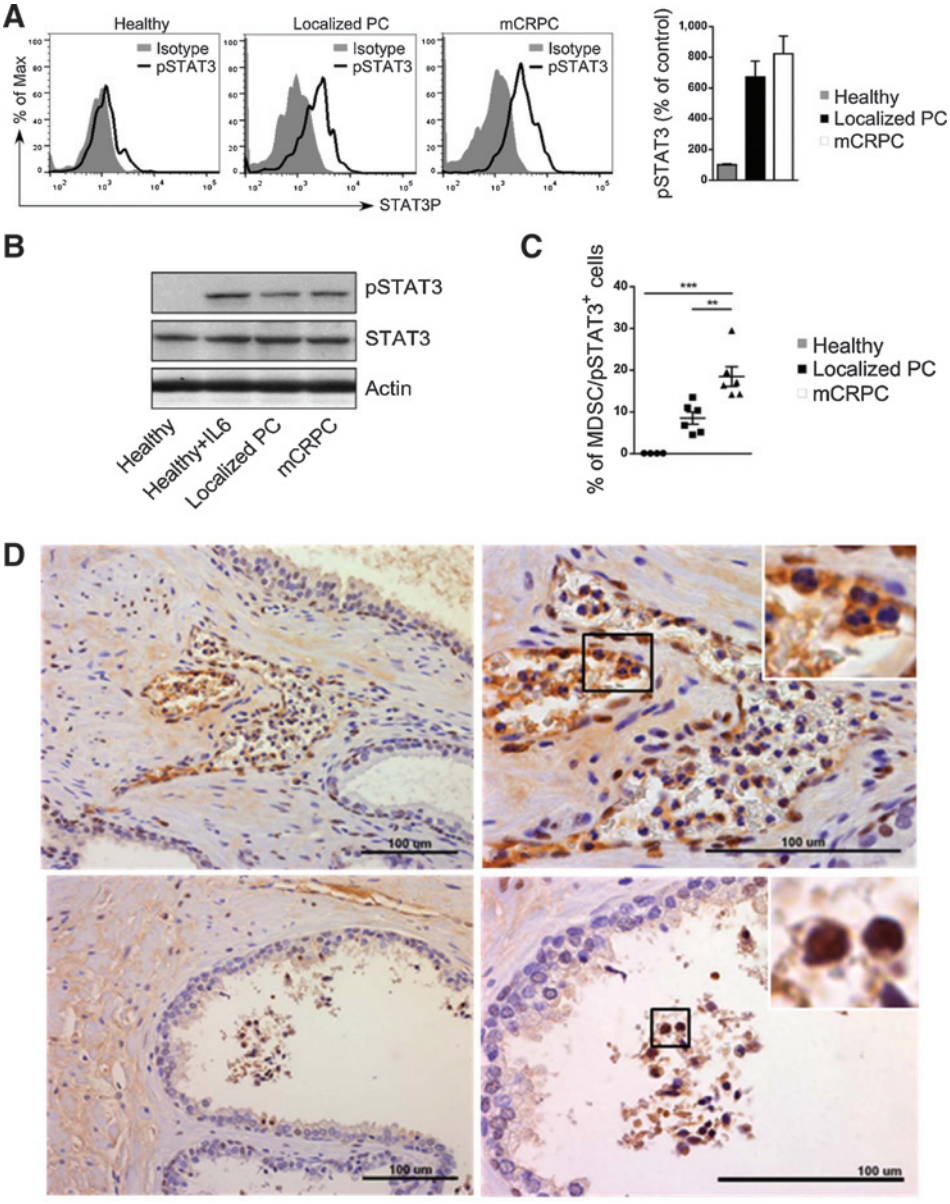

Figure 3.
STAT3 activity is elevated in $CD15^{HI}$ MDSCs in prostate cancer patients. A, flow cytometric analysis of activated STAT3 (pSTAT3) in granulocytic MDSCs ($CD15^{HI}CD33^{LO}$) from patients with localized ($n = 6$) and metastatic ($n = 6$) prostate cancers compared with granulocytes from healthy individuals ($n = 5$). Shown are representative histogram overlays and bar graph summary of data from all patients; average of mean fluorescence intensities (MFI) ± SD. B, prostate cancer patients' granulocytic cells show increased STAT3 phosphorylation without changes in the total STAT3 protein levels. Western blotting analysis to compare pSTAT3 and total STAT3 protein levels in $CD15^+$ $CD14^-$ cells isolated from PBMCs pooled from prostate cancer patients or healthy donors. C, the percentage of MDSCs ($CD15^{HI}CD33^{LO}$) with activated STAT3 increases with prostate cancer progression. Summary of results from all tested patients; asterisks, statistically significant differences. D, increased infiltration of pSTAT3-positive cells with granulocytic (PMN) morphology in prostate tissues from high-risk prostate cancer patients. FFPE tissue sections were stained using immunohistochemistry for pSTAT3 and analyzed using bright-field microscopy. Arrows, $pSTAT3^+$ PMN cells accumulating within capillaries and venules (top) and involving the glandular lumen (bottom). Shown are representative images from two of 10 analyzed specimens; scale bars, 100 μm.

Published OnlineFirst May 12, 2015; DOI: 10.1158/1078-0432.CCR-14-3145

not monocytes from mCRPC patients, also strongly inhibited IFNγ (Fig. 2D) and granzyme B production by effector $CD8^+$ T cells (Fig. 2E). These results confirmed that $CD15^+$ myeloid cells accumulating in the circulation of prostate cancer patients are functionally MDSCs.

G-MDSCs in circulation show higher level of pSTAT3

Recent clinical studies suggested that STAT3 contributes not only to MDSC expansion, as suggested by mouse tumor models, but plays a critical role for the expression of several mediators of immunosuppression (21, 27). Thus, we used flow cytometry to assess levels of activated and tyrosine-phosphorylated STAT3 (pSTAT3) in G-MDSCs during prostate cancer progression. As shown in Fig. 3A, $CD15^{HI}CD33^{LO}$ cells from patients with both localized and metastatic disease had elevated levels of intracellular pSTAT3 compared to control healthy subjects. These changes reflected increase STAT3 activation rather than upregulated expression of STAT3 total protein, which did not change between healthy subjects and prostate cancer patients (Fig. 3B). Importantly, the percentage of G-MDSCs with high STAT3 activity increased significantly during disease progression, reaching maximum in mCRPC patients (Fig. 3C). Next, we verified whether $pSTAT3^+$ granulocytic cells are present not only in circulation but also in the prostate cancer microenvironment. Sections of prostatectomy-derived tumors ($n = 10$) were stained using immunohistochemistry for pSTAT3, counterstained, and microscopically analyzed. $pSTAT3^+$ cells with PMN morphology were present in patients' samples and could be found in prostate tissues, including lumen of benign glands (Fig. 3D). Thus, we conclude that granulocytic $CD15^+/pSTAT3^+$ cells are commonly present in mCRPC patients' circulation and likely reach into the prostate tumor microenvironment.

Prostate cancer–associated G-MDSCs secrete high levels of Arginase-1

To assess whether G-MDSCs actively contribute to prostate cancer–associated immune evasion, we compared *iNOS*, *IDO*, or *ARG1* mRNA levels in $CD15^+/pSTAT3^+$ G-MDSCs sorted from cancer patients in comparison with $CD15^+/pSTAT3^-$ cells in healthy control subjects. The qPCR analysis indicated more than 100-fold increase in *ARG1* levels in cancer patients' samples (Fig. 4A). In contrast, the *IDO* mRNA increased only 5-fold while there was no effect on *iNOS* expression in the same group of samples. These results were further corroborated by measuring ARG1 enzymatic activity directly in cellular lysates prepared from $CD15^+CD14^-$ cells derived from metastatic prostate cancer patients versus healthy subjects. $CD15^+CD14^-$ cells from mCRPC patients showed about 10-fold increase in ARG1 activity compared with controls (Fig. 4B). In addition, the overall frequency of ARG1 expressing $CD15^{HI}CD33^{LO}$ G-MDSCs increased with progression of the disease (Fig. 4C) corresponding to the increase in the percentage of $CD15^+pSTAT3^+$ cells (Fig. 3C). At the same time, the intracellular levels of ARG1 protein were comparably high in G-MDSCs from patients with both localized and metastatic prostate cancers (Fig. 4D). These changes were paralleled by significantly elevated enzymatic activity of ARG1 in patients' plasma samples during disease progression. Compared with baseline levels in healthy controls, the ARG1 activity was doubled or tripled in patients with localized or metastatic tumors, respectively (Fig. 4E). Overall, these data implicate the role of ARG1 in

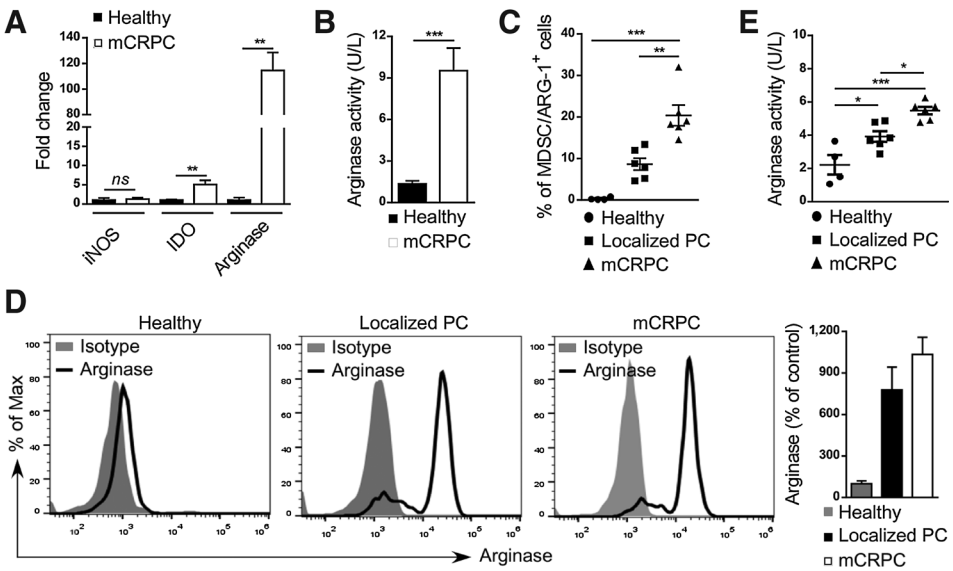

Figure 4.

The percentage of arginase-expressing MDSCs increases with prostate cancer progression. A and B, Arginase 1 expression and activity is highly elevated in G-MDSCs from mCRPC patients. Levels of *ARG1* mRNA in comparison with *IDO* and *iNOS* transcripts (A) as well as intracellular activity of Arginase 1 (B) were assessed in $CD15^+CD14^-$ G-MDSCs using real-time qPCR and QuantiChrom assays, respectively. Shown are means ± SD ($n = 4$). C, prostate cancer progression correlates with increase in the percentage of arginase-expressing $CD15^{HI}CD33^{LO}$ G-MDSCs. Flow cytometric analysis comparing PBMCs from healthy individuals ($n = 4$) with prostate cancer patients with localized disease ($n = 6$) or mCRPCs ($n = 6$); means ± SD. D, high intracellular levels of arginase expression in G-MDSCs from prostate cancer patients compared with granulocytes from healthy subjects as assessed using flow cytometry. Representative histograms (three left panels) and bar graph combining all data (right) from one of three experiments are shown; means ± SD. E, plasma levels of arginase activity increase with disease progression as measured in blood samples from healthy individuals ($n = 4$), prostate cancer patients with localized ($n = 6$) and metastatic disease ($n = 6$); means ± SD. Asterisks, statistically significant differences.

Published OnlineFirst May 12, 2015; DOI: 10.1158/1078-0432.CCR-14-3145

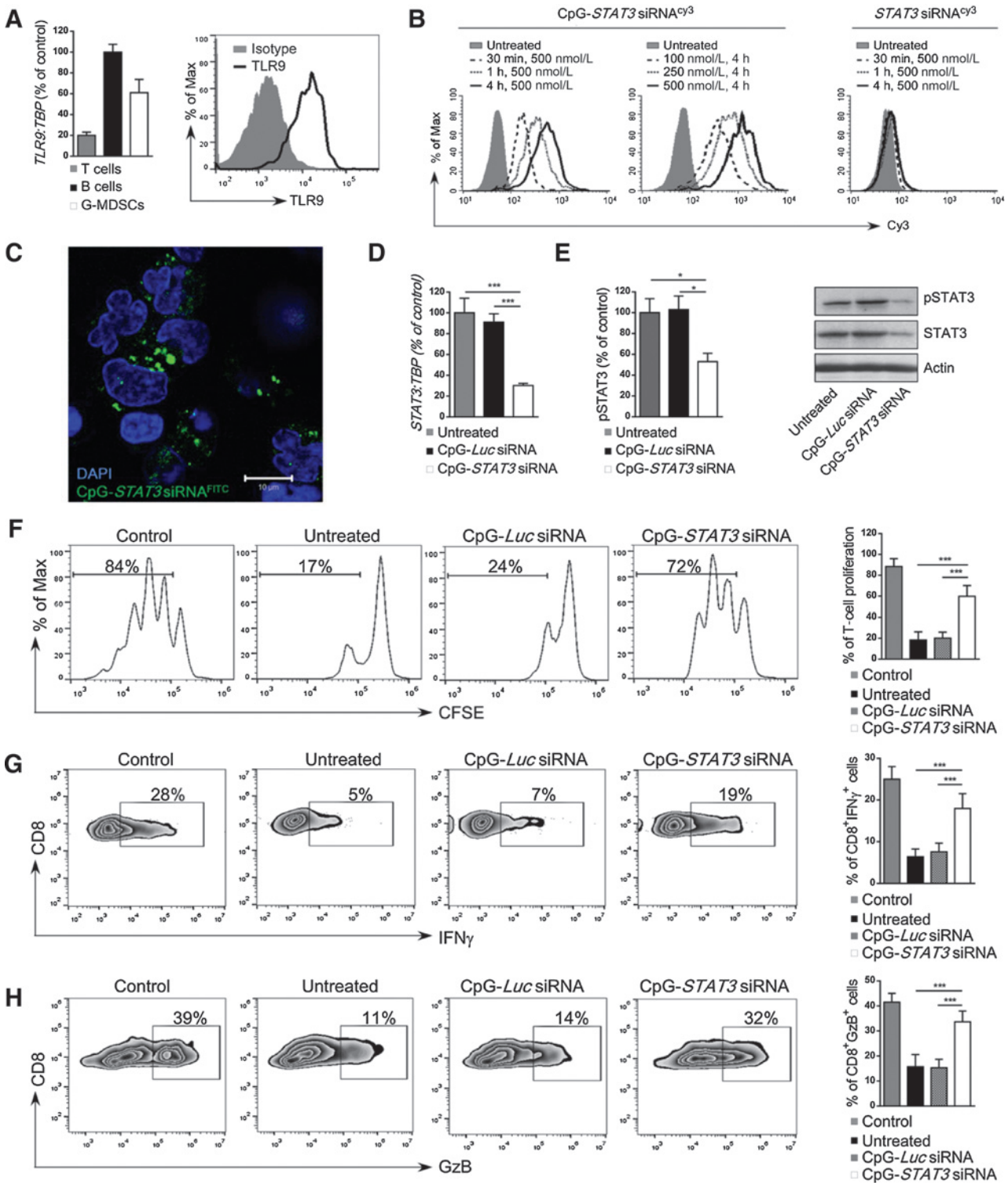

Figure 5.

Targeted STAT3 silencing using CpG-*STAT3*siRNA strategy abrogates immunosuppressive activity of granulocytic MDSCs. A, $CD15^{HI}CD33^{LO}$ G-MDSCs express TLR9 at mRNA or protein levels as assessed by using real-time qPCR (left) or flow cytometry (right), respectively. $CD19^{+}$ B cells and $CD3^{+}$ T cells were used as positive and negative controls for qPCR analysis (left), respectively. B, dose- and time-dependent internalization of CpG-*STAT3* siRNA by $CD15^{HI}CD33^{LO}$ MDSCs. PBMCs from prostate cancer patients were incubated with fluorescently-labeled CpG-*STAT3* $siRNA^{Cy3}$ conjugate or unconjugated *STAT3* $siRNA^{Cy3}$ for the indicated times and doses without any transfection reagents. (*Continued on the following page.*)

Published OnlineFirst May 12, 2015; DOI: 10.1158/1078-0432.CCR-14-3145

promoting and sustaining the immunosuppressive microenvironment in human prostate cancers.

Prostate cancer–associated G-MDSCs express TLR9 and are effectively targeted by CpG-*STAT3*siRNA conjugates

We previously demonstrated that ligands for the intracellular TLR9 receptor can deliver siRNA molecules into mouse and human target cells (23, 24). The unformulated CpG-siRNA conjugates silence specific genes both *in vitro* and *in vivo*. As verified using real-time qPCR, $CD15^{HI}CD33^{LO}$ G-MDSCs isolated from prostate cancer patients' blood express TLR9 at both mRNA and protein levels similar to B cells used as a positive control (Fig. 5A; ref. 24). Next, we determined whether G-MDSCs can internalize CpG-*STAT3*siRNA. PBMCs from late-stage prostate cancer patients were incubated for various times and doses with fluorescently labeled CpG-$siRNA^{Cy3}$ or unconjugated $siRNA^{Cy3}$ without any transfection reagents. Already after 30 minutes of incubation, the uptake of CpG-*STAT3*siRNA exceeded 80% of G-MDSCs and continued to increase with longer incubation times (Fig. 5B, left two panels). At 4 hours, the CpG-*STAT3*siRNA was internalized by the majority of cells already at the lowest 100 nmol/L concentration (Fig. 5B, middle). In contrast, the G-MDSCs did not internalize the unconjugated *STAT3*siRNA even after 4 hours of incubation at 500 nmol/L (Fig. 5B, right). Confocal microscopy studies showed perinuclear/cytoplasmic localization of the siRNA part of the molecule after uptake by target G-MDSCs (Fig. 5C). This is consistent with the TLR9-mediated mechanism of endosomal release of processed CpG-siRNA conjugates (23). Finally, we examined whether CpG-*STAT3*siRNA treatment will result in target gene silencing in G-MDSCs. Magnetically enriched G-MDSCs were incubated for 48 hours with 500 nmol/L CpG-siRNA conjugates targeting *STAT3* or *luciferase* genes, the latter being used as a negative, nontargeting control. Both *STAT3* expression and pSTAT3 levels were assessed using qPCR and flow cytometry together with western blotting. CpG-*STAT3* siRNA treatment reduced *STAT3* mRNA expression by approximately 70% (Fig. 5D) and as a result also STAT3 phosphorylation and total protein levels (Fig. 5E). Importantly, STAT3 inhibition did not affect G-MDSC viability as verified by flow cytometry (Supplementary Fig. S6). Next, we determined the effect of CpG-*STAT3*siRNA on immunosuppressive functions of G-MDSCs. The isolated $CD15^+CD14^-$ cells were pretreated using CpG-*STAT3* siRNA or control CpG-*Luc* siRNA overnight and then cocultured with autologous $CD3^+$ T cells (1:1 ratio) with CD3/CD28 costimulation for additional 72 hours. As shown in Fig. 5F, CpG-*STAT3* siRNA alleviated most of the G-MDSC–mediated effect on T-cell proliferation. Under the same experimental conditions, we analyzed IFNγ and granzyme B production by $CD8^+$ T cells. Both IFNγ (Fig. 5G) and granzyme B (Fig. 5H) expression levels were restored to approximately 70% and approximately 80% of control levels, respectively, after STAT3 blocking in G-MDSCs using CpG-*STAT3*siRNA. Overall, these results suggest the feasibility of using CpG-*STAT3*siRNA strategy for functional depletion of prostate cancer–associated MDSCs.

CpG-*STAT3*siRNA blocks ARG1 production and impairs G-MDSC activity

To gain insights into the mechanism(s) of G-MDSCs loss of function, we assessed the effect of STAT3 inhibition on ARG1 expression. $CD15^+CD14^-$ cells were isolated from late-stage prostate cancer PBMCs and cultured for 48 hours in the presence of 500 nmol/L CpG-*STAT3*siRNA or CpG-*Luc*siRNA. As assessed using flow cytometric and colorimetric assays, both ARG1 expression (Fig. 6A) and enzymatic activity (Fig. 6B) were reduced by approximately 60% in G-MDSCs following *STAT3* silencing. To verify whether ARG1 actually contributes to STAT3-mediated suppression of T-cell activity by G-MDSCs, we repeated T-cell proliferation assays using specific inhibitor of arginase activity (nor-NOHA; ref. 21). Prostate cancer-derived G-MDSCs ($CD15^+CD14^-$) were pretreated with nor-NOHA alone, CpG-*STAT3* siRNA alone, or both reagents combined and then cocultured with autologous T cells with CD3/CD28-mediated stimulation (Fig. 6C). As expected, G-MDSCs treated with nor-NOHA used as a single agent reduced by about half the immunosuppressive effect of G-MDSCs on T-cell proliferation (Fig. 6D). However, STAT3 blocking using CpG-siRNA alone eliminated most of the G-MDSC effect while the combination with nor-NOHA didn't improve this effect any further (Fig. 6D). Overall, these studies provide a proof-of-principle for targeting immunosuppressive STAT3–ARG1 signaling axis in G-MDSCs as a potential therapeutic strategy to disrupt the immunosuppressive microenvironment in prostate cancers.

Discussion

Here, we provide the first evidence of $TLR9^+$ granulocytic MDSCs that accumulate in prostate cancer patients in correlation with disease progression. We also document that these prostate cancer–associated G-MDSCs require high levels of immunosuppressive STAT3 signaling and Arginase-1 activity protein for suppressing effector T-cell activity. While our results are based on limited number of patients, pSTAT3-positive granulocytic cells were consistently found not only in blood but also patients' prostatectomy specimens. Finally, we suggest therapeutic strategy for the functional elimination of G-MDSCs using CpG oligonucleotide-mediated delivery of *STAT3* siRNA into these $TLR9^+$ myeloid cells. Overall, our findings indicate new and potentially safer therapeutic approach to mitigate immunosuppression in

(*Continued.*) Percentages of $Cy3^+$ $CD15^{HI}CD33^{LO}$ MDSCs were assessed by flow cytometry; shown are representative results from one of three experiments. C, *STAT3* siRNA localizes to perinuclear/cytoplasmic cell compartment shortly after internalization. G-MDSCs ($CD15^+CD14^-$) enriched from mCRPC patients were incubated with 500 nmol/L CpG-*STAT3*$siRNA^{FITC}$ for 1 hour. The localization of the labeled siRNA part of the conjugate was assessed using confocal microscopy; scale bar, 10 μm. D and E, CpG-*STAT3* siRNA induces *STAT3* silencing in fresh granulocytic MDSCs. The G-MDSCs enriched from prostate cancer patients' PBMCs were treated with 500 nmol/L CpG-*STAT3* siRNA or CpG-*Luc* siRNA, used as a negative control, for 48 hours. The level of STAT3 inhibition was measured at mRNA level (D) using real-time qPCR or at protein level using flow cytometry (E, left) or Western blotting (E, right) after staining with antibodies specific to pSTAT3 and/or total STAT3. Asterisks, statistically significant differences; shown are means ± SD ($n = 5$). F to H, $CD15^+CD14^-$ MDSCs isolated from prostate cancer patients were treated with CpG-*STAT3* siRNA or control CpG-*Luc* siRNA for 18 hours and then cocultured with autologous $CD3^+$ T cells at 1:1 ratio with anti-CD3/CD28 stimulation. F, T-cell proliferation was determined by CFSE dilution assay after 72 hours of coculture with fresh MDSC. Under same experimental conditions percentages of IFNγ- (G) or granzyme B- (H) producing $CD8^+$ T cells were assessed using flow cytometry. Shown are representative data from one of two experiments (left four panels) and bar graphs (right) combining results from analyses of 5 individual patients' samples; means ± SD. Asterisks, statistically significant differences.

Published OnlineFirst May 12, 2015; DOI: 10.1158/1078-0432.CCR-14-3145

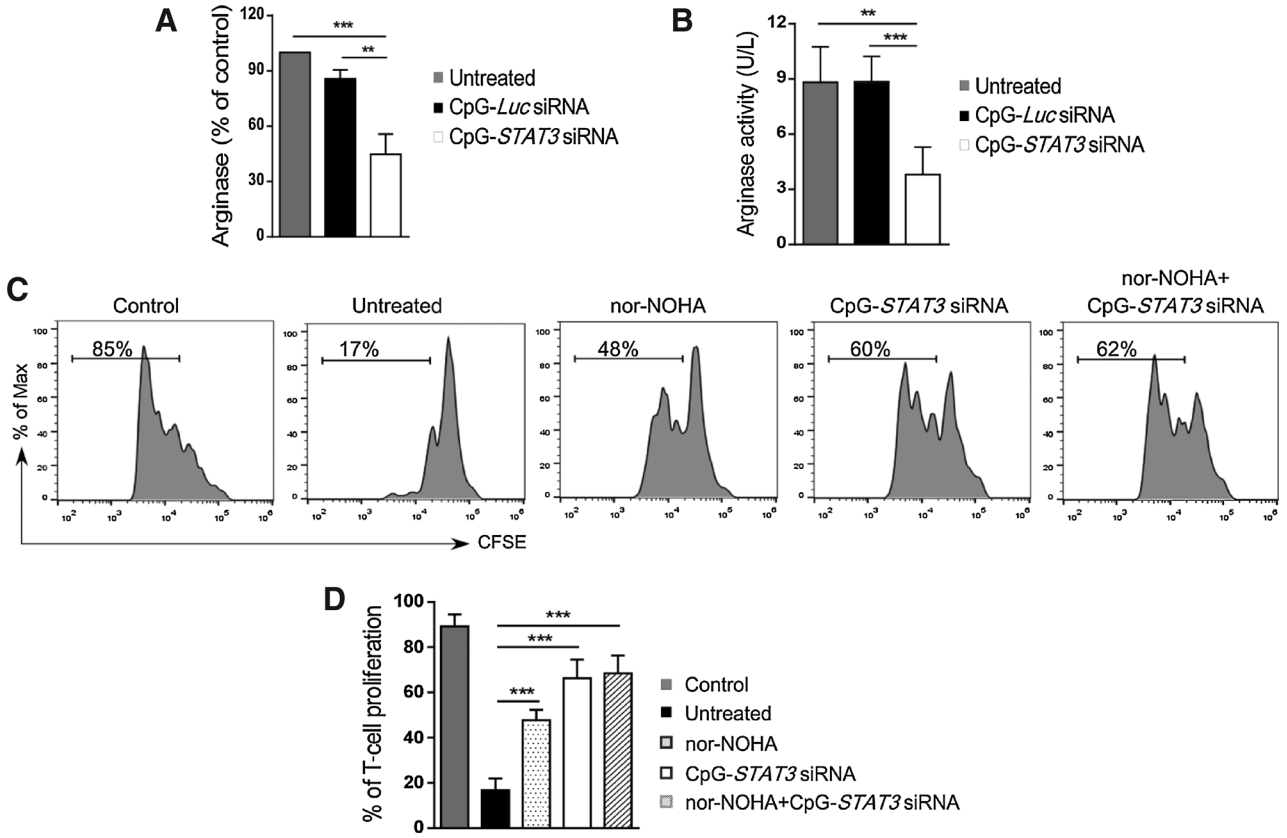

Figure 6.
CpG-*STAT3* siRNA blocks arginase expression and inhibits functions of granulocytic MDSCs. A and B, STAT3 targeting using CpG-siRNA strategy inhibits arginase expression and activity in granulocytic MDSCs. Levels of arginase mRNA (A) and enzymatic activity (B) were assessed in cell lysates using qPCR and QuantiChrom assays, respectively, in $CD15^{+}CD14^{-}$ granulocytic MDSCs after 48 hours of incubation with CpG-*STAT3* siRNA, CpG-*Luc* siRNA, or without any treatment. C and D, selective STAT3 inhibition alleviates immunosuppressive effect of MDSCs to greater extent than arginase inhibitor (nor-NOHA). Representative data from one of two experiments (C) and the summary of T-cell proliferation assays (D) cocultured in the presence or absence of MDSCs, nor-NOHA (20 μmol/L) and the indicated CpG-siRNAs (500 nmol/L). Shown are means ± SD ($n = 5$). Asterisks, statistically significant differences.

prostate cancer patients using gene- and cell type-specific inhibitory oligonucleotides.

The relevance of these results for human cancer therapy is underscored by the lack of clinically relevant strategies for eliminating MDSC-dependent immune evasion. In contrast to results of preclinical studies in mice (28), with notable exception of sunitinib effect in renal cancer patients, current cancer therapies usually fail to reduce the elevated levels of MDSCs (Supplementary Fig. S4; refs. 8, 15, 18). The G-MDSCs were found in circulation of patients with other genitourinary malignancies, such as renal and bladder cancers and several different solid tumors (11, 13, 15, 16). However, due to complex pattern of surface molecules, partly overlapping with other immune cell lineages, targeting MDSCs through antibody-mediated depletion is challenging. Successful targeting of MDSCs requires identification of functional markers associated with the tumor microenvironment, as shown by promising preclinical results on targeting CXCR2-mediated MDSC tumor trafficking (17). Our findings suggest that intracellular signaling mediators of immunosuppression may provide alternative and even more precise functional MDSC biomarkers. This is of importance given the difficulty in identifying MDSCs among other immune cell populations using surface markers or nuclear morphology, as in case of discerning G-MDSCs from mature neutrophils (29, 30). Thus, the contribution of mature neutrophils to the overall immunosuppressive effect cannot be excluded (29). The constitutive activation of STAT3, a known master regulator of immunosuppression, was lately reported in MDSCs associated with several types of human cancers, such as melanoma, head and neck, renal, breast, and pancreatic cancers (15, 21, 27, 31–33). Correspondingly, we have found that majority of granulocytic cells that were infiltrating prostate tissues showed activation of STAT3. These observations merit further studies in a larger set of specimens to validate whether the presence of $CD15^{+}$/$pSTAT3^{+}$ and/or $CD15^{+}$/$ARG1^{+}$ cells can serve as an indicator of the G-MDSC-induced immunosuppressive microenvironment in prostate cancers. It is known that immunosuppressive activity of G-MDSCs depends mainly on Arginase-1 expression rather than iNOS activity for their function (19). This is consistent with our data from patients' G-MDSCs, in comparison with normal granulocytic cells, that showed highly elevated levels of *ARG1*, weak induction of *IDO* and no detectable effect on *iNOS* expression. These results seem to reflect different level of STAT3 involvement in the regulation of these target genes. In MDSCs, STAT3 was shown to have potent and direct effect on *ARG1*, while it collaborates with noncanonical NF-κB signaling to promote *IDO* expression (19, 21, 32). In contrast, STAT3 activity is

not required for *iNOS* expression which is driven by STAT1 and NF-κB signaling activated in monocytic MDSCs but not in G-MDSCs (19).

TLR9 was recently found to be expressed by tumor-associated MDSCs in mice, with its highest levels observed in M-MDSCs (34, 35). This is consistent with the common expression of TLR9 in mouse myeloid cells (36). Although TLR9 expression in humans is more restricted than in mice, recent studies reported that environmental factors such as GM-CSF can induce TLR9 in differentiating monocytes and neutrophils (24, 37, 38). TLR9 expression in prostate cancer patients' G-MDSCs is likely associated with the multiple soluble factors released from the tumor microenvironment (Fig. 1G). Downstream TLR9 signaling through MyD88 and NF-κB contributes to myeloid cell-driven inflammatory responses in reaction to tissue stress and injury (39–41). Interestingly, two reports showed that intratumoral injections of high doses of synthetic TLR9 agonists, CpG oligodeoxynucleotides (ODN), can trigger MDSC differentiation and reduce their immunosuppressive potential in mice (34, 35). These effects were suggested to be either direct or mediated through activation of plasmacytoid DCs and production of type I IFNs. However, numerous clinical trials using CpG ODNs proved that generation of systemic antitumor immune responses is challenging due to immunosuppressive effects of the tumor microenvironment (42). Other studies in mouse tumor models showed that activation of TLRs in myeloid cells can in fact promote expression of immunosuppressive molecules critical for MDSC function, such as Arginase-1, S100A8, IL10, and PGE_2 (19, 43–45). The functional dichotomy of TLR9 effects results from cross-talk with other signaling pathways operating under normal or tumor-induced inflammatory conditions. The outcome of TLR9 signaling seems to be defined by a multilayered negative feedback regulation through STAT3 (41, 46). Our own studies in mouse solid tumor models revealed that preexisting STAT3 activity in tumor-associated myeloid cells, such as macrophages and MDSCs, can skew TLR9 signaling toward supporting tumor angiogenesis while blocking antitumor immunity (25, 46). Whether TLR9 contributes to immunosuppressive potential of prostate cancer–associated MDSCs remains to be established in more extensive molecular studies.

STAT3 provides an attractive therapeutic target in tumor-associated myeloid cells (20, 41). At the same time, the role of STAT3 signaling in T lymphocytes is complex. While STAT3 reduces antitumor activity of effector CD8 T cells and promotes generation of tumor-promoting Th17 cells, it is also necessary for the generation of memory T cells and prolonged antitumor immune responses (47–49). Thus, targeting STAT3 for cancer immunotherapy requires myeloid cell-specific strategies to avoid unpredictable adverse effects and toxicities. For example, recent study in mouse melanoma models demonstrated that small-molecule drug targeting upstream STAT3 activators, JAK1/2 kinases, reduced numbers of MDSCs while increasing their immunosuppressive potential and blocking T-cell proliferation (50). We previously demonstrated that TLR9 agonists, CpG ODN, can be utilized for delivery of therapeutic siRNA molecules into $TLR9^+$ cells in both mouse and human systems (23, 24). Targeting STAT3 with parallel TLR9 activation using CpG-*STAT3*siRNA was shown to eliminate tumorigenic effects of TLR signaling in mouse tumor models (25). Here, we demonstrated that CpG-siRNA strategy allows for targeting of $TLR9^+$ G-MDSCs to eliminate their immunosuppressive functions without myeloid cell depletion. Further studies should determine whether CpG-*STAT3*siRNA only modulates G-MDSC activity or induces their differentiation into mature granulocytes or DCs/macrophages. Correspondingly, we previously observed that CpG-STAT3siRNA induces activity of neutrophils against blood cancer xenotransplants in NSG mice (24). Independently from this article, we recently identified that prostate cancer propagating cells in human tumors express TLR9 and it is feasible to target this cancer cell population using CpG-siRNA approach (Moreira and Kortylewski; unpublished results). Taken together, our findings provide support for application of CpG-*STAT3*siRNA strategy to immunotherapy of advanced prostate cancers alone or in combination with immunotherapies, such as Sipuleucel-T treatment or emerging T cell-based therapies. Disruption of STAT3 signaling in the tumor microenvironment with concurrent TLR9 stimulation has potential to disrupt the central immunosuppressive circuit paving way to effective antitumor immune responses without toxicities associated with pharmacologic agents.

Disclosure of Potential Conflicts of Interest

No potential conflicts of interest were disclosed.

Disclaimer

The content of this article is solely the responsibility of the authors and does not necessarily represent the official views of the NIH.

Authors' Contributions

Conception and design: D.M.S. Hossain, S.K. Pal, J. Jones, M. Kortylewski
Development of methodology: D.M.S. Hossain, D. Moreira, M. Kortylewski
Acquisition of data (provided animals, acquired and managed patients, provided facilities, etc.): D.M.S. Hossain, D. Moreira, P. Duttagupta, Q. Zhang, M. D'Apuzzo, M. Kortylewski
Analysis and interpretation of data (e.g., statistical analysis, biostatistics, computational analysis): D.M.S. Hossain, D. Moreira, H. Won, M. D'Apuzzo, M. Kortylewski
Writing, review, and/or revision of the manuscript: D.M.S. Hossain, S.K. Pal, D. Moreira, P. Duttagupta, H. Won, J. Jones, S. Forman, M. Kortylewski
Administrative, technical, or material support (i.e., reporting or organizing data, constructing databases): D.M.S. Hossain, S.K. Pal, M. Kortylewski
Study supervision: S.K. Pal, M. Kortylewski

Acknowledgments

The authors thank Dr. Robert Hickey (Translational Biomarker Discovery Core) and acknowledge the dedication of staff members at the Analytical Cytometry, Microscopy, Pathology Core Facilities, Animal Resource Center and at COH. This work was supported in part by the National Cancer Institute of the NIH award number R01CA155367, the Department of Defense grant W81XWH-12-1-0132, the Movember-Prostate Cancer Foundation Award, STOP CANCER Foundation Allison Tovo-Dwyer Memorial Career Development Award (to M. Kortylewski) and by the National Cancer Institute Grant P30 CA033572 (to COH).

The costs of publication of this article were defrayed in part by the payment of page charges. This article must therefore be hereby marked *advertisement* in accordance with 18 U.S.C. Section 1734 solely to indicate this fact.

Received December 4, 2014; revised April 3, 2015; accepted April 21, 2015; published OnlineFirst May 12, 2015.

References

1. Jemal A, Siegel R, Xu J, Ward E. Cancer statistics, 2010. CA Cancer J Clin 2010;60:277–300.
2. de Bono JS, Oudard S, Ozguroglu M, Hansen S, Machiels JP, Kocak I, et al. Prednisone plus cabazitaxel or mitoxantrone for metastatic castration-

resistant prostate cancer progressing after docetaxel treatment: a randomised open-label trial. Lancet 2010;376:1147–54.
3. Kantoff PW, Higano CS, Shore ND, Berger ER, Small EJ, Penson DF, et al. Sipuleucel-T immunotherapy for castration-resistant prostate cancer. N Engl J Med 2010;363:411–22.
4. Whiteside TL. Inhibiting the inhibitors: evaluating agents targeting cancer immunosuppression. Expert Opin Biol Ther 2010;10:1019–35.
5. May KF Jr, Gulley JL, Drake CG, Dranoff G, Kantoff PW. Prostate cancer immunotherapy. Clin Cancer Res 2011;17:5233–8.
6. Sottnik JL, Zhang J, Macoska JA, Keller ET. The PCa tumor microenvironment. Cancer Microenviron 2011;3:283–97.
7. Topalian SL, Hodi FS, Brahmer JR, Gettinger SN, Smith DC, McDermott DF, et al. Safety, activity, and immune correlates of anti-PD-1 antibody in cancer. N Engl J Med 2012;366:2443–54.
8. Gabrilovich DI, Ostrand-Rosenberg S, Bronte V. Coordinated regulation of myeloid cells by tumours. Nat Rev Immunol 2012;12:253–68.
9. Diaz-Montero CM, Salem ML, Nishimura MI, Garrett-Mayer E, Cole DJ, Montero AJ. Increased circulating myeloid-derived suppressor cells correlate with clinical cancer stage, metastatic tumor burden, and doxorubicin-cyclophosphamide chemotherapy. Cancer Immunol Immunother 2009;58:49–59.
10. Greten TF, Manns MP, Korangy F. Myeloid derived suppressor cells in human diseases. Int Immunopharmacol 2011;11:802–7.
11. Youn JI, Kumar V, Collazo M, Nefedova Y, Condamine T, Cheng P, et al. Epigenetic silencing of retinoblastoma gene regulates pathologic differentiation of myeloid cells in cancer. Nat Immunol 2013;14:211–20.
12. Vuk-Pavlovic S, Bulur PA, Lin Y, Qin R, Szumlanski CL, Zhao X, et al. Immunosuppressive CD14+HLA-DRlow/− monocytes in prostate cancer. Prostate 2009;70:443–55.
13. Kusmartsev S, Su Z, Heiser A, Dannull J, Eruslanov E, Kubler H, et al. Reversal of myeloid cell-mediated immunosuppression in patients with metastatic renal cell carcinoma. Clin Cancer Res 2008;14:8270–8.
14. Rodriguez PC, Ernstoff MS, Hernandez C, Atkins M, Zabaleta J, Sierra R, et al. Arginase I-producing myeloid-derived suppressor cells in renal cell carcinoma are a subpopulation of activated granulocytes. Cancer Res 2009;69:1553–60.
15. Ko JS, Zea AH, Rini BI, Ireland JL, Elson P, Cohen P, et al. Sunitinib mediates reversal of myeloid-derived suppressor cell accumulation in renal cell carcinoma patients. Clin Cancer Res 2009;15:2148–57.
16. Eruslanov E, Neuberger M, Daurkin I, Perrin GQ, Algood C, Dahm P, et al. Circulating and tumor-infiltrating myeloid cell subsets in patients with bladder cancer. Int J Cancer 2012;130:1109–19.
17. Highfill SL, Cui Y, Giles AJ, Smith JP, Zhang H, Morse E, et al. Disruption of CXCR2-mediated MDSC tumor trafficking enhances anti-PD1 efficacy. Sci Transl Med 2014;6:237ra67.
18. Pal SK, Sakib Hossain DM, Zhang Q, Frankel PH, Jones JO, Carmichael C, et al. Pazopanib as third-line therapy for metastatic renal cell carcinoma: clinical efficacy and temporal analysis of cytokine profile. J Urol 2014;14:4591–1.
19. Gabrilovich DI, Nagaraj S. Myeloid-derived suppressor cells as regulators of the immune system. Nat Rev Immunol 2009;9:162–74.
20. Yu H, Kortylewski M, Pardoll D. Crosstalk between cancer and immune cells: role of STAT3 in the tumour microenvironment. Nat Rev Immunol 2007;7:41–51.
21. Vasquez-Dunddel D, Pan F, Zeng Q, Gorbounov M, Albesiano E, Fu J, et al. STAT3 regulates arginase-I in myeloid-derived suppressor cells from cancer patients. J Clin Invest 2013;123:1580–9.
22. Wesolowski R, Markowitz J, Carson WE III. Myeloid derived suppressor cells - a new therapeutic target in the treatment of cancer. J Immunother Cancer 2013;1:10.
23. Kortylewski M, Swiderski P, Herrmann A, Wang L, Kowolik C, Kujawski M, et al. *In vivo* delivery of siRNA to immune cells by conjugation to a TLR9 agonist enhances antitumor immune responses. Nat Biotechnol 2009;27:925–32.
24. Zhang Q, Hossain DM, Nechaev S, Kozlowska A, Zhang W, Liu Y, et al. TLR9-mediated siRNA delivery for targeting of normal and malignant human hematopoietic cells *in vivo*. Blood 2013;121:1304–15.
25. Gao C, Kozlowska A, Nechaev S, Li H, Zhang Q, Hossain DM, et al. TLR9 signaling in the tumor microenvironment initiates cancer recurrence after radiotherapy. Cancer Res 2013;73:7211–21.
26. Waight JD, Hu Q, Miller A, Liu S, Abrams SI. Tumor-derived G-CSF facilitates neoplastic growth through a granulocytic myeloid-derived suppressor cell-dependent mechanism. PLoS One 2011;6:e27690.
27. Poschke I, Mougiakakos D, Hansson J, Masucci GV, Kiessling R. Immature immunosuppressive CD14+HLA-DR-/low cells in melanoma patients are Stat3hi and overexpress CD80, CD83, and DC-sign. Cancer Res 2010;70:4335–45.
28. Kodumudi KN, Woan K, Gilvary DL, Sahakian E, Wei S, Djeu JY. A novel chemoimmunomodulating property of docetaxel: suppression of myeloid-derived suppressor cells in tumor bearers. Clin Cancer Res 2010;16:4583–94.
29. Brandau S, Moses K, Lang S. The kinship of neutrophils and granulocytic myeloid-derived suppressor cells in cancer: cousins, siblings or twins? Semin Cancer Biol 2013;23:171–82.
30. Pillay J, Kamp VM, van Hoffen E, Visser T, Tak T, Lammers JW, et al. A subset of neutrophils in human systemic inflammation inhibits T cell responses through Mac-1. J Clin Invest 2012;122:327–36.
31. Mace TA, Ameen Z, Collins A, Wojcik S, Mair M, Young GS, et al. Pancreatic cancer-associated stellate cells promote differentiation of myeloid-derived suppressor cells in a STAT3-dependent manner. Cancer Res 2013;73:3007–18.
32. Yu J, Wang Y, Yan F, Zhang P, Li H, Zhao H, et al. Noncanonical NF-kappaB activation mediates STAT3-stimulated IDO upregulation in myeloid-derived suppressor cells in breast cancer. J Immunol 2014;193:2574–86.
33. Waight JD, Netherby C, Hensen ML, Miller A, Hu Q, Liu S, et al. Myeloid-derived suppressor cell development is regulated by a STAT/IRF-8 axis. J Clin Invest 2013;123:4464–78.
34. Zoglmeier C, Bauer H, Norenberg D, Wedekind G, Bittner P, Sandholzer N, et al. CpG blocks immunosuppression by myeloid-derived suppressor cells in tumor-bearing mice. Clin Cancer Res 2011;17:1765–75.
35. Shirota Y, Shirota H, Klinman DM. Intratumoral injection of CpG oligonucleotides induces the differentiation and reduces the immunosuppressive activity of myeloid-derived suppressor cells. J Immunol 2012;188:1592–9.
36. Hemmi H, Takeuchi O, Kawai T, Kaisho T, Sato S, Sanjo H, et al. A Toll-like receptor recognizes bacterial DNA. Nature 2000;408:740–5.
37. Hayashi F, Means TK, Luster AD. Toll-like receptors stimulate human neutrophil function. Blood 2003;102:2660–9.
38. Hoene V, Peiser M, Wanner R. Human monocyte-derived dendritic cells express TLR9 and react directly to the CpG-A oligonucleotide D19. J Leukoc Biol 2006;80:1328–36.
39. Trinchieri G, Sher A. Cooperation of Toll-like receptor signals in innate immune defence. Nat Rev Immunol 2007;7:179–90.
40. Kawai T, Akira S. The role of pattern-recognition receptors in innate immunity: update on Toll-like receptors. Nat Immunol 2010;11:373–84.
41. Murray PJ, Smale ST. Restraint of inflammatory signaling by interdependent strata of negative regulatory pathways. Nat Immunol 2012;13:916–24.
42. Krieg AM. CpG still rocks! Update on an accidental drug. Nucleic Acid Ther 2012;22:77–89.
43. El Kasmi KC, Qualls JE, Pesce JT, Smith AM, Thompson RW, Henao-Tamayo M, et al. Toll-like receptor-induced arginase 1 in macrophages thwarts effective immunity against intracellular pathogens. Nat Immunol 2008;9:1399–406.
44. Parker KH, Sinha P, Horn LA, Clements VK, Yang H, Li J, et al. HMGB1 enhances immune suppression by facilitating the differentiation and suppressive activity of myeloid-derived suppressor cells. Cancer Res 2014;74:5723–33.
45. Hsu K, Chung YM, Endoh Y, Geczy CL. TLR9 ligands induce S100A8 in macrophages via a STAT3-dependent pathway which requires IL-10 and PGE2. PLoS ONE 2014;9:e103629.
46. Kortylewski M, Kujawski M, Herrmann A, Yang C, Wang L, Liu Y, et al. Toll-like receptor 9 activation of signal transducer and activator of transcription 3 constrains its agonist-based immunotherapy. Cancer Res 2009;69:2497–505.
47. Kujawski M, Zhang C, Herrmann A, Reckamp K, Scuto A, Jensen M, et al. Targeting STAT3 in adoptively transferred T cells promotes their *in vivo* expansion and antitumor effects. Cancer Res 2010;70:9599–610.
48. Wang L, Yi T, Kortylewski M, Pardoll DM, Zeng D, Yu H. IL-17 can promote tumor growth through an IL-6-Stat3 signaling pathway. J Exp Med 2009;206:1457–64.
49. Kaech SM, Cui W. Transcriptional control of effector and memory CD8+ T cell differentiation. Nat Rev Immunol 2012;12:749–61.
50. Maenhout SK, Du Four S, Corthals J, Neyns B, Thielemans K, Aerts JL. AZD1480 delays tumor growth in a melanoma model while enhancing the suppressive activity of myeloid-derived suppressor cells. Oncotarget 2014;5:6801–15.

AACR American Association for Cancer Research

Clinical Cancer Research

TLR9-Targeted STAT3 Silencing Abrogates Immunosuppressive Activity of Myeloid-Derived Suppressor Cells from Prostate Cancer Patients

Dewan M. S. Hossain, Sumanta K. Pal, Dayson Moreira, et al.

Clin Cancer Res Published OnlineFirst May 12, 2015.

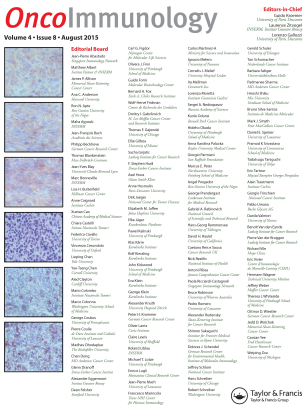

OncoImmunology
Publication details, including instructions for authors and subscription information:
http://www.tandfonline.com/loi/koni20

Breaking Bad Habits: Targeting MDSCs to Alleviate Immunosuppression in Prostate Cancer

Sumanta K. Pal[a] & Marcin Kortylewski[b]

[a] Department of Cancer Immunotherapeutics & Tumor Immunology

[b] Department of Medical Oncology & Experimental Therapeutics at Beckman Research Institute, City of Hope National Medical Center, Duarte, CA 91010, USA

Accepted author version posted online: 24 Aug 2015.

Breaking Bad Habits: Targeting MDSCs to Alleviate Immunosuppression in Prostate Cancer

Sumanta K. Pal[1] and Marcin Kortylewski[2]*,

[1]Department of Cancer Immunotherapeutics & Tumor Immunology; [2]Department of Medical Oncology & Experimental Therapeutics at Beckman Research Institute, City of Hope National Medical Center, Duarte, CA 91010, USA

Keywords: MDSC, myeloid-derived suppressor cells, TLR9, STAT3, arginase, prostate cancer, immunotherapy

**Author for correspondence:*
Marcin Kortylewski, Ph.D., 1500 East Duarte Rd., Duarte, CA 91010;
phone: (626) 218-4120; fax: (626) 471-3602; e-mail: mkortylewski@coh.org

Abstract

The myeloid-derived suppressor cells (MDSCs) contribute to tumor immune evasion and still remain an elusive therapeutic target. Our study identified granulocytic MDSCs accumulating in prostate cancer patients during disease progression. We demonstrate the feasibility of using STAT3siRNA-based strategy for targeting MDSCs to alleviate arginase-dependent suppression of T cell activity.

Metastatic castration-resistant prostate cancers are known for being resistant to current standard therapies and even to the emerging immunotherapeutic regimens. Growing evidence suggests that advanced prostate cancers develop potently immunosuppressive microenvironment which partly relies on the heterogeneous population of myeloid-derived suppressor cells (MDSCs). The MDSCs play pivotal role in cancer progression and poor patients' survival.[1] The MDSCs are immature myeloid cells which lack expression of multiple immune cell surface markers, including antigen-presenting molecules. Depending on the expression of myeloid lineage markers, human MDSCs can be divided into $CD14^{+}CD15^{LO}CD33^{HI}$ monocytic MDSCs (M-MDSCs) and $CD14^{-}CD15^{HI}CD33^{LO}$ granulocytic MDSCs (G-MDSCs).[1] The M-MDSCs were previously found in prostate cancer patients and their levels correlated with levels of PSA used as a marker of tumor burden.[2] Even though G-MDSCs were recently observed in other genitourinary tumors, the contribution of G-MDSCs to prostate cancer progression remained unknown.

Our recently published study focused on the phenotypic analysis of immune cell populations in blood derived from patients with localized or metastatic prostate cancers compared to healthy subjects.[3] In contrast to earlier studies, our flow cytometric analysis revealed significant accumulation of granulocytic ($CD15^{HI}CD33^{LO}$) but not monocytic ($CD15^{LO}CD33^{HI}$) cell populations in patients' circulation with progression of the disease. Further studies of both myeloid cell populations confirmed that only $CD15^{HI}CD33^{LO}$ myeloid cells were functionally MDSCs as indicated by their potent inhibitory effect on T cell proliferation and activity. Due to complex identification which relies on markers common to other immune cell lineages, eliminating MDSCs using monoclonal antibodies is challenging. Thus, it seems more practical to target signaling molecules which control MDSC function in the specific tumor microenvironment. Our analysis of cytokine and growth factor (GF) profiles revealed elevated levels of factors related to recruitment and expansion of myeloid cells, such as G-CSF and IL-8 among others. Given the critical role of STAT3 transcription factor in the downstream signaling of G-CSF as well as other GFs present in the tumor microenvironment[3], we assessed levels of activated STAT3 (pSTAT3) in prostate cancer-associated G-MDSCs using flow cytometric and immunohistochemical analyses. We observed elevated pSTAT3 in circulating G-MDSCs and also in polymorphonuclear cells infiltrating prostate tissue biopsies from cancer patients. In addition, STAT3 activation clearly correlated with high levels of Arginase-1 (ARG1) expression in G-MDSCs compared to healthy granulocytes, and also with detectable ARG1 activity in blood samples from cancer patients. Highly elevated levels of ARG1 in G-MDSCs with weak induction of *IDO* and undetectable *iNOS* mRNA expression likely reflected different levels of STAT3 involvement in the regulation of these target genes. In G-MDSCs, STAT3 was shown to have potent and direct effect on ARG1, while it collaborates with noncanonical NF-κB signaling to promote IDO expression. In contrast, STAT3 activity is not required for iNOS expression which is driven by STAT1 and NF-κB signaling activated in monocytic MDSCs but not in G-MDSCs.[1] Altogether, these observations strengthened the evidence that G-MDSCs are commonly present in prostate cancer patients' circulation and likely reach into the prostate tumor microenvironment.

TLR9 was recently found to be expressed by tumor-associated MDSCs in mice, with its highest levels observed in M-MDSCs.[4] However, the pattern of TLR9 expression differs dramatically between mouse and human immune systems. While in mice TLR9 is ubiquitous in myeloid cells, it is expressed specifically by human plasmacytoid

DCs in healthy subjects.[5] Thus, the expression of TLR9 in prostate cancer patients' MDSCs and specifically in G-MDSCs was a novel finding of our study. Whether downstream TLR9 signaling restricts or supports the immunosuppressive functions of G-MDSCs remains unclear. Treatments with synthetic TLR9 agonists, CpG oligodeoxynucleotides (ODN), can trigger MDSC differentiation and reduce their immunosuppressive potential in mice.[4] However, other studies suggested that activation of TLRs in myeloid cells can promote expression of molecules critical for MDSC function, such as ARG1, S100A8, IL-10 and PGE2.[1] The functional dichotomy of TLR9 effects results from crosstalk with other signaling pathways operating under normal or tumor-induced inflammatory conditions. The outcome of TLR9 signaling seems to be defined by a multilayered negative feedback regulation through STAT3 regardless whether it is triggered by synthetic ligands or release of natural agonists (e.g. mitochondrial DNA) from dying cells.[6, 7]

We previously demonstrated that TLR9 agonists, CpG ODN, can be harnessed for delivery of therapeutic siRNA molecules into $TLR9^+$ cells in both mouse and human systems.[8, 9] Targeting STAT3 with simultanous TLR9 activation using CpG-STAT3siRNA was shown to eliminate tumorigenic effects of TLR9 signaling in mouse tumor models.[7] Here, we demonstrated that CpG-STAT3siRNA allows for targeting of $TLR9^+$ G-MDSCs to eliminate their immunosuppressive functions without myeloid cell depletion. Further studies should determine whether our approach only modulates G-MDSC activity or induces their differentiation into mature granulocytes or DCs/macrophages. In fact, we previously observed that CpG-STAT3siRNA induces activity of neutrophils against blood cancer xenotransplants in NSG mice.[9] In a parallel study, we recently identified that prostate cancer stem cells in human tumors rely on TLR9 signaling through NF-κB and STAT3 signaling crucial for their self-renewal and tumor-propagating potential. We demonstrated that it is feasible to target tumorigenic signaling in cancer stem cells using CpG-siRNA approach.[10] Taken together, our findings provide support for application of CpG-STAT3siRNA strategy to immunotherapy of advanced prostate cancers alone or in combination with immunotherapies, such as emerging T cell-based therapies. Disruption of STAT3 signaling in the tumor microenvironment with concurrent TLR9 stimulation has potential to disrupt the central immunosuppressive circuit paving way to effective antitumor immune responses without toxicities associated with pharmacological agents.

Financial & competing interests disclosure

No potential conflicts of interests were disclosed.

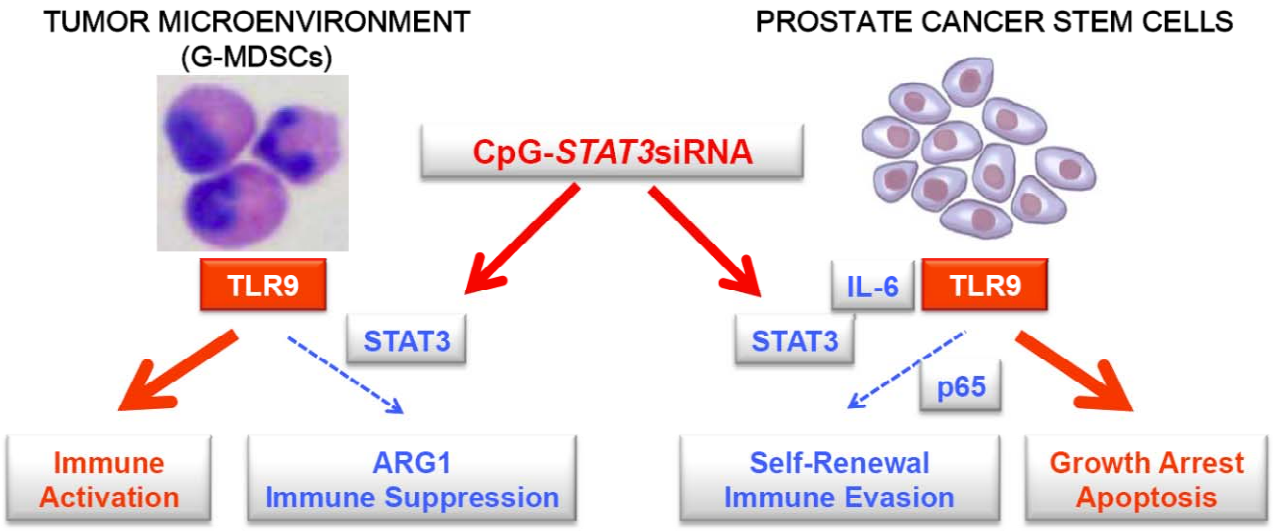

Figure 1. TLR9-targeted STAT3 inhibition allows for two-pronged therapeutic effect against prostate cancers. CpG-*STAT3*siRNA conjugates target STAT3 signaling in TLR9^{+} G-MDSCs, an immunosuppressive population of myeloid cells which accumulate during prostate cancer progression from localized to metastatic disease. *STAT3* silencing reduces production of a potently immunosuppressive mediator, arginase-1 (ARG1), thereby restoring effector T cell proliferation and activity. As shown in a parallel study, CpG-siRNA strategy allows for delivery of therapeutic siRNAs to prostate cancer stem cells which express TLR9 and rely on NF-κB/STAT3 signaling for self-renewal and tumor-propagating potential. The combination of breaking immune suppression in the tumor microenvironment and decreasing cancer cell survival is likely to augment the overall therapeutic effect against prostate cancer.

References

1. Gabrilovich DI, Ostrand-Rosenberg S, Bronte V. Coordinated regulation of myeloid cells by tumours. Nat Rev Immunol 2012; 12:253-68.
2. Vuk-Pavlovic S, Bulur PA, Lin Y, Qin R, Szumlanski CL, Zhao X, et al. Immunosuppressive CD14+HLA-DRlow/- monocytes in prostate cancer. Prostate 2009; 70:443-55.
3. Hossain DM, Pal SK, Moreira DFD, Duttagupta P, Zhang Q, Won H, et al. TLR9-Targeted STAT3 Silencing Abrogates Immunosuppressive Activity of Myeloid-Derived Suppressor Cells from Prostate Cancer Patients. Clin Cancer Res 2015.
4. Zoglmeier C, Bauer H, Norenberg D, Wedekind G, Bittner P, Sandholzer N, et al. CpG blocks immunosuppression by myeloid-derived suppressor cells in tumor-bearing mice. Clin Cancer Res 2011; 17:1765-75.
5. Krieg AM. CpG still rocks! Update on an accidental drug. Nucleic acid therapeutics 2012; 22:77-89.
6. Kortylewski M, Kujawski M, Herrmann A, Yang C, Wang L, Liu Y, et al. Toll-like receptor 9 activation of signal transducer and activator of transcription 3 constrains its agonist-based immunotherapy. Cancer Res 2009; 69:2497-505.
7. Gao C, Kozlowska A, Nechaev S, Li H, Zhang Q, Hossain DM, et al. TLR9 Signaling in the Tumor Microenvironment Initiates Cancer Recurrence after Radiotherapy. Cancer Res 2013; 73:7211-21.
8. Kortylewski M, Swiderski P, Herrmann A, Wang L, Kowolik C, Kujawski M, et al. In vivo delivery of siRNA to immune cells by conjugation to a TLR9 agonist enhances antitumor immune responses. Nat Biotechnol 2009; 27:925-32.
9. Zhang Q, Hossain DM, Nechaev S, Kozlowska A, Zhang W, Liu Y, et al. TLR9-mediated siRNA delivery for targeting of normal and malignant human hematopoietic cells in vivo. Blood 2013; 121:1304-15.
10. Moreira D, Zhang Q, Hossain DM, Nechaev S, Li H, Kowolik CM, et al. TLR9 signaling through NF-kappaB/RELA and STAT3 promotes tumor-propagating potential of prostate cancer cells. Oncotarget 2015.